

GEOLOGICA ULTRAIECTINA

Mededelingen van de
Faculteit Geowetenschappen
Universiteit Utrecht

No. 240

Fluxes, diagenesis, and the variation of proxies in eastern Mediterranean sediments

Patrick van Santvoort

ISBN 90-5744-099-7

Fluxes, diagenesis, and the variation of proxies in eastern Mediterranean sediments

Fluxen, diagenese en de variatie van proxies in sedimenten in de oostelijke
Middellandse zee

(met een samenvatting in het Nederlands)

PROEFSCHRIFT

TER VERKRIJGING VAN DE GRAAD VAN DOCTOR
AAN DE UNIVERSITEIT UTRECHT
OP GEZAG VAN DE RECTOR MAGNIFICUS, PROF. DR. W.H. GISPEN
INGEVOLGE HET BESLUIT VAN HET COLLEGE VOOR PROMOTIES
IN HET OPENBAAR TE VERDEDIGEN
OP MAANDAG 22 MAART 2004 DES MIDDAGS TE 14.30 UUR

DOOR

PETRUS JOHANNES MARIA VAN SANTVOORT

geboren op 3 juli 1965, te Rosmalen

Promotoren: Prof. Dr. G.J. de Lange
Department of Earth Sciences - Geochemistry
Faculty of Geosciences
Utrecht University
Utrecht, The Netherlands

Prof. Dr. C.H. van der Weijden
Department of Earth Sciences - Geochemistry
Faculty of Geosciences
Utrecht University
Utrecht, The Netherlands

The research described in this thesis was carried out at the Department of Earth Sciences - Geochemistry, Faculty of Geosciences, Utrecht University, Budapestlaan 4, PO Box 80021, 3508 TA Utrecht, The Netherlands.

This work was supported by the European Union Marine Science and Technology programme, contract numbers MAS2-CT93-0051 (PALAEOFLUX), MAS3-CT97-0137 (SAP) and EVK3-2000-00042 (BIODEEP)

*Ein Haus,
darin Menschen wohnen
die sich verstehen.*

*Ein Himmel,
durch den
die Sonne scheint.*

*Eine Erde,
die bunte Wiesen trägt.*

Mehr kann Glück nicht sein

*Ga tot het einde der aarde
Tot het uiterste
Daar zal liefde zijn
Ga!*

Contents

Chapter 1	Introduction and summary	9
Chapter 2	Oxidation and origin of organic matter in surficial eastern Mediterranean hemipelagic sediments	15
Chapter 3	Messinian salt fluxes into the present-day eastern Mediterranean: implications for budget calculations and stagnation	33
Chapter 4	Active post-depositional oxidation of the most recent sapropel (S1) in sediments of the eastern Mediterranean Sea	45
Chapter 5	Geochemical and paleomagnetic evidence for the occurrence of “missing” sapropels in eastern Mediterranean sediments	65
Chapter 6	Components of eastern Mediterranean sediments	85
	References	107
	Appendix	123
	Samenvatting in het Nederlands (summary in Dutch)	129
	Dankbetuiging (acknowledgements)	134
	Curriculum Vitae	135

Chapter 1

Introduction and summary

1.1 Setting

The Mediterranean is a semi-enclosed basin, bordered by the African and Eurasian continents. The only connection to the world oceans is through the narrow and shallow Strait of Gibraltar. The sill in the Strait of Sicily divides the basin into an eastern and western basin. The eastern basin is shown in Figure 1.1. Evaporation exceeds precipitation and river runoff resulting in more saline and denser surface water. This is balanced by the inflow of nutrient-depleted Atlantic surface waters into the Mediterranean. At the same time, nutrient-enriched Mediterranean Intermediate Water flows out over the sill of Gibraltar. Due to the export of nutrients, the present-day Mediterranean Sea can be considered a nutrient desert. The production of organic matter in the surface waters is therefore very low (e.g. Sarmiento et al., 1988; Béthoux, 1989).

The formation of the deep water takes place in the eastern basin where the dense surface water is moved to greater depths. The mechanism of deep water formation has changed dramatically since 1987. The source of deep water moved from the Adriatic Sea to the Aegean Sea. The new deep water is more warm and saline than before, resulting in an uplift of isopycnals by about 500 m (Klein et al., 1999; Lascaratos et al., 1999; Theocharis et al., 2002). Notable changes have been found in the nutrient distributions. Nutrient-rich water is now found closer to the euphotic zone than previously, which might induce enhanced biological activity (Klein et al., 1999). This major event can be attributed to important meteorological anomalies in the eastern Mediterranean and to changes of circulation patterns (Lascaratos et al., 1999). Only an extended dry period (1988-1993) and a few exceptionally cold winters (1987, 1992-1993) was enough to dramatically alter this large scale process.

1.2 Brine basins and mud volcanoes

The geodynamic evolution of the Mediterranean has been largely determined by the convergence of Europe and Africa, resulting from differential spreading along the Atlantic oceanic ridge. As a consequence, the African plate collided with Eurasia and subducted under the European margin. This still ongoing process has resulted in the formation of volcanic arcs and other tectonical phenomena such as faults and fractures; not only on land, but also below the seafloor.

The sediments of the Mediterranean are deposited on top of an extremely thick layer of evaporites, formed during what is called the Messinian Salinity Crisis. The most common explanation is that the evaporites were deposited in a deep and desiccated Mediterranean basin that had been repeatedly isolated from the Atlantic Ocean. Krijgsman et al. (1999) showed that the onset of evaporite precipitation, astronomically dated at 5.96 Myr, was remarkably synchronous over the entire Mediterranean basin. The origin of the Messinian Salinity Crisis was found to be dominantly tectonic.

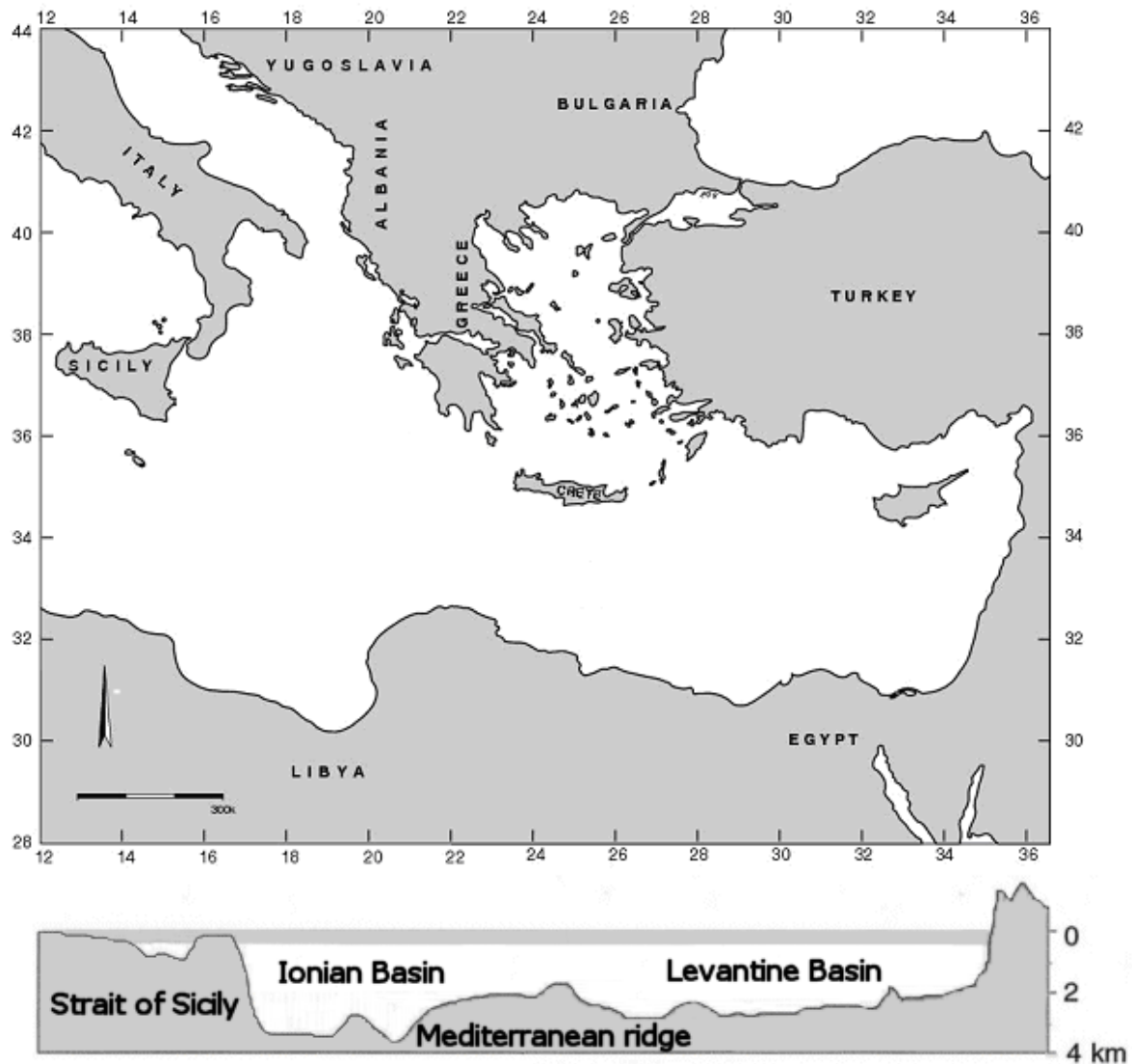


Figure 1.1 *The eastern Mediterranean Sea.*

Tectonic process and the fact that evaporites have a lower density than sediment resulting in an up rising of salt domes. When a salt dome reaches the seafloor, it is rapidly dissolved and a deep basin is formed. In recent years, several of these basins have been discovered: Tyro, Bannock, Atalante, Urania and Discovery Basin (De Lange and Ten Haven, 1983; Jongsma et al., 1983; Scientific staff of Cruise Bannock 1984-2, 1985; MEDRIFF Consortium, 1995). The brines that are formed during this dissolution process, are extremely dense, with salinities up to ten times seawater (De Lange et al., 1990b). The interface of brine and seawater is very sharp: the salinity changes from normal seawater to brine values within ten centimeter. Due to the density difference there is no mixing with seawater, resulting in anoxic conditions in the brine.

Tectonic dislocations can occur at rates that are fast enough to increase the pore water pressure in low-permeability sediments (Bray and Karig, 1985), for example in the Mediterranean Ridge (a morphological high south of Greece and Crete). Increased pore pressure and overthrust faults and folds have been identified as triggers for mud diapirs and volcanoes. During active periods, sediment and a fluid phase (water and gas) is erupted and

deposited on the seafloor, building up the mud volcano. Fluids, that are also expelled during dormant periods, are the result of dissolution of evaporites at greater depth and are in general more saline than eastern Mediterranean seawater.

1.3 Eastern Mediterranean sediments

Sediments that are presently deposited at hemi-pelagic sites in the eastern Mediterranean contain less than half a weight percent of organic carbon (C_{org}). Intercalated in these light-brown sediments are distinctive olive-green to black, organic rich layers, called sapropels. Kidd et al. (1978) proposed the following definition: discrete layers, greater than 1 cm in thickness, set in open marine environment and containing more than 2% organic carbon. Sapropels range in thickness from a few centimeters to decimeters and may contain up to 30 weight percent of C_{org} .

The origin of sapropels is thought to be related to paleoclimatic changes in the Mediterranean area. They were formed at maxima in the Northern Hemisphere insolation of the Sun, during periods of wetter climatic conditions (e.g. Rossignol-Strick et al., 1982; Rossignol-Strick, 1985). These conditions caused enhanced river run-off and nutrient supply to the eastern Mediterranean. The variations in insolation are mainly controlled by the precession of the Earth's orbit, which has a period of about 23 kyr. (e.g. Hilgen, 1991, Lourens et al., 1992).

The exact formation mechanism of sapropels is still a matter of debate. The numerous scenarios that have been proposed can be subdivided in three groups. (1) Enhanced primary production in the photic zone (since the nutrient supply to the basin was higher at these times) is the cause of an increased organic matter accumulation in the sediments. (2) Primary production remains unchanged during times of sapropel formation, but anoxia in the bottom water causes a better preservation of organic material. Anoxia may be caused by stratification of the water column and stagnation of circulation. (3) An increased primary production is accompanied by suboxic to anoxic bottom waters.

1.4 Diagenesis

Early diagenetic processes start immediately after deposition of sediments. The most important of these processes is the decomposition of organic matter by bacteria. Available oxidants are consumed in order of decreasing energy production per mole of C_{org} oxidized, namely oxygen, nitrate, manganese oxides, iron oxides and sulphate (e.g. Froelich et al., 1979). In most organic-rich sediments, oxygen and nitrate are consumed by bacteria in the uppermost millimeters of the sediment, while in organic-poor sediments oxygen can be encountered at much greater depths. Deeper in the sediment other oxidants are used for the decomposition of organic matter. This consumption of oxidants results in the development of several redox zones in the sediment. Usually, sediments are progressively more reducing with depth, with a downward succession of oxic, suboxic and anoxic sediments.

In the suboxic redox zone, solid phase manganese and iron oxides are used for the oxidation of C_{org} . As a result, dissolved species of iron and manganese appear in the pore waters as well as trace metals that were adsorbed on or incorporated in the oxides. These dissolved species can diffuse to other levels in the sediment. On upward diffusion, these ionic species are reprecipitated as oxides when finite oxygen tensions are reencountered.

When anoxic conditions prevail, sulphate is consumed by bacteria, resulting in the formation of sulfide. Sulfide can precipitate with dissolved iron to form pyrite. As a consequence of this sulphate reduction the sulphate concentrations in the pore water drop and barite (barium sulphate) may start to dissolve. Barium is reprecipitated at levels with higher pore water sulphate concentrations.

Diagenetic processes are responsible for the removal of C_{org} and redistribution of (trace)metals in sediments. The alternation of organic poor and organic rich sediments in the eastern Mediterranean provide an unique setting to study the diagenetic interactions between organic-poor and organic-rich sediments.

1.5 This thesis

In this thesis diagenetic processes in both organic-poor and organic-rich eastern Mediterranean sediments are studied. Furthermore, (present-day) fluxes and the variations in several proxies are discussed.

Chapter 2 deals with the aerobic mineralisation of C_{org} in surface sediments of the deep eastern Mediterranean Sea. Quantification was done with the modeling environment for early diagenetic problems MEDIA. The reactive fraction comprises 60-80% of the total C_{org} reaching the sediments and is largely oxidized within the surficial 10 cm. A non-reactive fraction dominates at depths > 10 cm, and makes up 20-40% of the total flux. Total mineralization rates in the surface sediments are typical for oligotrophic, deep-sea environments. The low fluxes and rapid remineralisation of C_{org} are accompanied by $^{210}Pb_{excess}$ surface mixed layers which are only 2 cm deep, among the thinnest reported for oxygenated marine sediments. The $\delta^{13}C_{org}$ values become less negative with increasing depth and decreasing C_{org} concentrations. The major $\delta^{13}C_{org}$ change occurs in the top 3-4 cm and coincides with the interval where most of the C_{org} oxidation takes place. Paleoproductivity estimates calculated from the sediment data yield low surface productivities.

In Chapter 3 a semi-quantitative study is made of sedimentary salt fluxes into the eastern Mediterranean deep water. Different sources can be distinguished with mud diapirs/volcanoes and normal pore waters as the most important ones. Compared with the "salt input" by evaporation, the sedimentary salt input is rather small and has little influence on the models used for the water- and salt budgets. Salt input from the sediment is too low to initiate stagnation of the water column, but will enhance the stagnation process once it is initiated by other processes.

Chapter 4 investigates the diagenetic signals above the most recent sapropel S1. Generally, two Mn-rich layers are observed above this sapropel, one immediately above the sapropel top, and one a few centimeters closer to the sediment surface. Pore water profiles show that the lower Mn peak is actively forming at this moment. Paleoproductivity profiles, using the barium-organic carbon relationship, are used to calculate the initial organic carbon profile of the S1 sapropel. The profiles generated by this method demonstrate that the original sapropel unit was bounded by the upper Mn peak. This implies that the interval between the two Mn peaks, where a low organic carbon content is now observed, was originally part of the sapropel. The initially deposited C_{org} has been oxidized by a progressive downwards-moving oxidation front and is still ongoing. As the upper Mn peak marks the end of sapropel formation, the deposition of sapropel

sediment has ceased more recently than is indicated by radiocarbon dating of the visible top of S1.

The concept of oxidation of sapropels is extended in Chapter 5. The occurrence of sapropels appears to be associated with maxima in the summer insolation target curve. However, sapropels are not observed at each maximum. Geochemical and magnetic signals allow for the detection of completely oxidized or “missing” sapropels. An important parameter to reveal missing sapropels is Ba. Elevated concentrations are always found in visible sapropels, and even after oxidation of part of sapropel, the initial Ba profile remains visible. Using this tool, at least 8 of 11 sampled intervals around insolation maxima contain evidence of a completely oxidized sapropel: Ba, trace metal distributions and magnetic parameters are similar to those observed around visible sapropels.

Chapter 6 discusses the different types of sediment found in the eastern Mediterranean, making use of a very long piston core. Apart from normal hemi-pelagic sediments and sapropels, layers containing volcanic material can be found. More than 5% of the sediment in this piston core is the result of turbiditic events. The composition of these turbidites is similar to the sediments in which they are embedded, pointing to a local source area. One layer is identified as a, possibly displaced, sapropel with low organic carbon content. A comparison between sapropel and normal sediments show that these are remarkably similar. Climatic variations that cause the formation of sapropels, do not have a very significant impact on the sediment composition on this location. Climate related cyclic variations have not been found in this core.

Chapter 2

Oxidation and origin of organic matter in surficial eastern Mediterranean hemipelagic sediments¹

Abstract – Aerobic mineralisation of C_{org} in surface sediments of the deep (> 2000 m water depth) eastern Mediterranean Sea has been quantified by analysis of detailed box core C_{org} concentration versus depth profiles and the modelling environment for early diagenetic problems MEDIA. The reactive fraction comprises 60–80% of the total C_{org} reaching the sediments and is largely oxidised within the surficial 10 cm. A non-reactive C_{org} fraction (G_{NR}) dominates at depths > 10 cm, and makes up 20–40% of the total C_{org} flux to the sediments. First-order rate constants for decomposition of the reactive fraction calculated from the C_{org} profiles range from $5.4 \cdot 10^{-3}$ to $8.0 \cdot 10^{-3} \text{ yr}^{-1}$. Total mineralization rates in the surface sediment are between 1.7 and $2.6 \mu\text{mol C cm}^{-2} \text{ yr}^{-1}$ and thus are typical for oligotrophic, deep-sea environments. The low fluxes and rapid remineralisation of C_{org} are accompanied by $^{210}\text{Pb}_{excess}$ surface mixed layers which are only 2 cm deep, among the thinnest reported for oxygenated marine sediments. Model results indicate a mismatch between the C_{org} profiles and O_2 microprofiles which were measured onboard ship. This can be attributed to a combination of decompression artefacts affecting onboard measurement of the O_2 profiles or the leakage of oxygen into the core during handling on deck. Furthermore, the used D_b values, based on ^{210}Pb , may not be fully appropriate; calculations with higher D_b values improve the O_2 fits. The surficial sediment $\delta^{13}\text{C}_{org}$ values of $\sim -22\text{‰}$ become less negative with increasing depth and decreasing C_{org} concentrations. The major $\delta^{13}\text{C}$ change occurs in the top 3 to 4 cm and coincides with the interval where most of the organic carbon oxidation takes place. This indicates that the reactive fraction of organic matter, commonly assumed to be marine, has a more negative $\delta^{13}\text{C}_{org}$ than the refractory fraction, usually held to be terrestrial. Palaeoproductivity estimates calculated from the sediment data by means of literature algorithms yield low surface productivities ($12 - 88 \text{ gC m}^{-2} \text{ yr}^{-1}$), which are in good agreement with field measurements of primary productivity in other studies. Such values are, however, significantly lower than those indicated by recent productivity maps of the area derived from satellite imagery ($> 100 \text{ gC m}^{-2} \text{ yr}^{-1}$).

2.1 Introduction

Eastern Mediterranean sediments record two different sedimentation regimes: short (few thousand year) episodes of organic-rich deposition characterised by sapropel sediments with $> 2 \text{ wt.}\%$ C_{org} , interbedded with longer (tens of thousands of years) periods of organic-poor, hemipelagic sediment deposition. These contrasts in C_{org} concentrations indicate the singular character of the eastern Mediterranean basin, because on the one hand, low sediment C_{org} contents ($< 0.5 \text{ wt.}\%$) are expected under oligotrophic areas or in slowly-accumulated open ocean sediments such as red clays, while on the other hand, high

¹ This paper has been published as: P.J.M. van Santvoort, G.J. de Lange, J. Thomson, S. Colley, F.J.R. Meysman and C.P. Slomp, 2002, *Aquatic Geochemistry*, 8, 153 – 175. Copyright 2002, with kind permission of Kluwer Academic Publishers.

values (> 2 wt.%) only occur in highly productive, upwelling continental margin areas (e.g. compilation by Müller and Suess, 1979).

Geochemical research on eastern Mediterranean sediments has mainly focused on the sapropels and the transitions between sapropels and the organic-poor sediments (e.g. Sigl et al., 1978; Anastasakis and Stanley, 1986; De Lange et al., 1989, 1999; Pruyssers et al., 1993; Higgs et al., 1994; Thomson et al., 1995; Van Santvoort et al., 1996²). The C_{org}-poor, deep-water sediments have been largely ignored, despite the fact that they compose most of the sedimentary column. The inorganic geochemical composition of the hemipelagic sediments of the basin are usually explained by differences in lithological source and the relative contribution of biogenic carbonate (Pruyssers et al., 1991; Dekkers et al., 1994; Van Os et al., 1994, Nijenhuis et al., 2001). Oxic sediments immediately above sapropels can exhibit high concentrations of redox-sensitive (trace-)elements, but these are generally sapropel sediments which have been oxidised after deposition (e.g. Thomson et al., 1995; Van Santvoort et al., 1996; De Lange et al., 1999; Thomson et al., 1999). Sediment C_{org} concentrations between sapropel units are low and fairly constant, ranging between 0.1 and 0.2 wt.%. This concentration range seems to be independent of depth in core, sedimentation rate and water depth (e.g. Pruyssers et al., 1991; this study).

This study focuses on the process of C_{org} oxidation in the top layer of eastern Mediterranean sediments. The aerobic mineralisation of C_{org} is quantified using the modeling environment for early diagenetic problems MEDIA (Meysman, 2001; Meysman et al., 2003), with sediment ²¹⁰Pb_{excess} data utilised to quantify bioturbation. δ¹³C values of the sedimentary organic carbon are discussed. Finally, based on the organic carbon data in the sediment, primary production rates are calculated.

2.2 Material and methods

Three sub-cores are studied from box cores UM15, UM26 and UM35, recovered during the 1994 Palaeoflux cruise with R.V. Urania (Figure 2.1 and Table 2.1). Pore water analyses of these cores have been reported elsewhere (Van Santvoort et al., 1996). Sediment oxygen profiles were measured within 3 hours after core recovery by means of an oxygen electrode mounted on a computer-controlled micro manipulator (Cussen et al., 1994), and showed that the sediments are oxic down to the top of the most recent sapropel (S1), present at 22.3–28.5 cm depth in the different cores.

Sub-cores for C_{org} analyses were sampled at high resolution (2–3 mm). Samples were freeze-dried and finely ground in an agate mortar. Organic carbon was determined on a Fisons Instruments NCS NA 1500 analyser using dry combustion at 1030°C. Inorganic carbon (carbonate) was removed before analysis by shaking 1 g samples twice for 24 hours in 1 M HCl. After drying at 80°C, the sample was ground in an agate mortar. CO₂ gas released upon combustion from 30 mg acid-treated samples was cryogenically separated from the other gases and the δ¹³C_{org} was measured with a VG SIRA 24 mass spectrometer. The precision was < 0.1‰, and international and in-house standards were used to check the accuracy of the method. Standard deviations were always < 1.5%.

² Van Santvoort et al. (1996) is chapter 4 of this thesis.

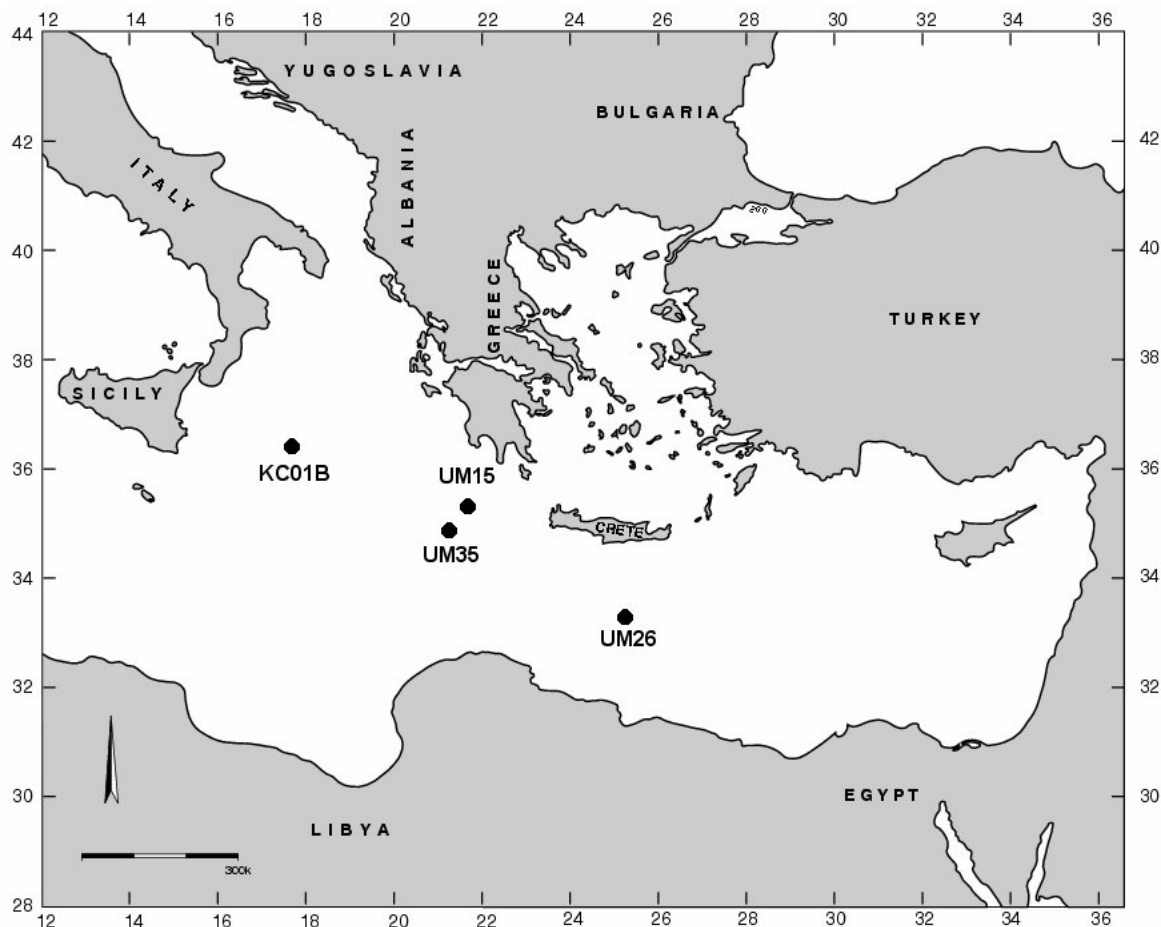


Figure 2.1 Sample locations of the cores used in this study. Position, water depth, and sediment accumulation rates for the UM boxcores are listed in Table 2.1.

Several tests have been carried out to check the removal of refractory carbonates such as dolomites by the HCl treatment. Test results show that all carbonates are removed from the sample so that the $\delta^{13}\text{C}$ measurements are not influenced by these components. Dissolved organic carbon (DOC) analyses of the HCl fractions after shaking revealed that negligible amounts of C_{org} were removed from the sample. These tests were not only performed on the samples but also on standards. The obtained DOC concentrations are below the detection limits of 0.5 ppm. Based on these results it can be assumed safely that the method for the removal of inorganic carbon as described above, only affects the inorganic carbon fraction of the sample.

The $^{210}\text{Pb}_{\text{excess}}$ method was employed to quantify bioturbation at the top of the cores (Nozaki et al., 1977; Soetaert et al., 1996). Samples (1 g) were leached with 6 M HCl in the presence of a ^{209}Po tracer. The Po isotopes were then plated on Ag planchettes by the method of Flynn (1968) for proxy determination of ^{210}Pb via ^{210}Po by alpha spectrometry.

Table 2.1 Summary of the cores studied. Accumulation rates for the UM boxcores were calculated from the base of the sapropel, assuming an age of 9.0 kyr and a constant sedimentation rate since then. In the absence of the base of the sapropel in the core, the sediment accumulation rate for UM15 is calculated on the basis of the depth of the upper Mn-peak alone (see Van Santvoort et al., 1996 for details).

Core	Location	Water depth (m)	Sediment accumulation rate (cm kyr ⁻¹)
UM15	35°17.4' N, 21°24.8' E	3307	4.7
UM26	33°23.6' N, 25°00.9' E	2160	3.1
UM35	35°11.0' N, 21°12.5' E	2670	3.3
KC01B	36°15.2' N, 17°44.3' E	3643	-

2.3 Results and discussion

2.3.1 Oxidation of organic material

C_{org} profiles (Figure 2.2a) have highest concentrations near the sediment surface and decrease with depth to achieve asymptotic values between 0.13 to 0.16 wt.% within the upper 5–10 cm of the sediment. The corresponding pore water O_2 profiles from the three box cores studied (Figure 2.2a) suggest that O_2 consumption, as revealed by the concave curvature in the profiles, is intense over the uppermost 2–3 cm. Between this surface zone and the top of the oxidized sapropel only minor additional O_2 is consumed. O_2 is fully removed at a greater depth (22.3–28.5 cm) where it is used to oxidise the most recent sapropel, S1 (Van Santvoort et al., 1996). The sediments of all three cores are therefore oxic down to the S1 unit.

C_{org} oxidation by O_2 in the upper layer of the core was reproduced using the object-oriented modeling environment MEDIA (Modelling Early DIAgenesis) (Meysman 2001, Meysman et al., 2003). This general-purpose software package for early diagenetic problems provides both transient and steady-state model description of reactive transport processes affecting organic matter, nutrients, oxidants and reduced by-products in aqueous sediments. In this study, the package was used to quantify aerobic C_{org} oxidation and to check the consistency of the C_{org} and O_2 profiles. To model the decreasing degradability of the organic matter, MEDIA implements the multi-G formulation of Westrich and Berner (1984). In this approach the total pool of sedimentary organic material G_T is subdivided into several classes, each having a different reactivity towards oxidation (Jørgensen, 1978).

$$G_T = \sum_1^n G_i$$

where G_T is the amount of total decomposable organic matter (wt.%) and G_i is the amount of organic matter in fraction i (wt.%). Each fraction degrades independently via different first-order kinetics.

$$\frac{dG_i}{dt} = -k_i G_i$$

where t is time (yr) and k_i is the first-order decay constant for organic matter in fraction i (yr^{-1}).

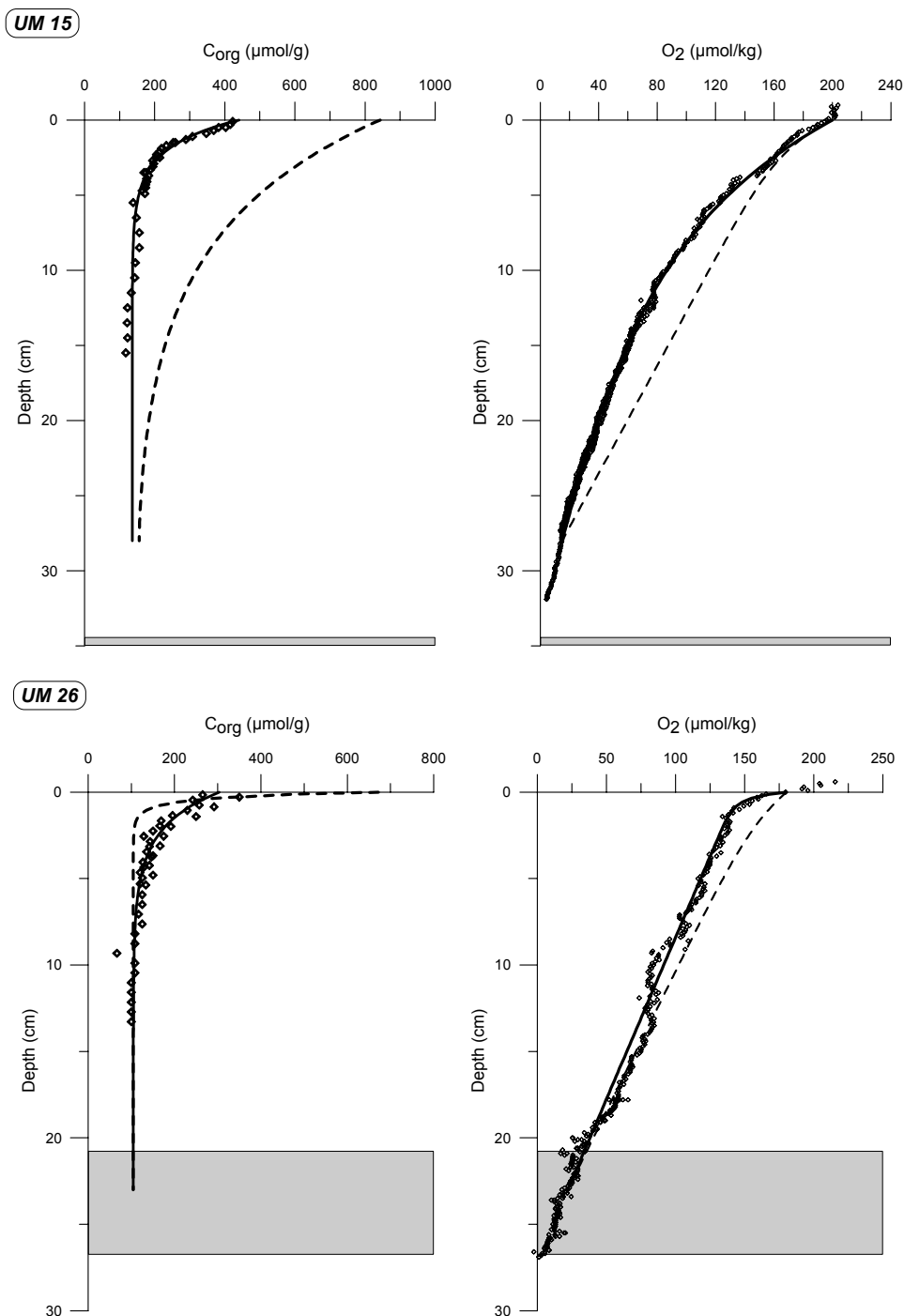


Figure 2.2a Organic carbon concentration and oxygen concentration versus depth profiles for cores UM15, UM26, and UM35. Part of the O_2 profile of UM15 was re-profiled at a different position in the core at 12 cm, which explains the overlap in the profile. The S1 sapropel (> 2 wt.% organic carbon) is indicated by the shaded area. Solid lines are the fits of MEDIA to the C_{org} data and the corresponding O_2 profiles. Dotted lines are the fits of MEDIA to the O_2 profiles and the corresponding C_{org} profiles. ^{210}Pb derived D_b values are used for the fits.

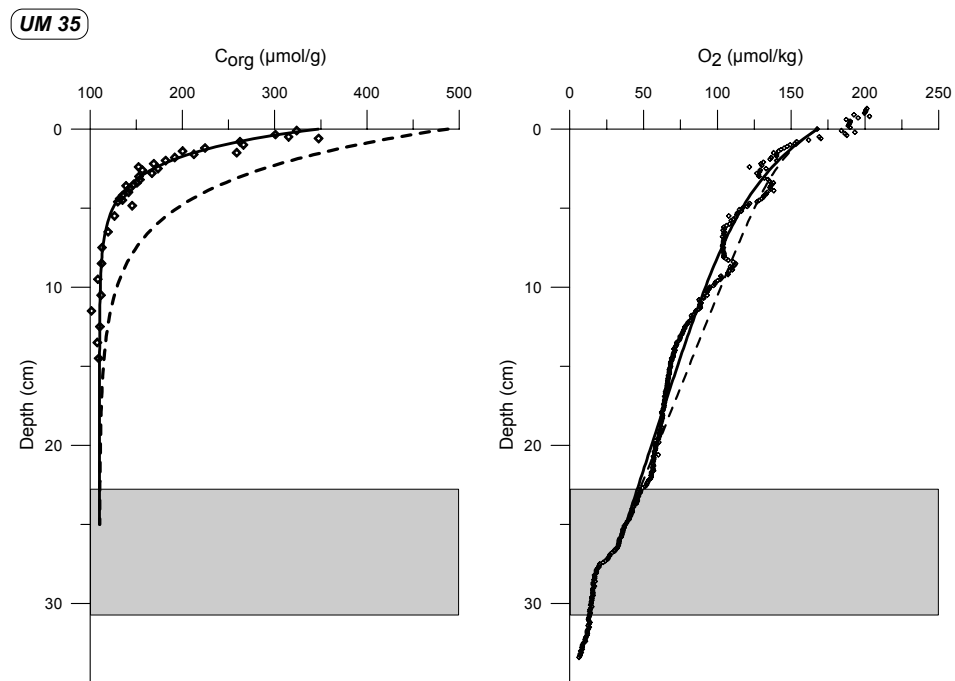


Figure 2.2a Continued.

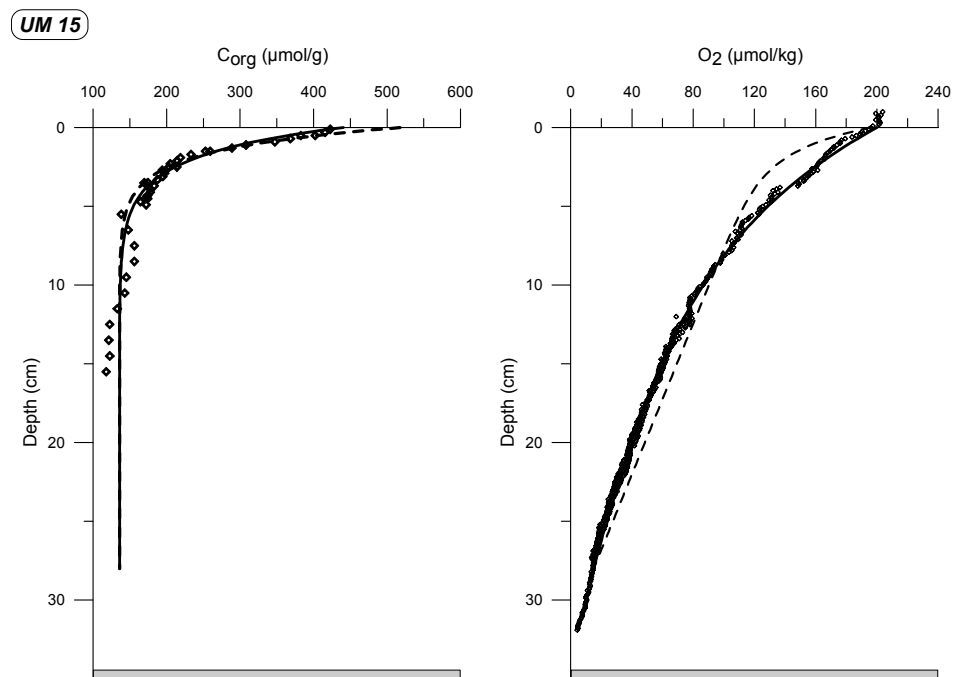


Figure 2.2b The same plots as in Figure 2.2a, but now MEDIA derived D_b values are used.

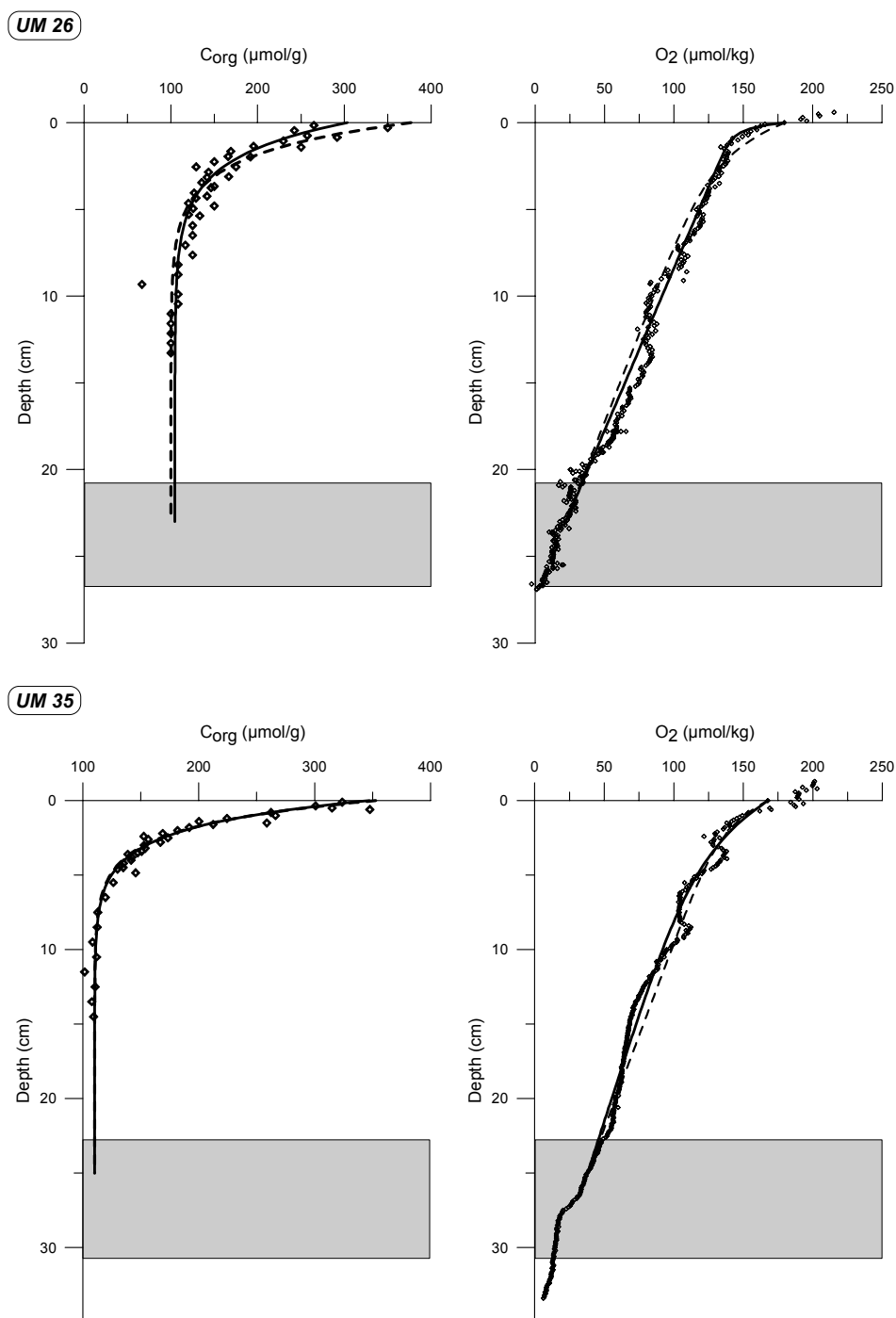


Figure 2.2b *Continued.*

Transport of solids is thought to be influenced by sediment accumulation and bioturbation. Sediment density was assumed to be equal to 2.6 g cm^{-3} . The porosity was fixed at 0.7, which is a typical value for deep-basin sediments in the eastern Mediterranean (Slomp et al., 2002), and was assumed constant with depth (no compaction). Advection velocities were calculated based on the depth location of the sapropel, i.e. either the base of the sapropel or the depth of Mn-peak (see Van Santvoort et al., 1996 for details). Bioturbation is described via the analogy of Fickian diffusion (Goldberg and Koide, 1962, Boudreau,

1986). Biodiffusion coefficients D_b ($\text{m}^2 \text{yr}^{-1}$) were calculated from the ^{210}Pb profiles for each site (section 2.3.3, Figure 2.5, Table 2.4). The modelled sediment stratum ranged from the sediment water interface to the top of the sapropel, and appropriate boundary conditions were imposed. For organic matter, a fixed flux (Neumann condition) was assumed at the sediment water interface, while no gradient boundary condition was used at the top of the sapropel. For O_2 , fixed concentrations (Dirichlet conditions) were used at both the upper and lower boundary. At the lower boundary, being the top of sapropel S1, oxygen is absent, due to the oxidation of the sapropel. To verify the performance of MEDIA, simulated C_{org} and O_2 profiles were compared to the solutions of an (approximate) analytical model (as used e.g. by Hammond et al., 1996) and matching results were obtained.

Table 2.2 Organic matter fluxes at the sediment-water interface (G_T = total, G_R = reactive, G_{NR} = non-reactive) and the first-order rate constant for organic matter decomposition (k_R) obtained by fitting the C_{org} profiles with the model MEDIA. Corresponding model fits to the C_{org} and O_2 profiles are shown in Figure 2.2a. The organic matter concentrations at the sediment-water interface, the time needed to reach the 50% and 1% level of the reactive fraction ($t_{50\%}$ and $t_{100\%}$), and C_{org} -oxidation rates in the sediment above the sapropel are also listed. At the bottom of the table, the G_T flux is listed as obtained from the MEDIA fits. Values in brackets are percentages of the total organic matter flux or concentration.

	UM15	UM26	UM35
C_{org} flux ($\mu\text{mol cm}^{-2} \text{yr}^{-1}$)			
G_T	3.03	1.92	2.93
G_R	2.53 (84%)	1.67 (87%)	2.64 (90%)
G_{NR}	0.50 (16%)	0.25 (13%)	0.28 (10%)
C_{org} concentration (wt.%)			
G_T	0.56	0.38	0.43
G_R	0.39 (71%)	0.26 (67%)	0.30 (70%)
G_{NR}	0.16 (29%)	0.13 (33%)	0.13 (30%)
k_R (yr^{-1})	$6.0 \cdot 10^{-3}$	$5.4 \cdot 10^{-3}$	$8.0 \cdot 10^{-3}$
$t_{50\%}$ (G_R) (yr)	116	129	87
$t_{1\%}$ (G_R) (yr)	770	858	575
C-ox. above S1 ($\mu\text{mol cm}^{-2} \text{yr}^{-1}$) :	2.53	1.67	2.64
flux G_T (MEDIA) ($\mu\text{mol cm}^{-2} \text{yr}^{-1}$)	9.23	4.43	3.52

C_{org} decomposition in the box cores was well-described by decay of one reactive fraction and a refractory fraction. Distinction of more fractions produced only marginal (less than a few percent) improvement to the fits and therefore the simplest model has been chosen. The model fits to the C_{org} profiles reveal that 85–90% of the organic matter reaching the sediment surface is reactive. Approximately 40–50% of the total organic material in the sediment is oxidised within the first 3 cm of the sediment in all cores (Figure 2.2a; Table 2.2). Over the next 6–7 cm, a further 20–30% is degraded and below this depth only the refractory fraction persists (fraction G_{NR} , which constitutes ca. 30% of the total C_{org} present in surficial sediments). The fitted k_R values for the three locations range between $5.4 \cdot 10^{-3}$ and $8.0 \cdot 10^{-3} \text{yr}^{-1}$. These values are within the range expected for oligotrophic, deep-sea low-sedimentation rate environments (e.g. Grundmanis and Murray, 1982; Boudreau, 1997), where the organic matter generally has a low reactivity. C_{org} -

oxidation rates in the sediment above the sapropel vary from 1.7 to 2.6 $\mu\text{mol cm}^{-2} \text{yr}^{-1}$ (Table 2.2) and are typical for deep-sea environments where very little reactive organic matter survives transport through the water column before reaching the sediment (e.g. Emerson et al., 1985; Hammond et al., 1996).

Corresponding model-calculated O_2 profiles show a concave curvature in the surface sediment, and near-linear profiles down to the top of the sapropel (Figure 2.2a). Calibrating the model to the C_{org} profiles, the measured O_2 profiles show a stronger decrease with depth than the modeled profiles for all three cores. Additional simulations showed that this discrepancy between the modeled and measured O_2 values is not the effect of nitrification. Due to low nitrate concentrations, its inclusion in the model has a negligible effect on the O_2 profiles. Therefore, it is most likely the result of a decompression artefact in the on-deck O_2 -measurements. The occurrence of such pressure-related artefacts in O_2 -microprofiles of deep-sea sediments measured on-deck was demonstrated earlier by Glud et al. (1994) who showed that measurements on recovered sediment cores showed lower O_2 penetration depths and higher diffusive uptake rates than *in situ* measurements. The differences increased with increasing water depth and were ascribed to three factors: (1) expelling of pore water due to the release of the hydrostatic pressure; (2) transiently-increased temperature during core recovery and handling on deck, causing an increase of respiration processes which increases the O_2 uptake and (3) a combination of both processes could be lethal to some species of bacteria and meiofauna. The availability of more organic compounds will increase the O_2 uptake.

To assess the magnitude of the change in respiration rates needed to explain the O_2 profiles in our cores, we fitted the model to the O_2 profiles and calculated the corresponding C_{org} profiles. The results are shown as dotted lines in Figure 2.2a and again clearly show the mismatch between the C_{org} and O_2 profiles. In all cores, much higher surface concentrations and fluxes of C_{org} are required than those that were actually measured. Corresponding respiration rates were up to a factor 12 (UM26) higher than those calculated based on the measured C_{org} profiles. This clearly demonstrates the need for either (1) *in situ* O_2 measurements or (2) C_{org} profiles in combination with accurate sediment transport rates (D_b , ω) when assessing organic matter decomposition in deep-sea surface sediments.

In the above discussion the implicit assumptions were made that the calculated D_b values (based on the ^{210}Pb profiles) are correct and that the mismatch between calculated and measured O_2 concentrations is the result of incorrect O_2 measurements. A different approach is the assumption that the O_2 data are correct but that the D_b values as calculated from the ^{210}Pb profiles are not accurate. Soetaert et al. (1998) showed that mixing rates based on C_{org} can be one order of magnitude higher than mixing rates based on ^{210}Pb . The organic (reactive) particles are mixed faster than the inorganic (non-reactive) ^{210}Pb particles resulting in different mixing rates. Therefore, calculations were carried out with different (higher) D_b values (Table 2.4). This improves the O_2 fits as shown in Figure 2.2b.

A final remark about the O_2 profiles is that some oxygen may have leaked into the core during coring and handling of the cores on deck. It is not possible to quantify this effect. The eventually measured profiles are the result of the possibilities mentioned before. We consider the pressure effect as the most important factor. *In situ* measurements of oxygen could clarify the observed mismatches.

In the absence of sapropels or turbidites at shallow depth, oxygen penetration into Eastern Mediterranean sediments would be much deeper than observed. This is expected because in most non-sapropel intervals C_{org} concentrations are similar to the G_{NR} values

observed for the surface sediment (Table 2.2) and rates of C_{org} decomposition are low. For example, results for a long core profile from the eastern Mediterranean (Figure 2.3), mostly show a range of C_{org} values between 0.1 and 0.2 wt.% for depths of 2.5–37 m below the seafloor, corresponding to ages of 20 kyr – 1.1 Myr (Van Santvoort et al. 1997³). Note that the lowest C_{org} values in Figure 2.3, down to 0.05 wt.%, correspond to ash layer horizons, i.e. are due to admixture with C_{org} lean allochthonous material. The lack of a consistent decrease of non-sapropel organic carbon with depth in core KC01B indicates that little or no degradation of the remaining organic carbon takes place under oxygen-deficient conditions.

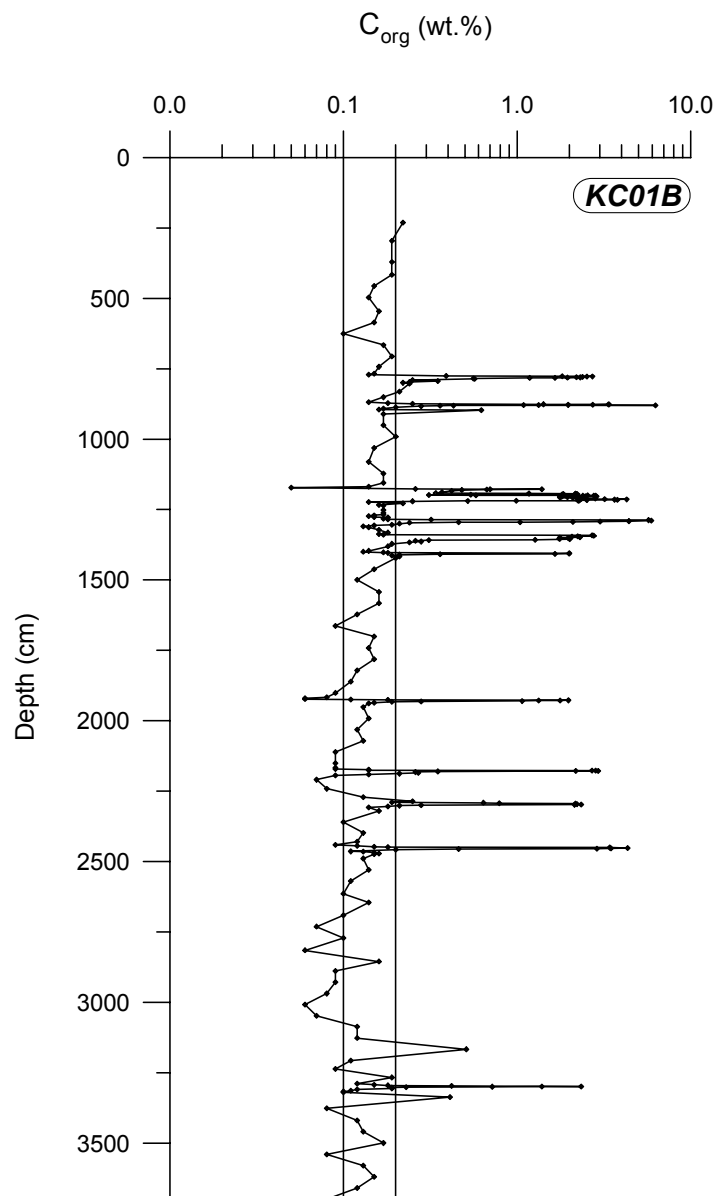


Figure 2.3 Organic carbon versus depth profile in piston core KC01B. Solid lines are drawn at 0.1 and 0.2 wt.% C_{org} . Organic carbon concentrations are mostly between these values, except in the sapropel(ic) intervals (much higher) and ash layers (lower). Note the logarithmic x-axis.

³ Van Santvoort et al. (1997) is chapter 5 of this thesis.

2.3.2 Organic matter $\delta^{13}\text{C}$ systematics

The quantity of organic matter represented by each component in the multi-G model is a model-fit parameter rather than a distinguishable class of compounds, and the model yields no information on organic matter sources. In an enclosed basin like the eastern Mediterranean, sedimentary C_{org} in principle may be expected to consist of both marine material produced in the photic zone and land-derived (terrestrial) material. $\delta^{13}\text{C}_{\text{org}}$ systematics are often used to differentiate between these sources, with values of -27‰ and -20‰ generally cited for terrestrial and marine C_{org} , respectively (Degens, 1969; Emerson and Hedges, 1988; Prahl et al., 1989). Naturally, these are average values for terrestrial and marine C_{org} , different compounds may have different $\delta^{13}\text{C}_{\text{org}}$ values (e.g. Jasper and Hayes, 1993). The most striking example for this is the difference between C_3 and C_4 plants. The $\delta^{13}\text{C}$ values of C_3 plants, which include trees, shrubs and cool-climate grasses, range from -22 to -32‰ . In contrast, C_4 plants, which include many tropical grasses, sedges and seagrasses, usually exhibit $\delta^{13}\text{C}$ values in the range of -9 to -16‰ . Several studies showed (e.g. Goñi et al., 1998; Huang et al., 2000) that the C_3/C_4 ratio can change over time by changes in climatic and atmospheric conditions. Furthermore, individual marine cores may record factors such as changes in aeolian transport pathways and wind strength (Sarnthein et al., 1981).

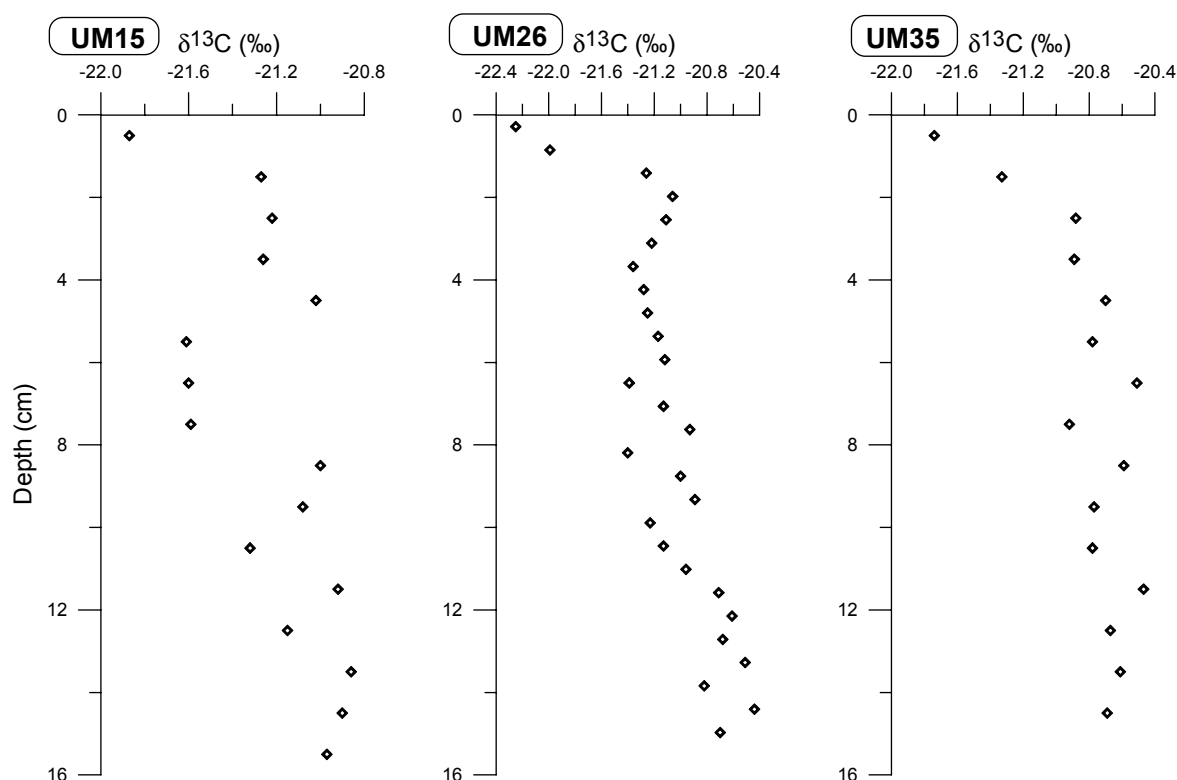


Figure 2.4 $\delta^{13}\text{C}$ (‰) versus depth profiles for UM15, UM26 and UM35. Values become less negative with increasing depth in all three cores.

The marine fraction is commonly assumed to be subject to more rapid oxidation (Emerson and Hedges, 1988; Prahl et al., 1980), whereas the terrestrial fraction is thought to be relatively resistant to further remineralisation in the marine environment since it has already been exposed to degradation on land and during transport (Prahl et al., 1989;

Hedges et al., 1994; Hedges and Keil, 1995). Our model calculations clearly indicate that the organic matter decomposition systematics can be adequately described using two fractions, namely a refractory and a reactive fraction. Concurring with commonly taken assumptions, we will tentatively assume that these fractions correspond to a predominantly ‘terrestrial’ and ‘marine’ component respectively. If in line with our model results, the organic matter remaining in sediments below 10 cm is assumed to be the refractory terrestrial component alone. Then from the model-calculated relative proportions of refractory and reactive fractions in the topmost sediment (avg. 30 and 70%; Table 2.2), and the C_{org} and $\delta^{13}C_{org}$ values for these respective sediments (Figure 2.4), an average $\delta^{13}C_{org}$ of $-20.8 \pm 0.2\text{‰}$ and $-22.6 \pm 0.4\text{‰}$ for terrestrial and marine components is calculated (Table 2.3). These values being more negative for the marine than for the terrestrial component deviate from what is commonly reported for oceanic sediments. However, in eastern Mediterranean sediments clearly a prominent decrease in reactive organic carbon concurs with a change to less negative $\delta^{13}C$ values (Figure 2.4). This cannot but indicate that the reactive fraction of organic matter, commonly assumed to be marine, has a more negative $\delta^{13}C_{org}$ than the refractory fraction, usually held to be terrestrial. Although these average $\delta^{13}C_{org}$ values, being more negative for marine than for terrestrial organic matter, deviate from the oceanic values usually reported, they fall within the respective range of average values reported for terrestrial and for marine organic matter. A similar $\delta^{13}C_{org}$ change was observed by Gacia et al. (2002) in the western Mediterranean, reporting values of -25‰ for organic material in the water column and of -20‰ for C_{org} in the underlying sediments.

Table 2.3 Calculated $\delta^{13}C_{org}$ values for the reactive and refractory organic carbon fractions. The non-reactive fraction is the organic material that remains deeper than 10 cm in the sediment, all other organic matter is assumed to be reactive. The calculated $\delta^{13}C_{org}$ is obtained by using the following equation:

$$\delta^{13}C_{org} (R) = \frac{(\%C_{org} (T) \cdot \delta^{13}C_{org} (T)) - (\%C_{org} (NR) \cdot \delta^{13}C_{org} (NR))}{\%C_{org} (R)}$$

where (R), (NR) and (T) represent the reactive, non-reactive and total fractions, respectively.

	UM15	UM26	UM35
Total C_{org} (wt.%)	0.56	0.38	0.43
Total $\delta^{13}C_{org}$ (‰)	-22.0	-22.4	-22.0
Non-reactive C_{org} (wt.%)	0.16	0.13	0.13
Non-reactive $\delta^{13}C_{org}$ (‰)	-20.6	-20.9	-20.9
Reactive C_{org} (wt.%)	0.39	0.26	0.30
Reactive $\delta^{13}C_{org}$ (‰) (calculated)	-23.1	-22.3	-22.5

This deviation in relative marine and terrestrial $\delta^{13}C_{org}$ values found in the Mediterranean may be due to the highly oligotrophic nature of this semi-enclosed basin, where a major part of the primary production flows to the microbial foodweb (e.g. Turley, 1999). A detailed organic geochemical and ecological study, combined with compound-

specific $\delta^{13}\text{C}_{\text{org}}$ work, is needed to elucidate detailed background information for the sources and behavior of the $\delta^{13}\text{C}_{\text{org}}$ in the eastern Mediterranean.

2.3.3 $^{210}\text{Pb}_{\text{excess}}$ systematics: mixed layers, bioturbation intensities and inventories.

$^{210}\text{Pb}_{\text{excess}}$ is a useful short-term proxy tracer for C_{org} fluxes in the deep sea (Moore and Dymond, 1988). Following ^{222}Rn emanation from the continents to the atmosphere, a fraction of the ^{210}Pb then produced by ^{222}Rn decay is deposited on the surface ocean (Turekian et al., 1977). Biological scavenging processes remove this ^{210}Pb from the surface ocean to the underlying sediments (Moore and Dymond, 1988; Fisher et al. 1988), along with additional ^{210}Pb produced from dissolved ^{226}Ra present deeper in the water column (Cochran et al., 1990). The activity supplied to the sediments in this way is termed $^{210}\text{Pb}_{\text{excess}}$ because it is additional to the ^{210}Pb present in radioactive equilibrium with ^{226}Ra in detrital materials.

Table 2.4 $^{210}\text{Pb}_{\text{excess}}$ inventory and bioturbation coefficients (D_b) of the UM box cores. *dpm* = disintegrations per minute. The estimated bioturbation coefficients for MEDIA fits (last row) were used in the exercise where it was assumed that the measured oxygen data are correct. An alternative D_b value was used to improve the fits as shown in Figure 2.2b.

	UM15	UM26	UM35
$^{210}\text{Pb}_{\text{excess}}$ inventory (dpm cm^{-2})	24.2	10.2	13.8
bioturbation coefficient ($\text{cm}^2 \text{yr}^{-1}$) as calculated from ^{210}Pb profiles	0.010	0.015	0.019
estimated bioturbation coefficient ($\text{cm}^2 \text{yr}^{-1}$) for MEDIA fits	0.037	0.038	0.026

Due to the bioturbative effects of sediment infauna, $^{210}\text{Pb}_{\text{excess}}$ is mixed downwards into the sediments from the sediment/water interface, resulting in a surface mixed layer (SML) in deep-sea sediments. The observed SML distributions of $^{210}\text{Pb}_{\text{excess}}$ may then be modeled to quantify bioturbation intensity and depth, where these measures are average values applicable to the past 100 yr (Nozaki et al., 1977). Like C_{org} concentration/depth profiles, surficial sediment $^{210}\text{Pb}_{\text{excess}}$ profiles are assumed at steady-state, i.e. a constant tracer supply balances consumption by radioactive decay ($t_{1/2} = 22.3$ yr). Assuming steady-state supply and decay, fluxes are related to inventory according to:

$$J = \lambda I$$

where J is the $^{210}\text{Pb}_{\text{excess}}$ flux ($\text{dpm cm}^{-2} \text{yr}^{-1}$), λ is the decay constant of ^{210}Pb (yr^{-1}) and I is the inventory (dpm cm^{-2}).

The inventory (I) is evaluated as

$$I = \sum (A_i \rho_i \Delta z_i)$$

where A_i is the $^{210}\text{Pb}_{\text{excess}}$ activity in for sample i (dpm g^{-1}), ρ_i is the dry bulk density (g cm^{-3} ; assumed constant = 0.7 g cm^{-3}) and Δz_i is the thickness (cm).

Assuming a constant biodiffusion constant D_b ($\text{cm}^2 \text{yr}^{-1}$), a constant sedimentation rate ω (cm yr^{-1}) and a constant dry bulk density ρ in the mixed zone, D_b is evaluated by fitting the following equation directly to the ^{210}Pb profiles using a least squares minimization routine:

$$A = A_0 \exp\left(\frac{\omega - \sqrt{\omega^2 + 4\lambda D_b}}{2D_b} z\right)$$

with boundary conditions $A = A_0$ at $z = 0$ and $A \rightarrow 0$ as $z \rightarrow \infty$.

Assuming no bioturbation, an advective velocity of 4 cm kyr^{-1} (Table 2.1) and a timespan of 4 times the ^{210}Pb half-life (i.e. about 100 yr), ^{210}Pb would penetrate the sediment only to around 4 mm. Hence, any deeper ^{210}Pb is due to mixing, and the zone over which significant non-zero ^{210}Pb activities are found, determines the thickness of the SML. The ^{210}Pb data from the three box core sub-cores (Figure 2.5) indicate shallow SMLs and low bioturbation intensities (Table 2.4). Like the overall sediment accumulation rate (Table 2.1) and C_{org} contents and fluxes (Table 2.2), the $^{210}\text{Pb}_{\text{excess}}$ inventory data of UM15 are greater than those of the other two cores (Table 2.4).

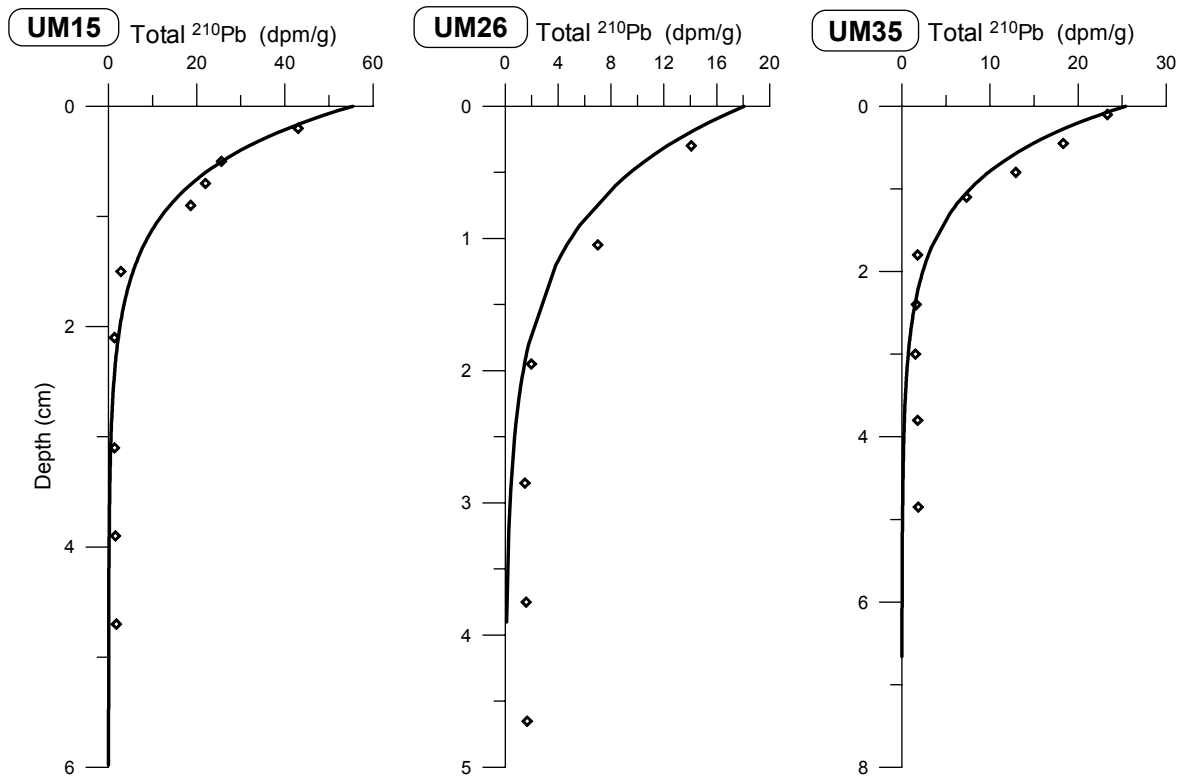


Figure 2.5 Specific activities of total ^{210}Pb versus depth for the three box cores studied. $^{210}\text{Pb}_{\text{excess}}$ is present only in the upper 2 cm of both types of core, below which depths low levels of supported ^{210}Pb (mean 1.63 dpm g^{-1}) are present in detrital materials ($^{210}\text{Pb}_{\text{excess}} = \text{total } ^{210}\text{Pb} - \text{detrital } ^{210}\text{Pb}$). $^{210}\text{Pb}_{\text{excess}}$ persists for only ~ 100 yr because of its short half-life. The observed $^{210}\text{Pb}_{\text{excess}}$ distribution is therefore not caused by sediment accumulation ($\sim 3 \text{ cm kyr}^{-1}$; Table 2.1), but rather by bioturbation in a surface mixed layer. Solid lines in the profiles are model fits to the data.

The indicated $^{210}\text{Pb}_{\text{excess}}$ SMLs in the studied cores are 2 cm thick (Figure 2.5) and are among the lowest reported for marine sediments (compare e.g. Trauth et al., 1997). They are similar to SML estimates made earlier from $^{210}\text{Pb}_{\text{excess}}$ profiles from other deep-water eastern Mediterranean sites (Table 2.4, Thomson et al., 1995). The thin $^{210}\text{Pb}_{\text{excess}}$ SMLs correspond to the depth layer with the most marked decrease in C_{org} , and it is anticipated that thin $^{210}\text{Pb}_{\text{excess}}$ SMLs will prove to be characteristic of deep-water eastern Mediterranean sediments. The D_b values are at the low end of the range observed in low sedimentation rate, deep-sea environments (Boudreau, 1994). As a result of the oligotrophic conditions in the area, C_{org} fluxes reaching the sea floor are low, and as a consequence of the low food supply flux and its rapid remineralisation, the intensity of bioturbation is low and the bioturbated zone is small in these sediments. In a suite of well-dated, deep-water eastern Atlantic cores, Trauth et al. (1997) observed that SML thickness increased directly with food supply from a minimum SML thickness of ~ 2 cm, but no such relationship was found with overall sediment accumulation rate. Thin SMLs and low mixing intensities, similar to those observed here, were also noted at the oligotrophic end-member of a transect down the west African continental slope from eutrophic to oligotrophic conditions (Legeleux et al. 1994).

From the correlation between C_{org} and $^{210}\text{Pb}_{\text{excess}}$ fluxes observed in sediment traps by Moore and Dymond (1988), it might be expected that low C_{org} fluxes from Eastern Mediterranean productivity could result in low $^{210}\text{Pb}_{\text{excess}}$ inventories in the underlying sediments. Direct wet and dry deposition measurements of $^{210}\text{Pb}_{\text{excess}}$ on the northern land margin of the Mediterranean Sea (O. Radakovitch, pers. comm. 1996) consistently yield values of ~ 0.6 dpm $\text{cm}^{-2} \text{yr}^{-1}$, which is similar to the value expected from the model of Turekian et al. (1977). This corresponds to a steady state $^{210}\text{Pb}_{\text{excess}}$ inventory or standing crop of 19 dpm cm^{-2} . The other potential source of $^{210}\text{Pb}_{\text{excess}}$ to the sediments is ^{226}Ra in the water column, but we have been unable to locate eastern Mediterranean water column $^{210}\text{Pb}/^{226}\text{Ra}$ data to evaluate this source. The atmospheric input expected to the sea surface alone is matched and exceeded only by the sediment inventory in core UM15 (24 dpm cm^{-2}), whereas the UM26 and UM35 inventories are less than that expected from atmospheric input alone (10–14 dpm cm^{-2} ; Table 2.4). For comparison, Cochran et al. (1990) found a mean deep North Atlantic inventory of 31 dpm cm^{-2} , (minimum 11, maximum 51 dpm cm^{-2}). The UM26 and UM35 data therefore are consistent with an inefficient scavenging of ^{210}Pb by primary production in surface water.

2.3.4 Organic carbon fluxes to the sediments and primary production

Previous studies have shown that the eastern Mediterranean is an area where the production of organic material is (very) low and is therefore classified as oligotrophic (e.g. Dugdale and Wilkerson, 1988). Using the model-calculated organic carbon fluxes (Table 2.2) it is possible to calculate estimates of the primary production (Suess, 1980; Betzer et al., 1984; Sarnthein et al., 1992). Equations and results are listed in Table 2.5 and range from 12 to 34 $\text{gC m}^{-2} \text{yr}^{-1}$ for the ^{210}Pb derived D_b values and from 21 to 88 $\text{gC m}^{-2} \text{yr}^{-1}$ for the MEDIA derived D_b values which all confirms the oligotrophic character of the eastern Mediterranean.

A different approach to make an estimate of the primary production is the utilisation of oxygen. For this, some assumptions must be made: (1) the average depth of the Eastern Mediterranean is 1791 m; (2) deep water is water below 200 m water depth; Levantine Intermediate Water and water from other Source areas is found below this depth (e.g. Bryden and Stommel, 1984; Roether and Well, 2001); (3) the residence time of the

deep water is 100 yr, which means that 1% of the deep water is refreshed every year (Roether and Well, 2001); (4) 90–98% of the export production is remineralised; (5) the primary production is ten times the export production (e.g. Müller and Suess, 1979); (6) the oxidation of organic carbon is the only process that utilises oxygen. Oxygen concentrations of 220 μM for the surface water (unpublished data) and 200 μM for the outflowing deep water (Roether and Well, 2001; unpublished data) were found. The surface water concentration used is slightly lower than the normally used concentration of 240 μM which is the equilibrium concentration with the atmosphere. Using the Redfield equation for the oxidation of organic matter gives an upper estimate for primary production of 30–33 $\text{gC m}^{-2} \text{yr}^{-1}$. The most important parameters in this calculation are the deep water residence time and the primary / export production ratio. On the basis of detailed hydrographic data and using sophisticated modelling, Roether and Well (2001) made an accurate assessment based on the same principle, resulting in a new productivity of 16 $\text{gC m}^{-2} \text{yr}^{-1}$.

Table 2.5 Calculation of the primary production ($\text{gC m}^{-2} \text{yr}^{-1}$) using different equations. The upper value is calculated with the fluxes (F_C) calculated with the ^{210}Pb derived D_b values, the lower with the MEDIA derived D_b values and fluxes (F_C). Since the terrestrial component can not be quantified confidently, the total C_{org} fluxes as listed in Table 2.2 are used. Actual values will therefore probably be lower.

	Reference	UM15	UM26	UM35
$F_C = \frac{P}{0.0238 \cdot z + 0.212}$	Suess (1980)	28 88	12 27	22 27
$F_C = \frac{P^{1.22}}{2.29 \cdot z^{0.5}}$	Sarnthein et al. (1992)	24 60	14 27	21 25
$F_C = \frac{P^{1.41}}{2.44 \cdot z^{0.63}}$	Betzer et al. (1984)	34 76	21 37	28 35

These estimates concur with those from the sediment data of this study, but differ from the mean annual values shown on satellite images (Longhurst et al., 1995 and Antoine et al., 1995). The Longhurst map shows productivities $> 100 \text{gC m}^{-2} \text{yr}^{-1}$ for the eastern Mediterranean, while Antoine et al. (1995) give an average productivity value for the Ionian Basin of $104 \text{gC m}^{-2} \text{yr}^{-1}$, also considerably higher than field values measured by others and the estimates made here (Table 2.5). According to the satellite derived values, more C_{org} is produced than is expected from the fluxes recorded at depth. To obtain these values in our calculation, the deep water residence time should be 2-3 times faster or the primary / export production ratio should be reduced by a similar factor of 2-3. Both possibilities are not very likely and therefore more in-depth investigations are necessary.

The processes that lead to sapropel formation are still not fully understood. This study contributes to this ongoing effort in that it clarifies some of the boundary conditions using subrecent sediments. Clearly, present-day primary production and water column conditions can not lead to sapropel formation. This is in good agreement with sapropel observations which indicate enhanced primary production and / or enhanced preservation due to suboxic water column conditions.

2.4 Conclusions

Organic carbon profiles for surficial sediments of the eastern Mediterranean can be modelled by the multi-G model using only two fractions, namely a reactive and a refractory one. In the uppermost 2–3 cm of the sediments approximately 40-50% of the total organic matter is oxidised; 20-30% is degraded over the next 6-7 cm and below this a refractory fraction persists. The k_R values are within the range expected for oligotrophic, deep-sea low-sedimentation rate environments that supply degraded C_{org} to the seafloor. All reactions in the sediments above sapropel S1 take place under oxic conditions and oxygen is never limiting in these intervals.

Unusual $\delta^{13}C$ values are observed: the values in the surface sediments are more negative than deeper in the core. The major changes take place in the top 3-4 cm where most of the organic carbon oxidation occurs. This indicates that the reactive fraction of organic matter, commonly assumed to be marine, has a more negative $\delta^{13}C_{org}$ than the refractory fraction, usually held to be terrestrial. A detailed organic geochemical study using compound specific $\delta^{13}C_{org}$ is needed to elucidate the more precise background information for the sources and behaviour of $\delta^{13}C_{org}$ in the eastern Mediterranean.

The surface mixed layers, the layer where $^{210}Pb_{excess}$ is present, are only 2 cm thick in these cores and are likely to be characteristic of deep-water eastern Mediterranean sediments. The most intense organic matter degradation takes place in the SMLs and is another confirmation of the low bioturbation depth in these sediments.

Estimates based on organic carbon fluxes and oxygen utilisation show low primary production values, ranging from 12 to 34 $gC\ m^{-2}\ yr^{-1}$ for the ^{210}Pb derived D_b values and from 21 to 88 $gC\ m^{-2}\ yr^{-1}$ for the MEDIA derived D_b values. These values are in good agreement with values found in other studies, but are low compared to satellite derived data. These data emphasize that the present primary production and water column conditions cannot lead to sapropel formation.

Acknowledgements - We are thankful to the captain and crew of R.V. Urania and chief scientist C. Corselli. H. de Waard, D. v.d. Meent, G. Nobbe, R. Alink and A. van Dijk are thanked for analytical assistance. A previous version of the manuscript benefited from reviews by J. Middelburg, R. Tyson and C. van der Weijden. This work was supported by the European Union Marine Science and Technology programme, contract numbers MAS2-CT93-0051 (PALAEOFLUX), MAS3-CT97-0137 (SAP) and EVK3-2000-00042. (BIODEEP). C.P. Slomp was supported by a fellowship of the Royal Netherlands Academy of Arts and Sciences. This is contribution 2003.05.13 of the Netherlands School of Sedimentary Geology.

Chapter 3

Messinian salt fluxes into the present-day eastern Mediterranean: implications for budget calculations and stagnation¹

Abstract - Although Messinian evaporites underly almost the entire Mediterranean, fluxes related to these evaporites have not been included in water- and salt budget calculations. Recently, long piston cores, recovered in the eastern Mediterranean, were sampled for pore waters in sufficient detail to allow a semi-quantitative study of the sedimentary fluxes. Six different salt sources can be distinguished, namely those coming from: 1. normal pore waters, 2. mud diapirs, 3. sediments of formerly brine filled basins, 4. brine filled basins, 5. sediments from areas with a cobblestone topography and 6. salt dissolution holes. Based on the chloride versus depth profiles, chloride fluxes from the sediment to the seafloor can be calculated. The fluxes were multiplied by the estimated areas for the different salt sources to obtain the total flux. These calculations show that mud diapirs and normal pore waters are the most important presently known salt sources in the eastern Mediterranean. Compared with the “salt input” by evaporation, the sedimentary salt input is rather small and has little influence on the models used for the water- and salt budgets.

Salt input from the sediment has a similar effect on the circulation of the eastern Mediterranean water column as the introduction of huge amounts of fresh water at the surface. The latter process may have resulted in the formation of sapropels. The known sedimentary salt input is too low to be directly responsible for stagnation of the water column. However, once stagnation is initiated by other factors (e.g. decrease of excess evaporation), the extra salt input into the deep water will enhance the stagnation process. Therefore, the circulation mechanism may be more sensitive to external changes than assumed until now.

3.1 Introduction

The water- and salt budgets in the Mediterranean have been studied extensively (e.g. Bryden and Stommel, 1984; Bryden and Kinder, 1991; Béthoux, 1979; Manzella et al., 1988; Sarmiento et al., 1988). All authors make use of the so-called Knudsen relations: 1. the difference between inflow and outflow through the Strait of Gibraltar is attributed to the net evaporation over the Mediterranean; 2. the total amount of salt flowing in is equal to that flowing out. Considerable disagreement exists for the estimated salinity difference in the Gibraltar Strait, and thereby for the excess evaporation.

Based on the Knudsen relations, all models assume that evaporation of inflowing Atlantic surface water is the only salinity input in the Mediterranean. However, salinity gradients are observed in the pore waters of eastern Mediterranean cores, indicating an additional salt flux from the sediments into the bottom water. These salinity gradients were found in DSDP cores (Presley et al., 1973; McDuff et al., 1978) and in normal piston cores

¹ This paper has been published as: P.J.M. van Santvoort and G.J. de Lange, 1996, *Marine Geology*, 132, 241 – 251. Copyright 1996, with permission from Elsevier.

(Ten Haven et al., 1987), but could not be adequately quantified due to the low sample resolution or the limited length of the cores. The high quality long piston cores with lengths up to 36 m, the high sample resolution, the careful sample processing procedure (De Lange, 1992) and the high precision chloride determination (De Lange, 1986) of the present sample set, allow for such a quantitative study.

In addition to the rather moderate increases in normal Mediterranean sediments (Presley et al., 1973; McDuff et al., 1978; Ten Haven et al., 1987), rather dramatic increases of salinity with depth have been reported (Klinkhammer and Lambert, 1989; De Lange, 1990a; 1990b; Henneke, 1993). All of these increases are thought to relate to the underlying Messinian salt deposits. Compositional and structural differences between the various occurrences (mud diapirs, brine-filled depressions and the various dissolution and collapse structures, such as the cobblestone areas and salt dissolution holes) probably depend on physical (tectonic related) circumstances, on the way of transport from the source areas to the sediment surface and on possible underway-interaction with sediment pore water and/or seawater (Kastens and Spiess, 1984; Camerlenghi and Cita, 1987; De Lange et al., 1990a, 1990b; Camerlenghi et al., 1992).

In this paper we will quantify the different Messinian salt sources and we will give possible implications for the salt budgets. Furthermore, implications for stagnation of the eastern Mediterranean water column will be discussed, since many authors have stated that such stagnation has resulted in the formation of sapropels (e.g. Olausson, 1961; Ryan, 1972; Thunell et al., 1977; Rossignol-Strick et al., 1982; Rossignol-Strick, 1985; Vergnaud-Grazzini et al., 1977).

3.2 Material and methods

Six piston cores and one box core have been selected for this study (Figure 3.1, Table 3.1). All piston cores have been collected during the first MAST-I Marflux cruise in June-July 1991, with the French R.V. 'Marion Dufresne'. The box core (ND2) has been taken during the third MAST-I Marflux cruise in March 1992 with the Dutch R.V. 'Tyro'.

Table 3.1 Cores (location, length and water depth) used in this study.

Core	Location	Length (m)	Water depth (m)
MD3	Calabrian Ridge, Pisano Plateau	25.25	3250
MD11	Napoli Dome, Olimpi Mud Diapirs	14.80	1925
MD14	Kretheus Basin	36.30	3314
MD15	Poseidon Basin	24.90	3305
MD19	Tyro ABC 19 PC site, Abyssal hill	29.64	2750
MD20	Top of Eratosthenes Seamount	12.04	882
ND2	Napoli Dome, Olimpi Mud Diapirs	0.28	1925

The shipboard procedure for sample processing has been described in detail by De Lange (1992). Piston core sediment samples were squeezed with modified Reeburgh-type squeezers in a glove box flushed with nitrogen. The box core was sampled in high resolution (3 mm) after which the sediment was centrifuged.

Chloride was analysed by potentiometric titration using a 0.06 M AgNO₃ solution (De Lange, 1986). Precision was on average better than 0.2 percent and always better than 1 percent.

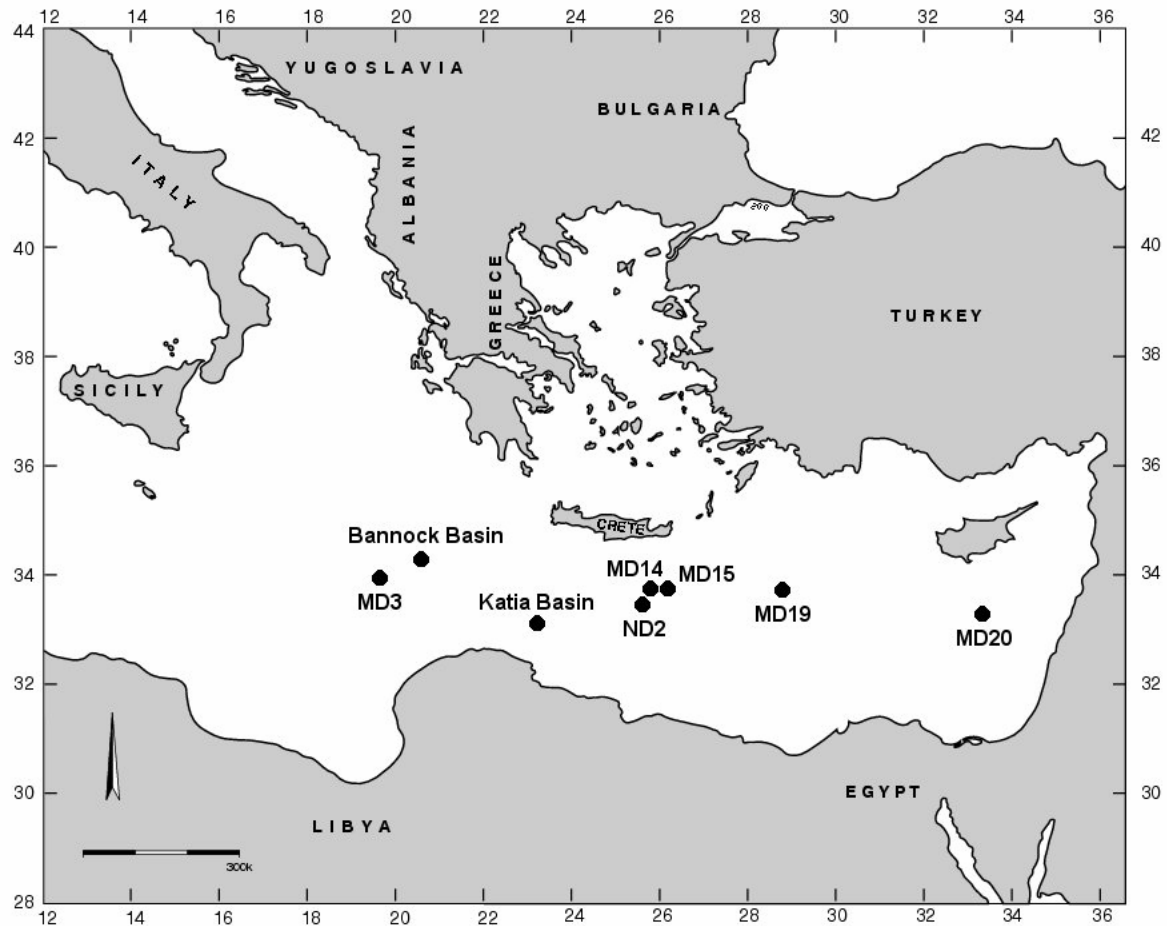


Figure 3.1 Map of the eastern Mediterranean showing the locations of the cores and basins referred to in the text. Cores MD14 and MD15 were recovered in the Tyro Basin area.

3.3 Results and discussion

Salinity is the sum of all dissolved species in water. Most of these species are more or less prone to diagenetic reactions. Chloride is one of the least reactive dissolved constituents and can be most accurately determined. Therefore, we have investigated the salt fluxes using the chloride concentration as a salinity proxy.

3.3.1 Chloride profiles

Considerable differences occur in the chloride versus depth profiles between different locations (Figure 3.2). Three different types of characteristic gradients can be distinguished: 1. the gradual increase of chloride with depth in the normal pelagic cores (MD3 and MD19); 2. the nearly constant concentration in the core from Erathostenes Seamount (MD20); 3. the steep increase in brine- and mud diapir related cores (MD11, MD14, MD15 and ND2).

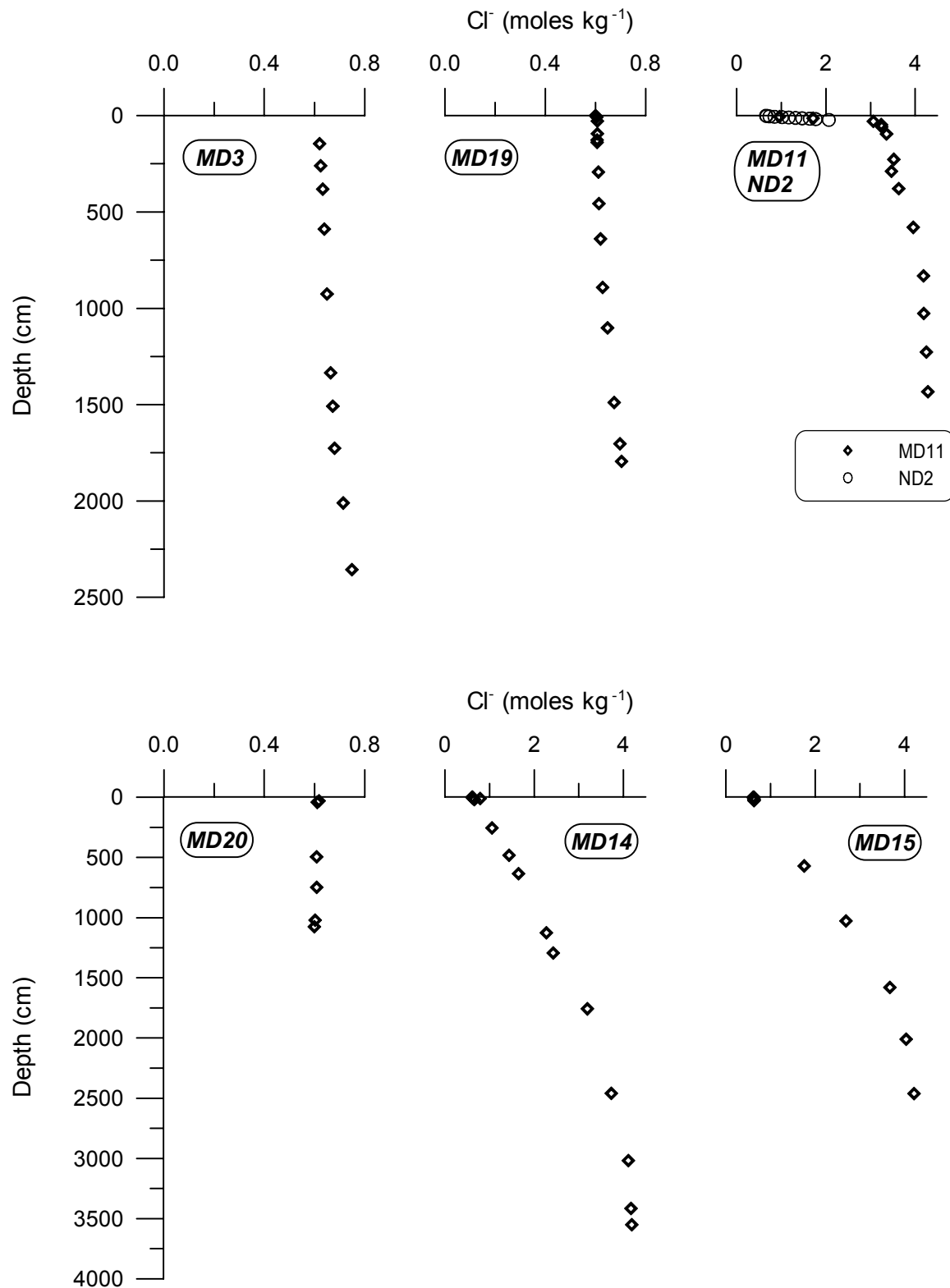


Figure 3.2 Chloride concentration versus depth profiles in pore waters.

The gradual salinity increases with depth can be explained by the (partial) dissolution of underlying Messinian evaporites and subsequent upward diffusion (e.g. Ten

Haven et al., 1987). Camerlenghi (1988) explains salinity gradients in a different way. The Plio-Quaternary sediments act as a huge membrane with seawater on one side and a brine on top of the evaporites on the other. This causes an osmotic pressure resulting in a downward transport of the 'fresher' seawater. The osmotically-induced advective flux of ions is larger than the molecular diffusion-induced flux acting in the opposite direction. On the Mediterranean and Calabrian Ridges (and probably seamounts) the osmotically induced flux can be established. The seawater that reaches the evaporites at these locations can flow down the regional slope of the ridges' flanks, along the evaporite / hemipelagic sediment lithologic discontinuity. The waterflux causes subsurface dissolution of evaporites and formation of brines. The brines are expected to accumulate in the lowest areas, the abyssal plains. Here the osmotically induced hydraulic gradient cannot trigger a seawater flux through the sediment because of the absence of a regional slope at the evaporite / hemipelagic sediment interface. No subsurface evaporite dissolution is expected, and only upward molecular diffusion will take place. A similar model for the Delaware Basin in Western Texas is proposed by Anderson and Kirkland (1980) and applied to the eastern Mediterranean by Kastens and Spiess (1984). The slight decrease of salinity with depth in core MD20 (Erathostenes Seamount) could confirm the Camerlenghi model, but could as well indicate the absence of underlying evaporites at this site and the presence of less saline bottom water and pore water conditions in the past (Hsü et al., 1978; Pierre and Fontes, 1978; De Lange, 1986). In this paper we will focus on the quantification of the different fluxes, independent of the mechanisms causing them.

3.3.1.1 *Normal pelagic cores*

Cores MD3 and MD19 show gradual increases of chloride with depth. In addition to using these profiles to calculate salinity fluxes, it is possible to use the observed profiles to estimate the depth of the salt deposits. To do so, the lower, linear part of the profile is extrapolated to a chloride concentration of $4.425 \text{ moles kg}^{-1}$. This is the concentration in the Tyro brine which differs only slightly from the concentration in the Bannock I brine (De Lange et al., 1990b) and may therefore be representative for most eastern Mediterranean brines. The calculated depth for the evaporites is 380 m for MD3 and 530 m for MD19. The approach we used here is valid since McDuff and Gieskes (1976) and Camerlenghi (1988) showed that for non-reactive elements like chlorine, steady-state conditions in sediments are reached within a few million years.

According to Camerlenghi (pers. comm.), seismic surveys show an evaporitic layer at a depth of 150-200 m at the location of MD3. The upper part is thought to consist of marls and gypsum (approximately 50 m) below which halite is found. Nile sediment input caused the deposition of an extremely thick (up to two km) Plio-Quaternary sequence above the Messinian evaporites in the area where MD19 was recovered. The whole sequence is gently folded and faulted, with salt diapirs growing in the cores of anticlines. Extrapolation of seismic data suggest that MD19 has been taken on top of one of the anticlines, where the thickness of the Plio-Quaternary sequence can be strongly reduced (locally to 500 m) (Camerlenghi, pers. comm.).

Some uncertainties exist for this kind of estimates: 1. the linear part of the profile in DSDP cores is found at greater depths than that reached with our long piston cores (e.g. McDuff et al., 1978); 2. different evaporite compositions will give different chloride concentrations for the initial brine; 3. it is unknown if diffusion is not hampered by a less permeable layer, such as dolomite or gypsum.

Nevertheless, the depths calculated from our pore water chloride data are in fairly good agreement with the depths estimated and extrapolated from seismic data.

3.3.1.2 *Erathostenes Seamount core*

The chloride profile for MD20 deviates from all other pore water profiles of the eastern Mediterranean as no salinity increase versus depth is observed. There are four possible explanations for this type of profiles: (1) Evaporitic layers are absent underneath Erathostenes Seamount. This would concur with a relative shallow water depth of this site during the Messinian; (2) The Plio-Quaternary sequence at this location is extremely thick, resulting in an extremely long diffusion path. Increases in pore water chlorinity near the sediment surface may then be too small to be noticed. In view of the time interval of approximately 5 Ma and the low sedimentation rate at this site during the last 0.6 Ma ($\sim 2 \text{ cm kyr}^{-1}$), this seems unlikely; (3) The Camerlenghi (1988) osmosis model predicts that cores taken at the Mediterranean and Calabrian Ridges and at seamounts will not show a diffusion type profile. The downward osmotically-induced advective flux at these locations is larger than the upward molecular diffusion-induced flux, so no increase in chloride concentration with depth will be observed; (4) Finally, interstitial waters in some of the sediments were brackish due to mixing of normal Mediterranean seawater and fresh water that intruded into the eastern Mediterranean (Hsü et al., 1978; Vengosh et al., 1994). The addition of fresh water, during periods of lowered sea levels, is confirmed by low $\delta^{18}\text{O}$ values of carbonates (Pierre and Fontes, 1978) and the occurrence of Cyprideis and Ammonia faunas (Hsü et al., 1978). The gradual decrease with depth in the chloride concentration is a consequence of diffusive exchange between the deeper low saline water and modern Mediterranean seawater.

3.3.1.3 *Brine related fluxes*

Several deep-seated brine pools have been discovered in recent years (De Lange and Ten Haven, 1983; Jongsma et al., 1983; Scientific staff of Cruise Bannock 1984-12, 1985). Most of these brine pools are characterized by an extremely sharp interface between brine and seawater, resulting in enhanced salinity fluxes across this boundary. Moreover, cores taken in some basins adjacent to such brine pools appear to have an extreme increase in salinity with depth. For example, the salinity increase with depth in the cores from Kretheus (MD14) and Poseidon basin (MD15) are thought to originate from an 'overflow' of the Tyro brine in these satellite basins (Ten Haven et al, 1987; Henneke, 1993).

Based on these profiles, it is possible to estimate the time at which hypersaline conditions changed to normal. For Kretheus basin this was 4000 yrs ago, and for Poseidon basin 1800 yrs ago. Henneke (1993) found slightly different ages, but could only use cores with a length of less than 6 m. The estimate for Kretheus basin is within the range calculated by Ten Haven et al. (1987). Similar post-brine filled satellite basins are known to occur at Bannock (De Lange et al., 1994) and Katia area².

3.3.1.4 *Mud diapir related cores*

The profiles of piston core MD11 and box core ND2 show very large increases in chloride with depth (up to $4.3 \text{ moles kg}^{-1}$). Tectonic dislocations can occur at rates that are fast enough to increase the pore water pressure in low-permeability sediments (Bray and Karig,

² More recent research has showed that there are no brine filled basins Katia area. However, other basins have been discovered, for example in the Nile delta area (Nautinil shipboard report, 2003).

1985). Evidence of such a pore pressure build-up is found in accretionary prisms, like the Mediterranean Ridge. Although formation of mud diapirs can be explained with a simple isostatic adjustment of a low viscosity and low density material when quickly loaded by other sediments (Chapman, 1974), they are related to a tectonic-induced increase of the pore pressure when associated with compressive structures. This can result in liquefaction of fine-grained sediments and their extrusion to the sea floor. Overthrust faults and folds have been identified as starting points of clay diapirs and volcanoes (Chapman, 1974). Where the permeability of the sediments allows a slow dewatering, the increased pore pressure can dissipate and produce a very low porosity. This means that porosity versus depth deviates towards low permeabilities due to the lithostatic overburden stress only (Bray and Karig, 1985). As a consequence an even larger flux of expelled pore water than in normal marine sediments has to be expected. We realise that formation of mud diapirs as described here, is only one of the possible mechanisms, but a more extensive discussion is beyond the scope of this paper.

The presence of indurated carbonate surfaces or hardgrounds is common in these sediments and points to active fluid escape (Camerlenghi et al., 1992). Such a carbonate layer was found in box core ND2 at a depth of 22 cm while the top metre of MD11 contained carbonate crust fragments. The two cores from Napoli Dome are the only cores taken on mud diapirs that are sampled for pore waters.

3.3.1.5 *Areas with a cobblestone topography and salt dissolution holes*

Two last potential salt sources are areas with a cobblestone topography and salt dissolution holes. Belderson et al. (1978) explained the depressions in the eastern Mediterranean seafloor by dissolution of subcropping Messinian evaporites, followed by collapse of the Plio-Quaternary sediment cover. A more extensive model for the tectonic related formation of areas with a cobblestone topography and larger basins was described by Camerlenghi and Cita (1987): initial compression of evaporites and Plio-Quaternary cover creates gentle anti- and synforms. In a more evolved stage, anticlines and synclines start growing and tensional fracturing of the crests of anticlines triggers evaporite dissolution and basin collapse. This situation explains the origin of small basins and is characterized by inversion of relief. In a much more evolved stage, anticlines may be reverse-faulted by continuing compression and increasing evaporite dissolution. Erosional processes occurring on basin slopes may result in exposure of Messinian evaporites. Large basins are found where main tectonic features complicate this pattern. Unfortunately, these structures have not been sampled for pore waters.

3.3.2 **Chloride flux calculations**

Chloride fluxes from sediment and brines to the deep water can be calculated using the profiles shown in Figure 3.2 (Table 3.2).

The following equation is used for the flux calculations:

$$J = -\Phi D \frac{\partial c}{\partial x}$$

in which J = chloride flux, Φ = porosity, D = diffusion coefficient and $\partial c/\partial x$ = concentration gradient at the sediment water interface.

The diffusion coefficient D is calculated as follows:

$$D = \frac{D^0}{\Phi F}$$

in which D^0 = tracer and self diffusion coefficient at infinite dilution and F = formation factor or resistivity.

The formation factor or resistivity, F , can be estimated according to Ullman and Aller (1982):

$$F = \Phi^{-n}$$

in which $n = 2$ for sediments with a porosity $\Phi \leq 0.7$ and $n = 2.5 - 3$ for sediments with a porosity $\Phi = 0.7 - 0.9$

In our calculations only the diffusive flux has been taken into account since the diffusive flux is far out the most important compared to the advective flux near the sediment-water interface. The D^0 for chloride was recalculated to the bottom water temperature of 13°C from the value given by Li and Gregory (1974). Concentration gradients were determined using the chloride profiles of Figure 3.2 and the water content of the sediments was used for the porosity calculations.

A major problem in calculating the fluxes is to estimate the average fluxes and the size of the different types of areas. Since all known diapiric belts are located in the crestal area of the Mediterranean Ridge (Camerlenghi et al., 1992), an estimate of (at most) 1 percent of the surface area of the eastern Mediterranean seafloor is thought to be realistic. Cores MD11 and ND2 are the only cores taken on mud diapirs that are sampled for pore water, so we have assumed that the flux on Napoli Dome is representative for all mud diapirs.³

Table 3.2 Eastern Mediterranean salt sources: area, fluxes and yearly input of chloride. Also listed is the evaporation over the entire Mediterranean.

Source	Area (cm ²)	Flux (moles cm ⁻² yr ⁻¹)	Total (moles yr ⁻¹)
Normal Mediterranean sediments	$1.65 \cdot 10^{16}$	$1.51 \cdot 10^{-5}$	$2.49 \cdot 10^{11}$
Deep brines	$1.5 \cdot 10^{12}$	$9.00 \cdot 10^{-3}$	$1.35 \cdot 10^{10}$
Mud diapirs	$1.65 \cdot 10^{14}$	$3.50 \cdot 10^{-2}$	$5.76 \cdot 10^{12}$
Former brine filled basins	$1 \cdot 10^{12}$	$6.82 \cdot 10^{-4}$	$6.82 \cdot 10^8$
Cobblestone areas and salt pits	$1 \cdot 10^{13}$	$1.51 \cdot 10^{-4}$	$1.51 \cdot 10^9$
		$1.51 \cdot 10^{-3}$	$1.51 \cdot 10^{10}$
		$1.51 \cdot 10^{-2}$	$1.51 \cdot 10^{11}$
Evaporation	$2.52 \cdot 10^{16}$	$3.65 \cdot 10^{-2}$	$9.25 \cdot 10^{14}$

³ In fact Napoli Dome appears not to be representative for all mud diapirs, since it contains brine filled lakes on top of it. This feature is observed more often in eastern Mediterranean mud diapirs, but not everywhere. Furthermore, not all mud diapirs provide an extra salt flux to the bottom water (G. de Lange, personal communication).

The total areas for the known brine filled and former brine filled basins (Tyro area, Bannock area, Katia area) are approximately 150 km² and 100 km², respectively. Data from De Lange et al. (1990b) are used for the flux calculations out of brine filled basins. The flux listed in Table 3.2 for the former brine filled basins is an average of the fluxes from the cores MD14 and MD15. The difference of almost 40% in these individual fluxes can be explained by the different times of changing from hypersaline to normal marine conditions in these basins, as is shown above.

For convenience, the cobblestone areas and salt dissolution holes are taken together for the flux calculations since these structures are thought to have a common origin (Kastens and Spiess, 1984; Camerlenghi and Cita, 1987). They cover an area of approximately 1000 km². Cores taken in these areas have not been sampled for pore water, consequently fluxes have to be estimated. As a first estimate we have taken values ranging from 10 up to 1000 times the normal flux. The statement of Kastens and Spiess (1984) that fluxes in these areas must be rather low because no elevated salinity is measured in the bottom water, should be rejected. The chloride concentration in the bottom water of box core ND2 (with extremely high chloride fluxes) is similar to the concentration in bottom water collected in normal hemipelagic areas.

The average flux in Table 3.2 for the normal Mediterranean sediments was calculated using the fluxes from cores MD3 and MD19. Values for both cores are almost identical (less than 1% difference).

Our flux calculations relate only to the eastern Mediterranean. The western Mediterranean is known to have underlying evaporites and to have enhanced brine fluxes too (Klinkhammer and Lambert, 1989). If we assume that the normal sediment fluxes and the cobblestone-type fluxes that take place in the Western Mediterranean are of a similar magnitude as those in the eastern Mediterranean, this results in an increase of 30 percent of the values listed in Table 3.2. A final assumption which has to be made is that the residence time of the Mediterranean deep water is relatively short and the Mediterranean circulation is a steady state process.

It is clear that mud diapirs are the major chloride source in the eastern Mediterranean (Table 3.2). Tabulated is only the diffusive flux, but there is also evidence for active fluid escape (Camerlenghi et al., 1992): gas escape structures suggest the occurrence of localized processes of fluid venting; the presence of indurated carbonate hardgrounds, which have been identified in three different diapiric fields, has been related to massive, simultaneous, ubiquitous fluid seepage; finally, reworked microfossils have been interpreted as contaminants from fluid mud expelled upslope and resedimentated in the surrounding hemipelagic area. No traces of chimneys have been found. Since it is impossible to estimate the amount of the escaping fluid, the contribution to the sedimentary salt input is unknown and is therefore not included in the calculations. Nevertheless, it is possible that these hypersaline fluids contribute significantly to the salt budget of the eastern Mediterranean or even would appear to be the major salt source. All other sources, except normal Mediterranean pore waters, are of minor importance. The minimum amount of chloride released by diffusion from the eastern Mediterranean seafloor to the deep water is $6.0 \cdot 10^{12}$ moles yr⁻¹; at most this is $6.2 \cdot 10^{12}$ moles yr⁻¹. Adding the estimates for the western Mediterranean will increase these values with $0.2 \cdot 10^{12}$ moles yr⁻¹.

Estimates of the excess evaporation (net evaporation) over the Mediterranean range from 55 to 85 cm yr⁻¹ (Bryden and Stommel, 1984; Bryden and Kinder, 1991; Béthoux, 1979; Van Os and Rohling, 1993; Sarmiento et al., 1988), with an average of approximately 65 cm yr⁻¹. Taking a chloride concentration of 0.574 moles l⁻¹, the

concentration of the inflowing Atlantic surface water and therefore the concentration of Mediterranean surface water, leads to a yearly evaporative input of $9.25 \cdot 10^{14}$ moles. This means that, on the basis of known diffusive fluxes alone, the sedimentary chloride influx is approximately 1 percent of the evaporative input. So, at present, evaporation is the most important parameter in the salt budget for the Mediterranean, accounting for 99 percent of the salt input. Therefore, the diffusive sedimentary salt input does not significantly change the water- and salt budgets of the Mediterranean. However, these percentages can change dramatically if data about the amount of fluid escaping from the mud diapirs become available.

3.3.3 Implications for stagnation

Stagnation of the water column during periods of sapropel formation is postulated by numerous authors. Factors proposed to have triggered stagnation are Black Sea overflow (Olausson, 1961; Ryan, 1972; Thunell et al., 1977), increased fluvial input of the Nile (Rossignol-Strick et al., 1982; Rossignol-Strick, 1985) and changed climatic and oceanographic conditions (like decreased evaporation and enhanced runoff) over the Mediterranean region (Vergnaud-Grazzini et al., 1977; Rohling, 1991; Van Os and Rohling, 1993). All models introduce a large body of fresh water which inhibits circulation. However, an extra input of salt into the deep water may cause similar effects. As shown above, the yearly input of chloride from the sediment is rather low compared to the evaporative input. It is evident that the sediment chloride flux alone may not have caused stagnation of the eastern Mediterranean circulation. However, if deep circulation slowed down due to an increased fresh water input, then the higher salinities induced in the bottom water by these salt fluxes will only increase the water column stability, hence stagnation.

According to Bryden and Stommel (1984), the interface between the Levantine intermediate water and the eastern Mediterranean deep water lies at a depth of about 1000 m. The salinity difference at this interface will increase if circulation is slowing down. If stagnation lasts for a few thousand years, and the residence time of the deep water is taken twice as long as during periods of normal circulation, then the salinity will increase to values of approximately 40‰. Lowering of the interface may lead to even higher salinities.

A similar hypothesis was proposed by Rossignol-Strick (1987) to explain the formation of brines. Leaching from evaporites caused a salinity flux to the bottom water, but the initial leachate was continuously flushed by bottom circulation. Accumulation of the leachate, and increase of salinity in the bottom water, started as circulation decreased. This process led eventually to the formation of brines in the deeper basins. In this view, brines are stagnant, fossil waters. It must be noted here that salinities in the pelagic areas cannot have been much higher than 40‰ during the S1 sapropel formation as no signs of sub-recent salinity excursions have been observed in the pore water profiles. The brine formation mechanism as proposed by Rossignol-Strick (1987) is therefore not valid for the pelagic regions, but probably only for the deep eastern Mediterranean basins. Up till now, bottom circulation was not strong enough to remove the brines from these basins.

The circulation mechanism in the eastern Mediterranean is probably more sensitive to external changes than assumed until now. It is difficult to quantify the effect of the sediment salt input on the stagnation process since there are too many unknown parameters (changing excess evaporation, residence time of deep water, the depth of the interface between the Levantine intermediate water and the deep water, etc.). But it is evident that

the sedimentary salt input will influence (i.e. enhance) the stagnation process, once initiated by other factors. Further research to quantify the presently unknown salinity fluxes is urged so as to better constrain circulation model calculations and conditions leading to bottom water stratification.

3.4 Conclusions

Six different salt sources can be distinguished in the Mediterranean, all related to Messinian evaporites: normal pore waters, mud diapirs, brine filled basins, pore water in sediments of basins that used to be filled with a brine, pore water in areas with a cobblestone topography and salt dissolution holes. Calculation of fluxes show that the most important source for diffusive salt fluxes are the mud diapirs, followed by the flux from the normal sediments. Compared with the input of chloride by evaporation, fluxes from the sediment are of minor importance. This means that the sedimentary input of chloride, based on diffusive fluxes alone, has little influence on the models used for the water- and salt budgets. Another implication is that the sediment chloride flux cannot be directly responsible for stagnation of the eastern Mediterranean water column. However, once stagnation is initiated, such as by introduction of a large body of fresh water at the surface (decrease of excess evaporation), the extra salt input will enhance the stagnation process. Salinities of 40‰ can be reached in the eastern Mediterranean deep water. Therefore, the present circulation mechanism is probably more sensitive to external changes than assumed until now.

Acknowledgements. - We thank the crews and the scientific parties of the R.V. 'Marion Dufresne' and R.V. 'Tyro' of the first and third MAST-I Marflux cruise. H. de Waard and M. Klein-Tank are thanked for analytical assistance. We thank C.H. van der Weijden for critically reading the manuscript. Two anonymous reviewers are thanked for constructive comments. This research was supported by the EC Marine Science and Technology (MAST) Programme, contracts 900022C (MARFLUX) and MAS2-CT93-0051 (PALAEOFLUX). NSG paper nr. 950315.

Chapter 4

Active post-depositional oxidation of the most recent sapropel (S1) in sediments of the eastern Mediterranean Sea¹

Abstract - Over a wide area of the eastern Mediterranean basin, two Mn-rich layers have been observed above the most recent sapropel (S1), one immediately above the sapropel top and one a few centimetres closer to the sediment surface. Different mechanisms have been proposed to explain the occurrence of these two Mn peaks: either both peaks have a diagenetic origin in which case the upper Mn peak is actively forming, or the lower peak is actively forming and the upper peak has a different formation mechanism. High-resolution pore water, including a gel sampler used for the first time in marine sediments, and solid phase data are now used to demonstrate that the oxidation front is located at the level of the lower Mn peak which, therefore, is presently being formed. A barium-organic carbon relationship is used to calculate the initial organic carbon profile of the S1 sapropel. The palaeoproductivity profiles generated by this method demonstrate that the original sapropel unit was bounded by the upper Mn peak. This implies that the interval between the two Mn peaks, where a low organic carbon content is now observed, was originally part of the sapropel. The initially deposited organic carbon has been oxidised by a progressive downwards-moving oxidation front. The penetration depth of this oxidation front, i.e. the distance between the two Mn peaks, is mainly determined by the organic carbon content, the sediment accumulation rate and the bioturbation depth. The upper Mn peak appears to have formed as a result of either Mn precipitation upon oxygenation of previously anoxic eastern Mediterranean deep water, or preservation of a surficial Mn peak at the end of the high productivity episode. In either case the upper Mn peak marks the end of sapropel formation as indicated by the Ba profiles. This means that formation of the S1 sapropel ceased more recently than is indicated by radiocarbon dating of the visible top of S1.

4.1 Introduction

Oxidation of organic matter is the driving force for early diagenetic reactions in deep-sea sediments. Available oxidants are consumed in order of decreasing energy production per mole of organic carbon oxidised, namely oxygen > nitrate ≥ manganese oxides > iron oxides > sulphate (e.g. Froelich et al., 1979; De Lange et al., 1986). Below the depth where the flux of reactive organic matter to the sediments consumes the available flux of oxygen from bottom waters, further decomposition takes place by nitrate and solid phase Fe- and Mn-oxide reduction. When this occurs, the redox condition of the pore water shifts from oxic to post-oxic (Berner, 1981), and Mn²⁺ and Fe²⁺ appear in the pore waters as reaction products. On upward diffusion, these ionic species are re-precipitated as oxides when finite oxygen tensions are re-encountered. Under steady-state conditions, this may lead to the

¹ This paper has been published as: P.J.M. van Santvoort, G.J. de Lange, J. Thomson, H. Cussen, T.R.S. Wilson, M.D. Krom and K. Ströhle, 1996, *Geochimica et Cosmochimica Acta*, 60, 4007 – 4024. Copyright 1996, with permission from Elsevier.

formation of Mn-rich layers at specific depths relative to the sediment surface (Froelich et al., 1979; Burdige and Gieskes, 1983; De Lange et al., 1989). In steady-state models, the downward fluxes of oxygen and nitrate are balanced by the upward Mn^{2+} and Fe^{2+} fluxes, and the depth of oxic conditions is determined by the constant organic matter and overall accumulation fluxes of the sediment and the constant bottom water oxygen content.

Changes in any of the parameters which determine steady-state conditions will force the system to re-adjust. For example, a change in organic matter flux to the sea floor will change the level at which available oxygen is consumed, i.e. the depth of (steady-state) oxic conditions. New Mn- and Fe-rich layers will then form at a different depth in the sediment when the new downward oxygen flux is re-balanced by the upward reductant flux. This concept of non steady-state diagenesis was originally developed to explain Mn-rich layers in the turbiditic sediments of the Madeira Abyssal Plain (e.g. Colley et al., 1984; Wilson et al., 1986). Wilson et al. (1985) proposed the mechanism of a progressive oxidation front, whereby bottom water oxygen diffuses into the re-deposited sediment surface of the turbidite. The initially rapid downward movement of the front decelerates with time, and forms Mn- and Fe-oxide peaks of characteristic shape.

The alternation of mainly organic-poor (< 0.5%) hemipelagic sediments, interrupted by occasional sapropel units of high (> 2%) organic carbon content in the eastern Mediterranean is an extreme example of changing sedimentary conditions. Manganese enrichments are commonly observed just above sapropel units (Murat and Got, 1987; Anastasakis and Stanley, 1986), which De Lange et al. (1989) and Pruyssers et al. (1993) ascribed to the post-depositional action of a progressive oxidation front. Pruyssers et al. (1993) noted that there were in fact two levels of marked Mn enrichment above the most recent sapropel S1, and proposed that both were diagenetic. The lower peak was formed first by a downward moving oxidation front, as described above. According to the interpretation of Pruyssers et al. (1993), the oxidation front then shifted upwards abruptly, in response to a postulated increase in organic carbon flux. Oxygen would then be preferentially consumed by this increased flux and a new oxygen-zero boundary would be located at a shallower depth in the sediment column. In this interpretation, the upper Mn peak is also diagenetic, and is in fact the actively-forming Mn peak. A similar process was described by Froelich et al. (1979) to explain double Mn peaks in sediments of the eastern equatorial Atlantic. Pore water Mn data support this interpretation for Atlantic sediments; the relatively low-resolution pore water data available to Pruyssers et al. (1993), however, did not allow to detect the exact location of the active oxidation front in these eastern Mediterranean sediments.

It has been inferred by some authors that bottom waters were anoxic during sapropel formation (e.g. Sigl et al., 1978; Anastasakis and Stanley, 1986), in which case Mn^{2+} would not have been immobilised by oxidation in the sediments but rather would have escaped into the bottom water. This phenomenon can be observed in the present-day anoxic hypersaline Tyro and Bannock basins in the eastern Mediterranean, where Mn^{2+} concentrations of $\sim 5 \mu\text{M}$ are found (De Lange et al., 1990). Higgs et al. (1994) and Thomson et al. (1995) used this concept to propose an alternative mechanism for the formation of the two Mn peaks observed above S1. They interpreted the upper Mn peak as a consequence of bottom water re-oxygenation at the end of sapropel formation (similar to the formation of Mn-rich layers in the world ocean, postulated by Mangini et al. (1991)), and the lower peak to be diagenetic and formed subsequently by the action of a progressive oxidation front. This interpretation implies that the deep eastern Mediterranean sediments

are still adjusting to changes which occurred at the end of sapropel formation, and that it is the lower Mn peak which is actively forming.

The different geochemical interpretations of Pruyssers et al. (1993) and Higgs et al. (1994) therefore hold important messages for the changes in the eastern Mediterranean environment as interpreted from the sedimentary record. In particular, both require a longer period of sapropel formation than is currently accepted. In this paper, high-resolution pore water and solid phase data are used to determine the exact position of the active oxidation front and hence the likely sequence of events leading to formation of the two Mn peaks. Conventional pore water extraction techniques are limited in their spatial resolution. Therefore pore waters were also sampled for iron and manganese using a new gel technique based on the procedures of Davison et al. (1991) and Krom et al. (1994). We present here the first use of this gel technology in a marine system. In addition, a new robust electrode (Cussen et al., 1994) is used to profile dissolved oxygen in the cores. Palaeoproductivity evidence from Ba profiles is presented to confirm the extensive post-depositional oxidation of organic carbon which has occurred in sapropel S1.

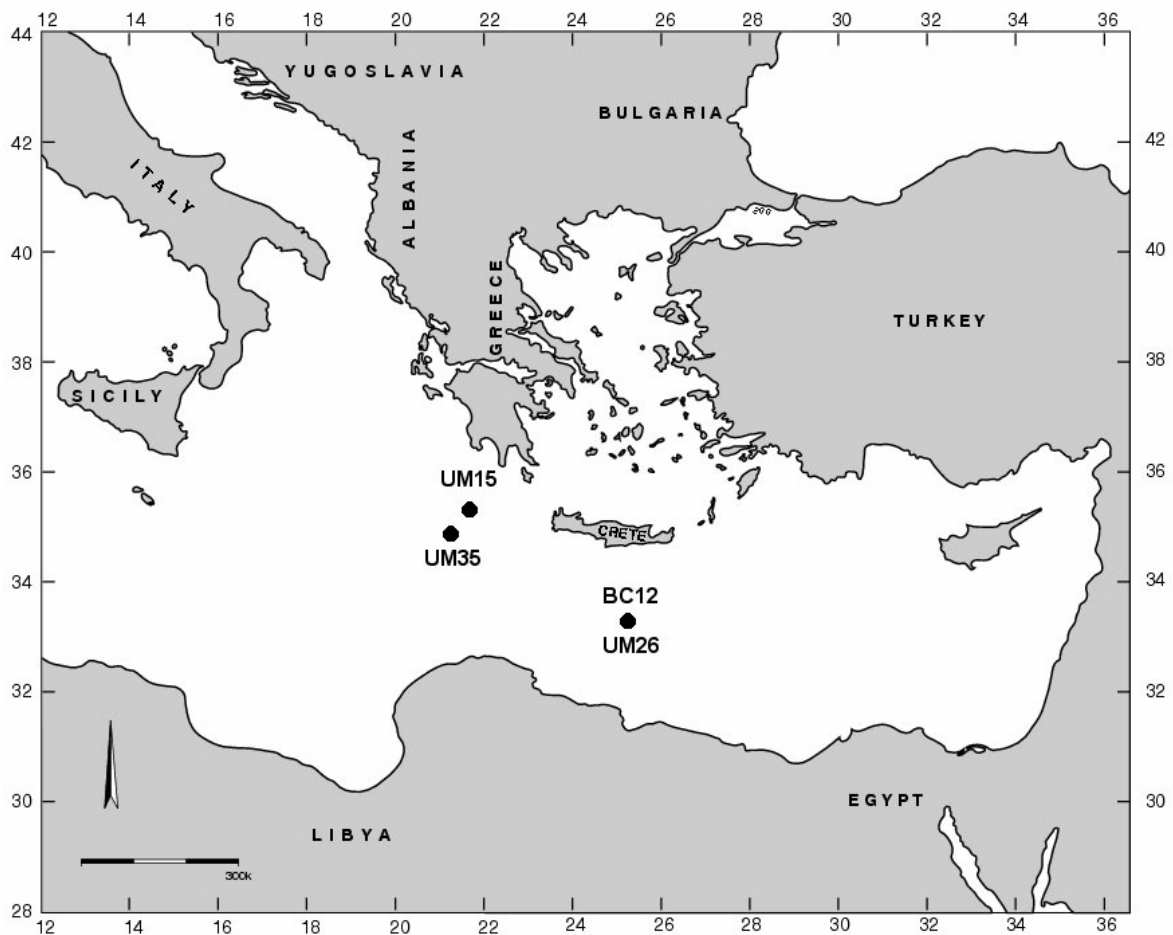


Figure 4.1 Map showing the locations of the box cores studied. Station UM15 is at $35^{\circ}17.4' N$, $21^{\circ}24.8' E$, 3307 m; UM26 is at $33^{\circ}23.6' N$, $25^{\circ}00.9' E$, 2160 m; UM35 is at $35^{\circ}11.0' N$, $21^{\circ}12.5' E$, 2670 m; station BC12 is at $33^{\circ}23.7' N$, $25^{\circ}01.3' E$, 2150 m.

4.2 Materials and methods

Box cores were recovered during two cruises: BC12 during the 1991 MARFLUX-I cruise of R.V. Marion Dufresne, and UM15, UM26 and UM35 during the 1994 PALAEOFLUX cruise of R.V. Urania (Figure 4.1)

4.2.1 Pore water measurements

Oxygen concentration and redox potential were measured onboard as soon as possible after core recovery. Pore waters were obtained by conventional sampling and subsequent squeezing, and by a gel technique. The shipboard routine has been described in detail elsewhere (De Lange, 1992). Box cores were extruded at 1 cm intervals and squeezed under nitrogen atmosphere in a glove-box. Sampling and pore water extraction took place at in situ temperature (13°C). The gel technique is briefly described below (*paragraph 4.2.1.4*).

4.2.1.1 Oxygen

Profiling dissolved oxygen in sediments presents practical problems. Although several workers (e.g. Revsbech et al., 1980; Reimers et al., 1986) have successfully used oxygen micro electrodes to profile the top few centimetres of sediments, such electrodes are too fragile to be driven to greater depths. In this study a new robust oxygen electrode, described elsewhere (Cussen et al., 1994), was used to profile the sediment cores to depths of a few decimetres. A computer-controlled manipulator inserted the electrode vertically into the core from above. The stiffness of the sediment and the relative size of the core tubes to the oxygen probe presented problems when forcing the probe to depths > 15 cm. For this reason the profiles were performed in two or three 15 cm sections by removal of the sediment already profiled. Part of UM15 is re-profiled at a different position in the core which explains the overlap as can be seen in Figure 4.3a.

4.2.1.2 Redox potential (*Eh*)

The redox potential was measured on split subcores as soon as possible after collection by a punch-in Ingoldt Eh electrode with a separate reference electrode. A Zobell standard solution ($Eh = 215$ mV at 13°C) was used for calibration.

4.2.1.3 Nitrate

Subsamples for nitrate analyses were taken onboard and analysed in the Utrecht laboratory. Nitrate was measured with a Skalar auto-analyser using an automated adaptation of the Strickland and Parsons (1968) method, following reduction of nitrate to nitrite. The difference between the nitrite concentration before and after reduction gives the nitrate concentration (Hydes and Hill, 1985). The analytical error is < 4%. The top samples contained high nitrate concentrations and were considered not to represent in-situ concentrations. A similar feature was observed by Cai et al. (1995) who found a relation for the size of the nitrate maximum and the time elapsed between core recovery and the start of sampling under anoxic conditions, suggesting that it is an artefact. These samples are therefore omitted from the profiles (Figures 4.3b, 4.4b, 4.5b).

4.2.1.4 Fe and Mn

After appropriate dilution, the squeezed pore waters were analysed at Utrecht University for Fe and Mn using a Perkin Elmer 4100 ZL Zeeman AAS. All samples were measured in

triplicate; reproducibility was better than 4% for Mn and better than 8% for Fe. Iron data of UM15 and UM35 are not used in this study due to contamination problems.

For the gel pore water technique, strips of polyacrylamide gel were mounted on 50 x 4 x 0.8 cm Perspex probes. The gel was held in place by a cover plate which exposed a 43 x 2 cm section of the gel to the pore waters. In order to protect the gel from contamination by sediment particles, a 0.45 μm Whatman membrane filter was placed on top of the exposed section of the gel, between the gel and the cover plate. The assembly was de-oxygenated for a minimum of 36 hours in a container filled with N_2 -purged distilled water. The probe was quickly (< 3 seconds) inserted into a box core subcore and left to equilibrate for 24 hours before transfer into a 10 mM solution of NaOH for 3 hours. This step ensured rapid oxidation and precipitation of mobile reduced iron and manganese and prevented further diffusion. The treated gel was carefully removed from the probe, sealed in airtight polyethylene bags and refrigerated until return to the laboratory on land.

Depending on the desired resolution, the gel was cut into 2.5 to 10 mm strips before analysis. The strips were placed into individual clean containers and leached with a known volume of 2 M HNO_3 overnight to release back into solution the metals previously fixed with NaOH. After appropriate dilution, all samples were analysed in Leeds on a Varian SpectrAA 10 AAS. Samples were measured in duplicate, and where duplicate analyses were in disagreement by more than 10%, in triplicate. Reproducibility was better than 2.8% at the 2σ level for Mn analysis and better than 8.7% for Fe analysis, as established by multiple injection of a single sample. Only Fe data from UM35 are presented due to contamination of two series of sample cups.

4.2.2 Solid phase measurements

Sediment samples were freeze-dried and finely ground in an agate mortar, then digested in a mixture of hydrofluoric, nitric and perchloric acids. Final solutions were analysed in 1 N HCl by ICP-AES on a Perkin Elmer Optima 3000 at Utrecht University, and in 1 N HNO_3 on a Philips PV8060 at IOS, for Al, Ba, Fe and Mn. The quality of the analyses was monitored by the inclusion of laboratory and international standards. The error in the analyses was < 4% for all elements. Br and I were analysed by XRF on powder briquettes. Selenium was measured by hydride-generation ICP-AES.

Organic carbon was determined on a Fisons Instruments NCS NA 1500 analyser using dry combustion at 1030°C. Inorganic carbon, as carbonate, was removed before analysis by shaking the sample for 24 hours in 1 N HCl. This procedure was repeated to ensure that all inorganic carbon had been removed. The sample was rinsed twice with distilled water and dried at 80°C. After drying, the sample was ground in an agate mortar. International and in-house standards were used to check the accuracy of the method. Standard deviations were always < 2%. Tests showed that the amount of organic carbon hydrolysed by the HCl treatment was negligible.

4.3 Results and discussion

The necessity for high-resolution sampling of both solid phase and pore waters in this study is demonstrated in Figure 4.2. Initially, the solid phase of core BC12 was sampled at the same resolution as the pore waters (1 to > 2.5 cm, Figure 4.2b), resulting in one broad Mn peak above sapropel S1 (Figure 4.2a). More detailed sampling of the solid phase at 5 mm resolution subsequently revealed two distinct Mn peaks instead of one (Figure 4.2c).

Especially at the levels of the two Mn peaks it is crucial to have high-resolution pore water data to locate the exact depth of the active oxidation front. In BC12, the initial sampling resolution decreased with depth (only one sample in the sapropel) and more detailed sampling was necessary at the deeper levels. The box cores from the Urania cruise were sampled with a resolution of 2.5 to 10 mm for pore water, and at 5 (UM26) or 10 mm (UM15 and UM35) resolution for solid phase analysis.

Concentration versus depth profiles of both solid phase and pore water data are presented in Figures 4.3, 4.4, 4.5 for UM15, UM26 and UM35, respectively. In each case, the S1 sapropel (samples with > 2% organic carbon) is indicated by the shaded area (Figures 4.3d, 4.4e, 4.5e). It should be noted that UM15 did not penetrate the complete sapropel unit. All three box cores have two solid phase Mn peaks above sapropel S1: one peak just above the sapropel (28.5 cm, 22.3 cm and 23.5 cm in UM15, UM26 and UM35, respectively) and the other at a shallower depth (at 23.5 cm, 15.5 cm and 16.5 cm in UM15, UM26 and UM35, respectively).

4.3.1 The active oxidation front

The oxygen profiles display similar characteristics for all three cores (Figures 4.3a, 4.4a, 4.5a). Core UM26 (Figure 4.4a) has a more scattered profile than the other two cores due to electrical pick-up by the electrode. Oxygen is the most important oxidant for organic matter degradation in deep marine sediments. According to Bender and Heggie (1984), more than 90% of the organic carbon reaching the deep sea floor is oxidised by O₂. From the more pronounced concave curves in the top few centimetres (< 3 cm) it can be seen that O₂ consumption is a dominant process at shallow sub-surface depths.

Below a depth of approximately 10 cm, all three cores exhibit near-linear diffusion curves with only the slightest evidence of O₂ consumption. A slight change in the slope of the curve can be seen at or close to the top of the sapropel. It is known that a well-polarised pO₂ electrode which is exposed to low pO₂ often shows a drift of the zero-line (Kessler, 1973). This artefact can be seen in all three profiles (Figures 4.3a, 4.4a, 4.5a) and makes it difficult to identify the exact depth at which pO₂ reaches zero. In our interpretation the change in the slope of the oxygen profiles at, or close to, the top of the sapropel indicates the point at which the sediment reaches zero pO₂ and below this point the electrode shows only zero base-line drift.

In such cores, oxygen is not fully utilised near the sediment surface, so that the excess oxygen can diffuse downwards to oxidise organic matter, sulphides and reduced pore water species present at depth in the sapropel. The profiles indicate that the oxidation processes have consumed the available oxygen at, or close to, the top of the sapropel.

Pore water nitrate displays a similar behaviour in the three box cores (Figures 4.3b, 4.4b, 4.5b). High initial concentrations occur near the tops of the cores (the first one or two samples) and decrease gradually to a constant background level of approximately 1 µM in the deeper parts of the cores. The lowest nitrate concentrations are reached near the lower solid phase Mn peak and remain at the same low level through the sapropel. The amount of nitrate at any particular depth is determined by the following processes. Degradation of organic matter liberates NH₄⁺ which is rapidly oxidised to nitrate (nitrification) (e.g. Froelich et al., 1979). This process produces high concentrations of NO₃⁻ near the top of the cores (greater than bottom water nitrate levels) where fresh organic material is rapidly oxidised. However, the anomalously high concentrations in the top can not be explained by this process (Cai et al., 1995). Below the nitrate maximum, nitrate diffuses downwards. The near-linear shape of our profiles indicates that, in the interval below the nitrate

maximum, nitrate is neither produced nor consumed (Bender et al., 1977). At low oxygen concentrations, decomposition of organic material occurs by utilisation of nitrate (denitrification) (e.g. Berner, 1980). Denitrification takes place at the depth where the lowest NO_3^- concentrations are reached, at the top of the sapropels.

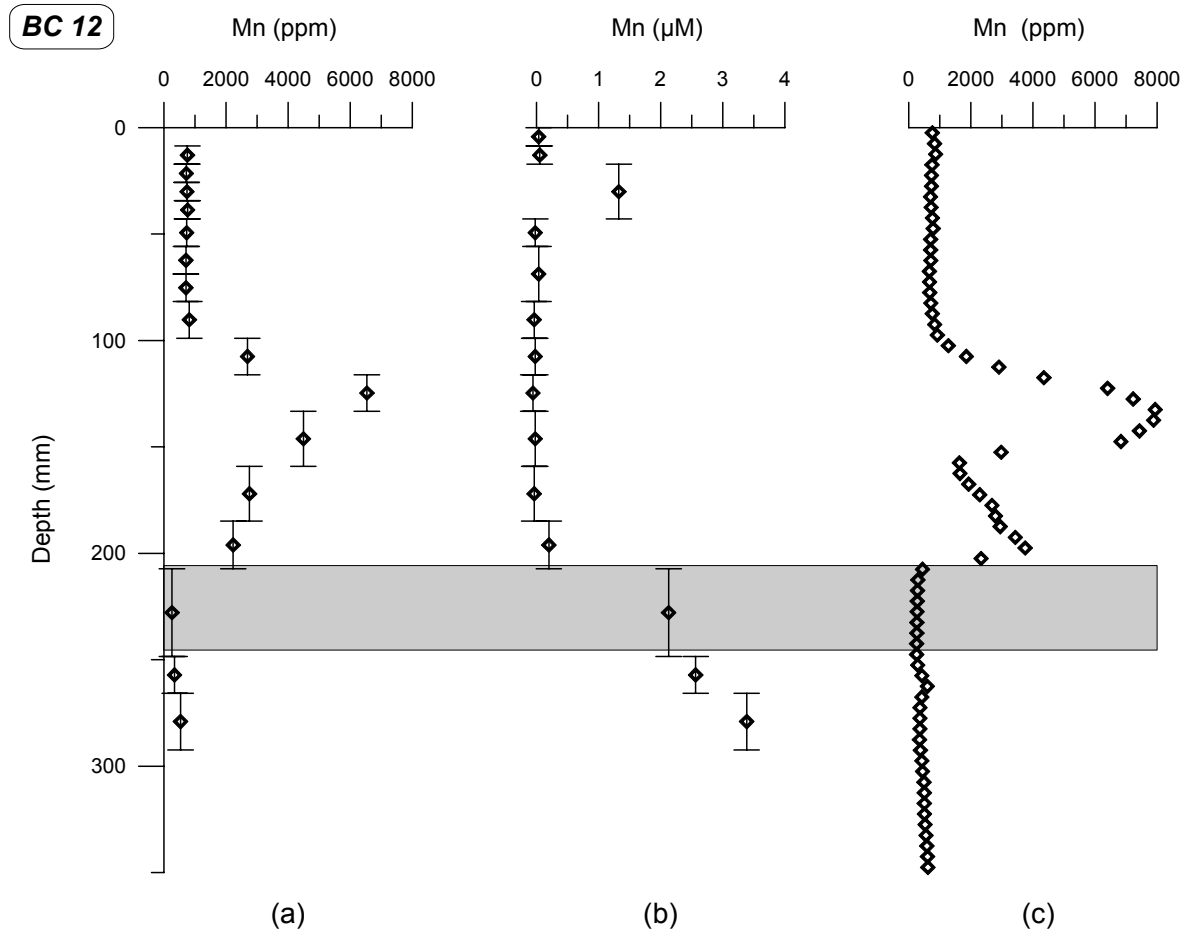


Figure 4.2 Concentration versus depth profiles of (a) solid phase Mn (1 to > 2.5 cm resolution), (b) pore water Mn (1 to > 2.5 cm resolution) and (c) high resolution (5 mm) solid phase Mn in core BC12. Initially solid phase Mn was analysed in the squeezed sediments (a). Sampling the core in a higher resolution revealed Mn peaks instead of one (c). The sapropel (sediment with > 2% organic carbon) is indicated by the shaded area.

Pore water Fe and Mn profiles, measured by conventional sampling or by gel sampler, are similar in all three box cores (Figures 4.3c, 4.4c, 4.4d, 4.5c, 4.5d). Concentrations only start to increase just below the solid phase Fe and lower Mn peak at the top of the layer where high concentrations organic carbon are present, and then increase with depth. Even at the resolution of the gel sampler, there is no significant increase in either Fe or Mn corresponding to the upper solid phase Mn peak. Under post-oxic conditions, manganese and iron oxides are utilised in the oxidation of organic matter, and Mn^{2+} and Fe^{2+} are released to pore water solution (Froelich et al., 1979; De Lange, 1986). Dissolved Mn and Fe can diffuse upwards and precipitate as Mn- and Fe-oxhydroxide when oxic conditions are encountered. Dissolved Mn^{2+} precipitates at slightly higher oxygen concentrations than Fe^{2+} , causing a separation of the solid phase Mn

and Fe peaks, with Mn maxima above Fe maxima (Figures 4.3e, 4.3f, 4.4f, 4.4g, 4.5f, 4.5g; De Lange et al., 1989; Pruyssers et al., 1993; Thomson et al., 1993; 1995). The source of the dissolved Mn^{2+} and Fe^{2+} is unknown in these cores. The amount of oxyhydroxides in the sapropel is very limited, so the main source should be located deeper in the core, below the sapropel. Ancient metal-rich layers that have formed above older sapropels may provide the dissolved species that precipitate now above S1.

The redox potential measured in fresh sub-cores of UM26 and UM35 (Figures 4.4h, 4.5h), is high in the upper part of the cores (~ 400 mV), decreases rapidly at the depth of the lower Fe and Mn peak and reaches a constant lower value in the sapropel and below. The high values above the sapropel point to oxic conditions, while the lower values in and below the sapropel are an indication of post-oxic conditions, characterised by reduction of Mn- and Fe-oxides (Berner, 1981). The gradual decrease in Eh in the upper part of the sapropel may reflect the transition from Mn-oxide to Fe-oxide reduction.

Solid phase I, Se and Br were measured in UM15 only (Figures 4.3g, 4.3h, 4.3i). Sharp I and Se peaks are found just at the top of the sapropel, while the concentrations in the sapropel are slightly higher for I, and approximately 10 times higher for Se than in the overlying sediments. Bromine does not show a peak, but appears to be closely correlated to the organic carbon content. Bromine, Se and I often show a positive correlation with organic carbon (e.g. Price and Calvert, 1977; Kennedy and Elderfield, 1987; Ten Haven et al., 1987), but it has been observed by Thomson et al. (1993, 1995) and Higgs et al. (1994) that sharp concentration maxima for solid phase I and Se are characteristically found on the inferred redox gradient across the oxic/post-oxic boundary. In contrast with Mn and Fe, which are immobile when re-precipitated in oxic conditions, the I and Se peaks are mobile and continuously move downward with the advancing oxidation front. In the absence of pore water data, solid phase I and Se may be useful to define the boundary between oxic and post-oxic conditions (Thomson et al., 1995).

The solid phase and pore water data discussed above all support the conclusion that the presently-active oxidation front is located at the level of the lower Mn and Fe peak. Oxidants, O_2 and NO_3^- , are present in the pore water only in very low concentrations below the lower Mn and Fe peak, while reduced species as Mn^{2+} and Fe^{2+} appear in solution immediately below this horizon. Furthermore, the fall in Eh just below this same level, and the sharp I and Se peaks are further evidence for the location of the oxidation front at this depth. The lack of any observed increase in Fe^{2+} and Mn^{2+} associated with the upper peak confirms that there is no diagenetic re-mobilisation occurring at this level at the present time. Our findings contrast with the conclusions of Pruyssers et al. (1993) who identified the active oxidation front at the depth of the upper Mn peak. The results by Pruyssers et al. (1993) were based on relatively shallow cores (~ 600 m water depth) whereas data from Higgs et al. (1994), Thomson et al. (1995) and this study are all based on deep cores (> 2000 m water depth). We conclude that the interpretation given here is representative of a wide area of the deep eastern Mediterranean, but may differ from the mechanisms in the more shallow parts.

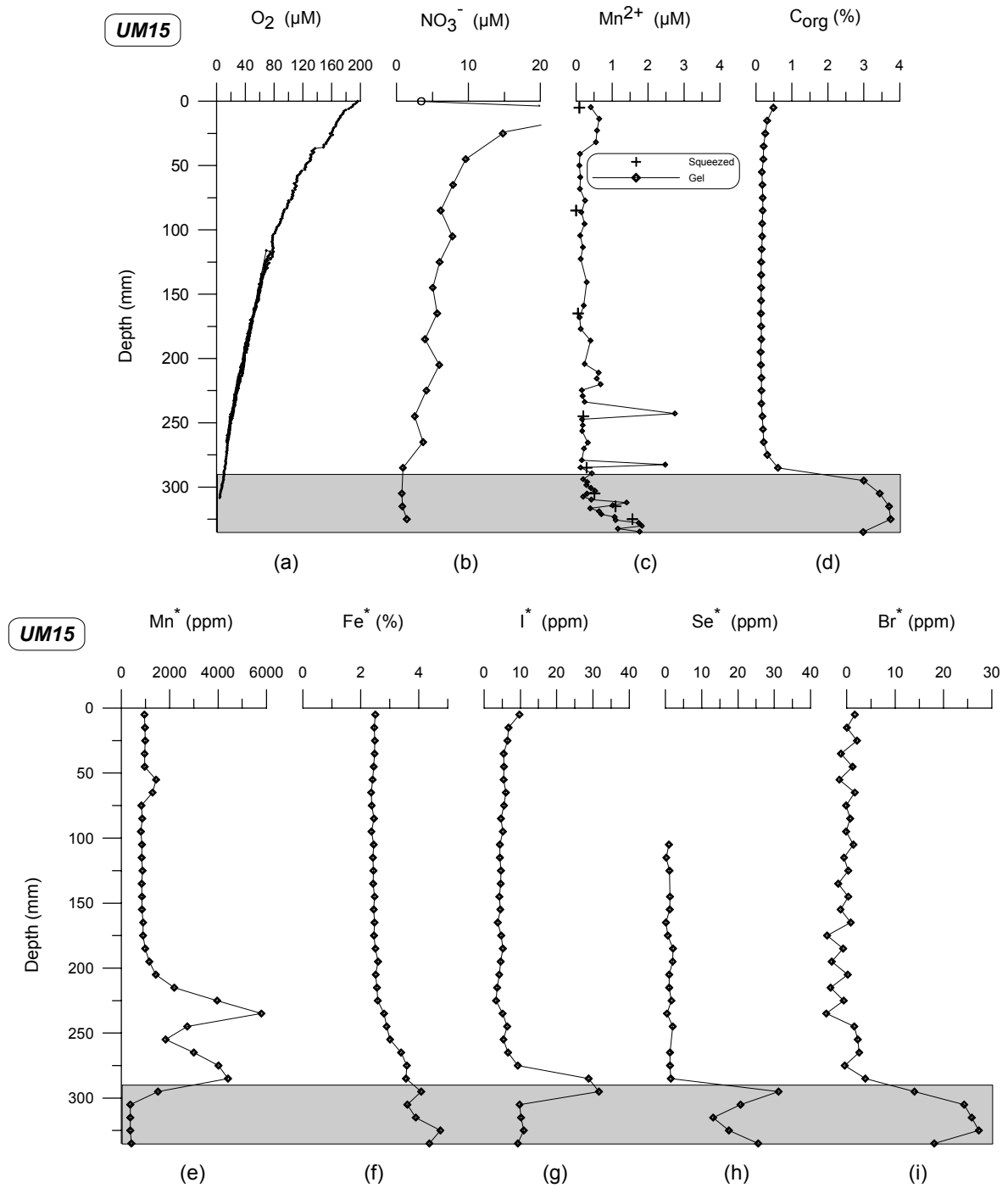


Figure 4.3 Concentration versus depth profiles of (a.) pore water O_2 , (b) pore water NO_3^- , (c) pore water Mn, data from squeezed pore waters are indicated by plus-signs, data from pore waters obtained by the gel technique by diamonds, (d) organic carbon, (e) solid phase Mn, (f) solid phase Fe, (g) solid phase I, (h) solid phase Se, and (i) solid phase Br in core UM15. Part of UM15 is reprofiled for oxygen at a different position in the core which explains the overlap in (a). Solid phase Mn, Fe, I, Se, and Br data are normalised to Al and multiplied by the average Al content to minimise the dilution effect by $CaCO_3$ (indicated by an asterisk). The sapropel (> 2% organic carbon) is indicated by the shaded area. Note that this core does not penetrate the bottom of the sapropel unit.

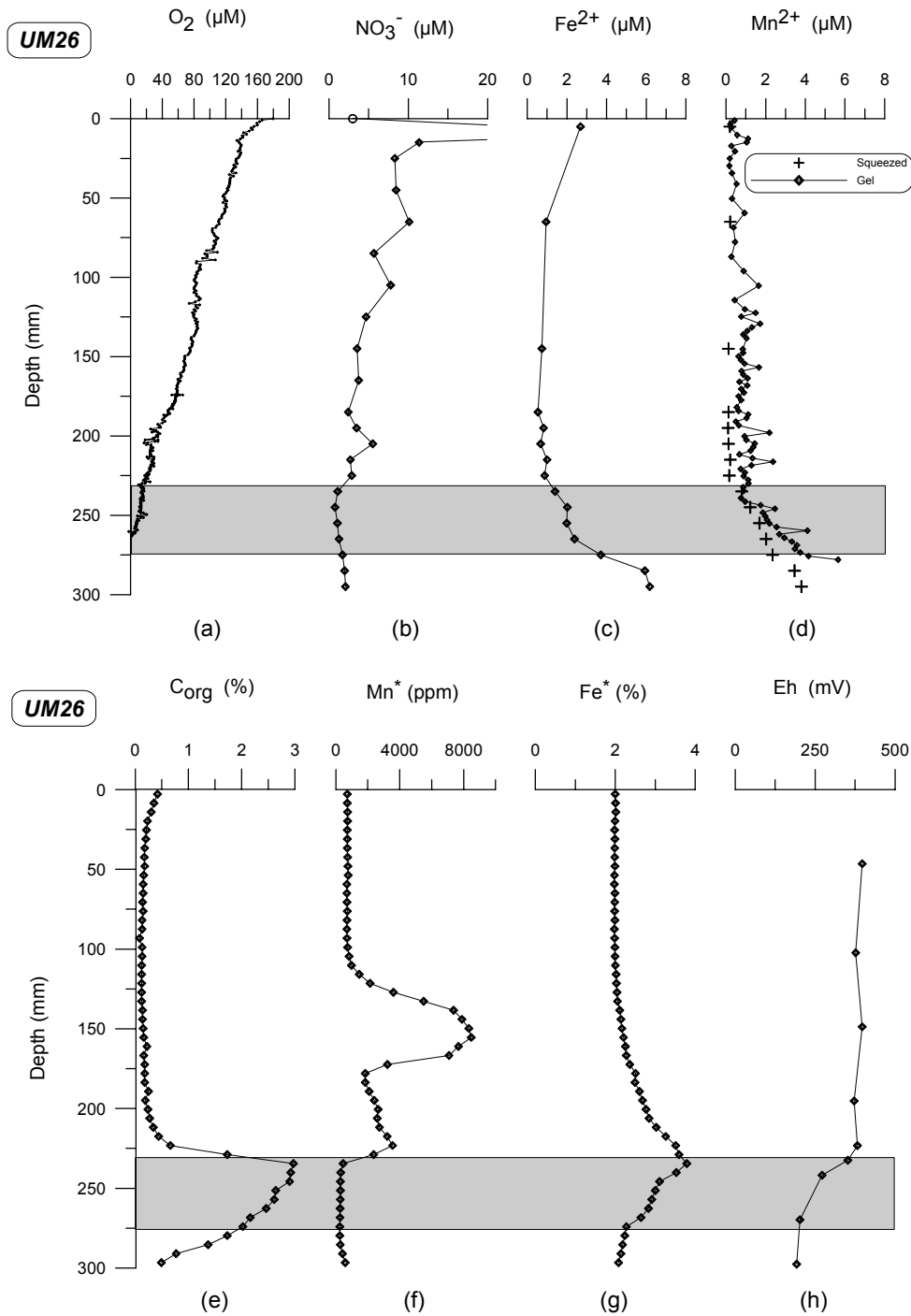


Figure 4.4 Concentration versus depth profiles of (a) pore water O_2 , (b) pore water NO_3^- , (c) porewater Fe, (d) pore water Mn, data from squeezed pore waters are indicated by plus-signs, data from pore waters obtained by the gel technique by diamonds, (e) organic carbon, (f) solid phase Mn, (g) solid phase Fe and (h) redox potential in core UM26. Solid phase Mn and Fe data are normalised to Al and multiplied by the average Al content to minimise the dilution effect by $CaCO_3$ (indicated by an asterisk). The sapropel (> 2% organic carbon) is indicated by the shaded area.

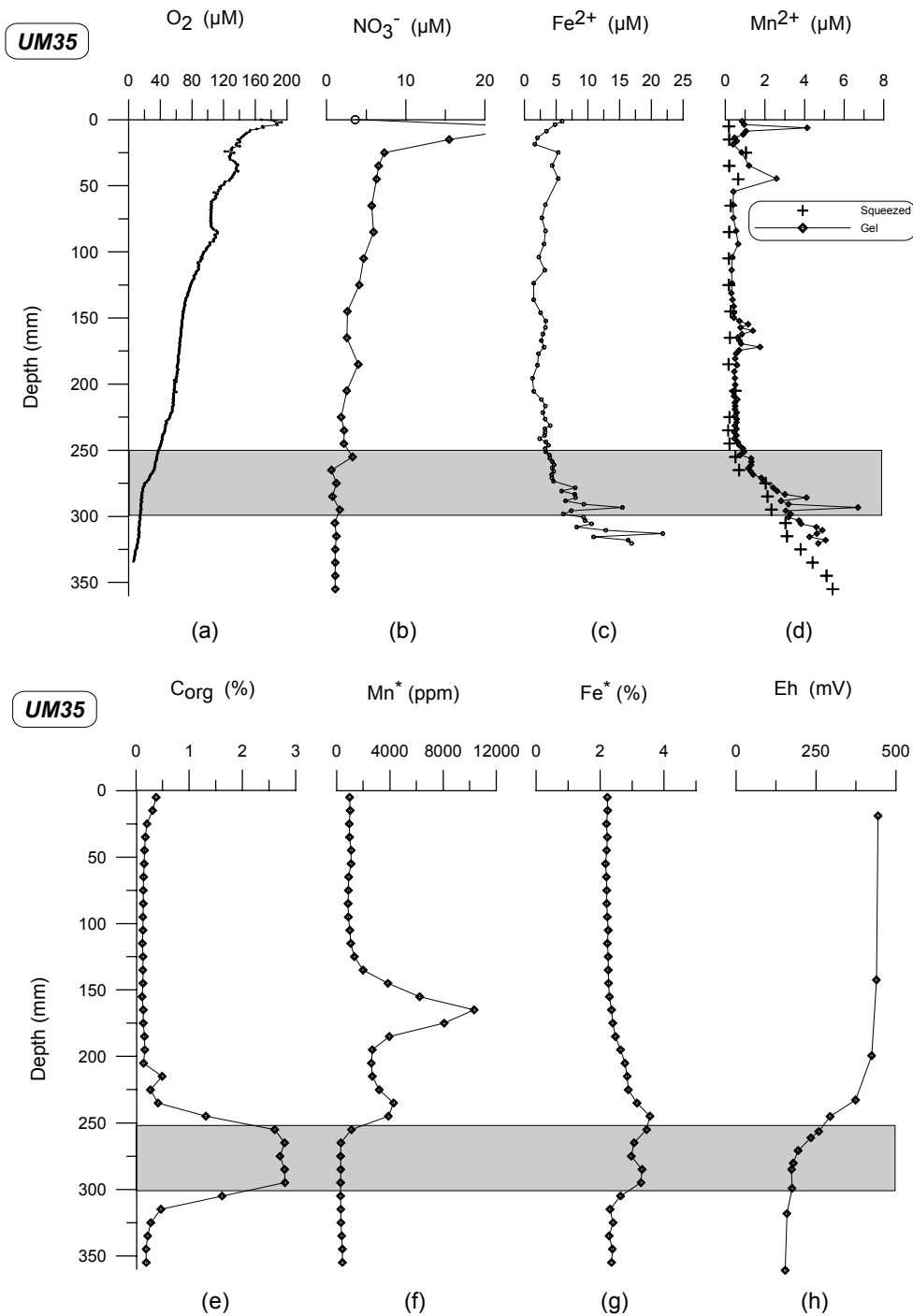


Figure 4.5 Concentration versus depth profiles of (a) pore water O_2 , (b) pore water NO_3^- , (c) porewater Fe, (d) pore water Mn, data from squeezed pore waters are indicated by plus-signs, data from pore waters obtained by the gel technique by diamonds, (e) organic carbon, (f) solid phase Mn, (g) solid phase Fe and (h) redox potential in core UM35. Solid phase Mn and Fe data are normalised to Al and multiplied by the average Al content to minimise the dilution effect by $CaCO_3$ (indicated by an asterisk). The sapropel (> 2% organic carbon) is indicated by the shaded area.

4.3.2 The upper Mn peak

Having demonstrated that the lower Mn peak is actively forming, the possible mechanisms for formation of the upper Mn peak will now be considered. Four possible explanations can be given for the formation of the upper peak.

4.3.2.1 *Hydrothermal origin*

Hydrothermal Mn-rich layers or crusts have been described for localities associated with mid-ocean ridges and island arcs (e.g. Hoffert et al., 1978; Moorby et al., 1984) and in the eastern Mediterranean (Varnavas et al., 1988; Cita et al., 1989). Since hydrothermal activity is a local phenomenon, a local occurrence of hydrothermally-formed Mn-rich layers is expected. However, the double Mn-peak feature has now been observed in many cores covering a large area in the eastern Mediterranean (Pruysers et al., 1993; Higgs et al., 1994; Thomson et al., 1995; De Lange et al., unpublished results; this study) and hydrothermal formation of the upper Mn peak therefore seems unlikely.

4.3.2.2 *Diagenetic formation by a downwards moving oxidation front*

We have demonstrated that the Fe and lower Mn peaks are presently being formed by this process. If the upper Mn peak was diagenetically formed, a solid phase Fe peak would be expected close to the same depth. However, no Fe enrichments are found at the level of the upper Mn peak (Figures 4.3f, 4.4g, 4.5g) which points to a non-diagenetic formation. Furthermore, if the upper Mn peak had a diagenetic origin, then the initial downward movement of the oxidation front must have been slow to have allowed the build up of peaks that are sometimes even larger than those that are actively forming (Figures 4.3e, 4.4f, 4.5f). This contrasts with the concept of a progressive downwards moving oxidation front Wilson et al. (1986): an increasing diffusion distance for oxygen causes a slower downward movement of the front. Therefore, the upper Mn peak in the sediments used in this study is not formed by diagenetic processes.

4.3.2.3 *Hydrogenetic origin (primary)*

Eastern Mediterranean bottom water has been interpreted to have been completely anoxic during periods of sapropel formation (e.g. Sigl et al., 1978; Anastasakis and Stanley, 1986). Most probably, a combination of increased productivity (and therefore an increased oxygen demand) and a stratified water column (no more new formation of oxygen-rich deep water) are most probably responsible for the anoxic conditions. Under such conditions dissolved Mn^{2+} is not immobilised in the sediments but escapes into the water column (Mangini et al., 1991). Upon re-oxygenation, dissolved Mn^{2+} is rapidly precipitated, forming a sharp Mn-oxyhydroxide peak in the sediment. Subsequent bioturbation causes broadening of the initially sharp peak. This mechanism would explain the occurrence of a Mn peak over large parts of the eastern basin if re-oxygenation was a basin-wide process.

4.3.2.4 *Fixation of surficial Mn*

If bottom waters were not completely anoxic during sapropel formation but rather contained some residual oxygen, then dissolved Mn would precipitate as the oxyhydroxide in a restricted surficial layer (e.g. Mucci and Edenborn, 1992). Continuous dissolution of Mn-oxyhydroxides occurs at the base of this Mn-rich layer and precipitation of Mn^{2+} takes place at the top. This process causes the Mn-rich zone to be maintained at the sediment surface. Upon re-establishing a higher (i.e. 'normal') oxygen concentration if, for example, there is a decrease in the organic carbon rain rate, the Mn-rich layer will be fixed in its

position and will not change depth. In such a scenario the oxygen concentration in the bottom waters is mainly determined by productivity. In this concept no changes in rates of bottom water formation are needed during or after the deposition of the sapropel. This mechanism provides a plausible explanation for the formation of the upper Mn peak, and will hereafter referred to as the fixation mechanism.

The mechanism for re-oxygenation of the deep eastern Mediterranean waters is still unsure. According to the stagnation theory, major hydrographic changes take place, one of them being the new formation of deep oxygen-rich water. Decreasing productivity causes a lower oxygen demand in the deeper parts of the water column, which may help build up the oxygen concentration. Most probably, both processes take place simultaneously, but which one is the most important is yet unknown.

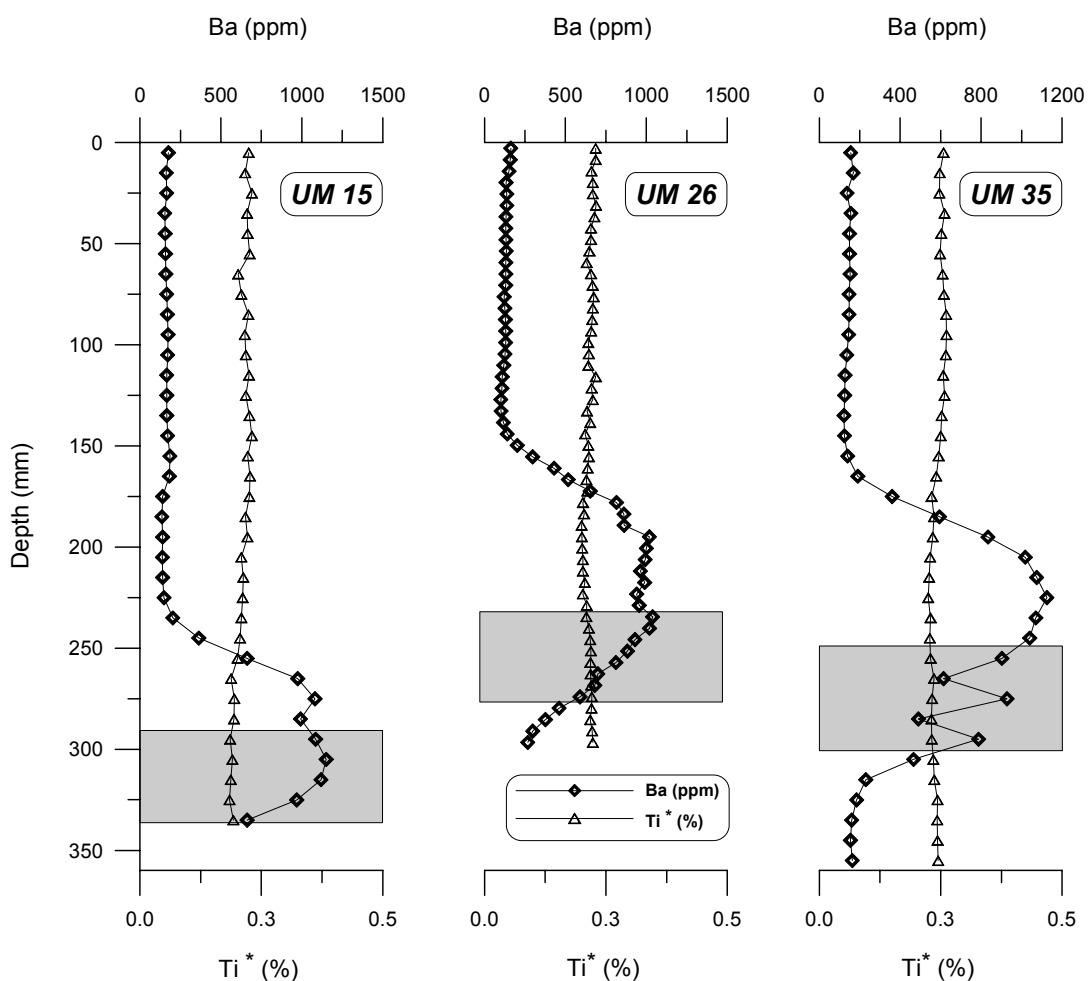


Figure 4.6 Concentration vs. depth profiles of Ba (diamonds) and Ti (triangles) in UM15, UM26, and UM35. Solid phase Ti data are normalised to Al and multiplied by the average Al content to minimise the dilution effect by CaCO_3 .

An important indication of primary hydrogenetic formation or formation by the fixation mechanism of the upper Mn peak, is that the sediments that host these peaks at different locations, have a similar age, which points to a basin wide event. Radiocarbon dating of pelagic foraminifera (Thomson et al., 1995), as well as model calculations (Higgs et al., 1994) indicates that the upper Mn peak is hosted by sediments with a ^{14}C age of

5.2 kyr. Simplified calculations using our data (taking 9.0 kyr as the ^{14}C age for the S1 bases and a constant accumulation rate) give similar results. Re-oxygenation of the oxygen-depleted deep water formed during sapropel formation could have caused Mn precipitation or fixation over the entire eastern basin. This re-oxygenation event marks the end of sapropel formation. In this interpretation the interval between the upper Mn peak and the lower Mn peak originally was part of the sapropel unit, which was oxidised by a downwards moving oxidation front after re-ventilation. This explains the wide range of radiocarbon ages reported for the top of S1 now observed. Radiocarbon dating of the sapropel at different locations gave similar ages of 8.6 kyr for the base while the top has been variously dated between 6 and 7.6 kyr (Vergnaud Grazzini et al., 1986; Fontugne et al., 1992; Troelstra et al., 1991; these ages are corrected by -400 yr for the reservoir effect, the ages given by Higgs et al. (1994) and Thomson et al. (1995) are not corrected). If the present interpretation is correct, then the radiocarbon age of the visible sapropel top depends on the sediment accumulation rate at the site and the amount of organic material oxidised. The presently-observed sapropel is always expected to be thinner than the unit initially deposited.

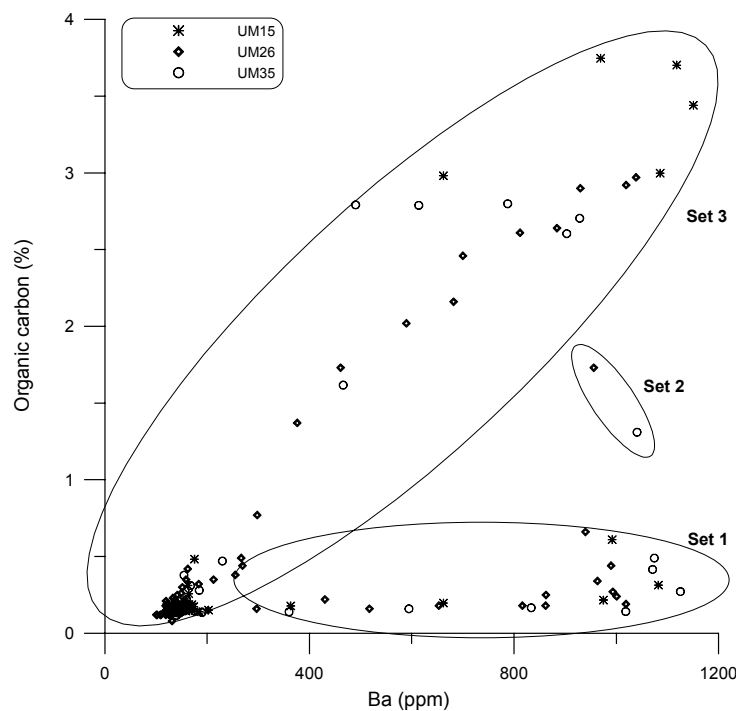


Figure 4.7 Barium vs. organic carbon plot of all data from cores UM15, UM26, and UM35. Three sets of data points can be distinguished: set 1 contains the samples which are located between the two solid phase Mn peaks; set 2 contains only two samples from the very top of the sapropel and are mixtures of sapropel and non-sapropel sediments; set 3 contains all other samples, in and below the sapropel, and above the upper Mn peak.

Further evidence consistent with oxidation of (the upper part of) the S1 sapropel is provided by Ba profiles. A good correlation between organic carbon and Ba is often observed both in organic-rich sediments (Calvert and Fontugne, 1988; Klinkhammer and Lambert, 1989) and sediment trap data (Dymond et al., 1992), so that Ba (present as biogenic barite) can be used as a palaeoproductivity proxy (De Lange et al., 1994; Francois

et al., 1995). Thomson et al. (1995) noted that Ba exhibited a quasi-Gaussian shape in three high resolution profiles through S1, and suggested that Ba might now be the best indicator of the original organic carbon signal in S1. Similar profiles were found by Pruyssers et al. (1991) and now in this study (Figure 4.6), covering a wide area of the eastern Mediterranean. An increase in Ba above detrital values is observed, starting at the base of the sapropel and a return to detrital values at the depth of the upper Mn peak. The Al-normalised Ti profiles (Figure 4.6) show near constant values over the entire interval which indicates that the higher Ba content of the sediment is not caused by an increased terrestrial input.

Our profiles give no indication for diagenetic mobilisation of Ba such as found by Van Os et al. (1991), since the increase and decrease are gradual and no sharp Ba peaks are found at the sapropel boundaries. Furthermore, it was shown by Thomson et al. (1995) that almost all Ba in the interval with raised concentrations is in the form of barite (typically 1-3 μm crystals) and only trivial amounts are oxyhydroxide sorbed. In case of diagenetic remobilisation a significant amount of oxyhydroxide sorbed Ba would be expected. Although the formation of Fe-sulphides indicates that conditions in the sapropel have been anoxic, Passier et al. (1996) showed that the $\delta^{34}\text{S}$ signal remains constant over the entire sapropel, indicating an open system. This means that the pore water sulphate concentration did not reach the low concentrations necessary for barite dissolution. A possible exception is the interval between 260 and 280 mm in core UM35 where two minor negative Ba spikes are found. The continuous supply of sulphate from the bottom water to the pore water and subsequent reduction leads to the high sulphur concentrations in the sapropel, mainly in the form of Fe-sulphides (Passier et al., 1996). The high sulphide concentrations are not necessarily indicative for barite dissolution, since the amount of barite related sulphate is much smaller than the total amount of sulphur found in the sapropels.

The distance between the top of the visible sapropel and the upper level at which the Ba content returns to detrital values is the distance over which oxidation of the original sapropel unit has taken place. The end of sapropel formation is marked by precipitation or fixation of a Mn peak and a simultaneous return of the Ba concentration to background levels.

For the three UM box cores, the Ba versus organic carbon data plot in three distinct fields (Figure 4.7). Set 1, with high Ba and low C_{org} values, contains only the data from the interval between the two solid phase Mn-peaks. The two data points in set 2 are located at the very top of the visible sapropel in UM26 and UM35, and are probably the result of mixing of sapropel and non-sapropel sediment during sampling by extrusion at fixed intervals. Organic carbon shows a clear correlation with barium content for the data in set 3, which contains all the samples in and below the sapropel and the samples above the upper Mn peak. The relationship in set 3 can be described by a second order polynomial function:

$$C_{\text{org}} = -2.04 \cdot 10^{-6} * [\text{Ba}]^2 + 5.84 \cdot 10^{-3} * [\text{Ba}] - 0.623$$

with $r = 0.964$. The samples in sets 1 and 2 were not included in this regression.

The $C_{\text{org}} : \text{Ba}$ ratio in the set 3 samples is 36 : 1, while Dymond et al. (1992) found a ratio of 25 : 1 in Atlantic, equatorial Pacific and California Current samples. The slightly

higher ratio in eastern Mediterranean sediments could point to enhanced preservation of organic carbon caused by lower oxygen concentrations or a partially anoxic water column, but could as well be explained by, for example, enhanced input of terrestrial organic carbon. Different environmental conditions (salinity, temperature, etc.) could have resulted in a different $C_{org} : Ba$ ratio of sinking particles in the eastern Mediterranean compared to the Dymond data. Sediment trap samples will be analysed in near future to compare the present fluxes to the burial fluxes that can be calculated with our sediment data.

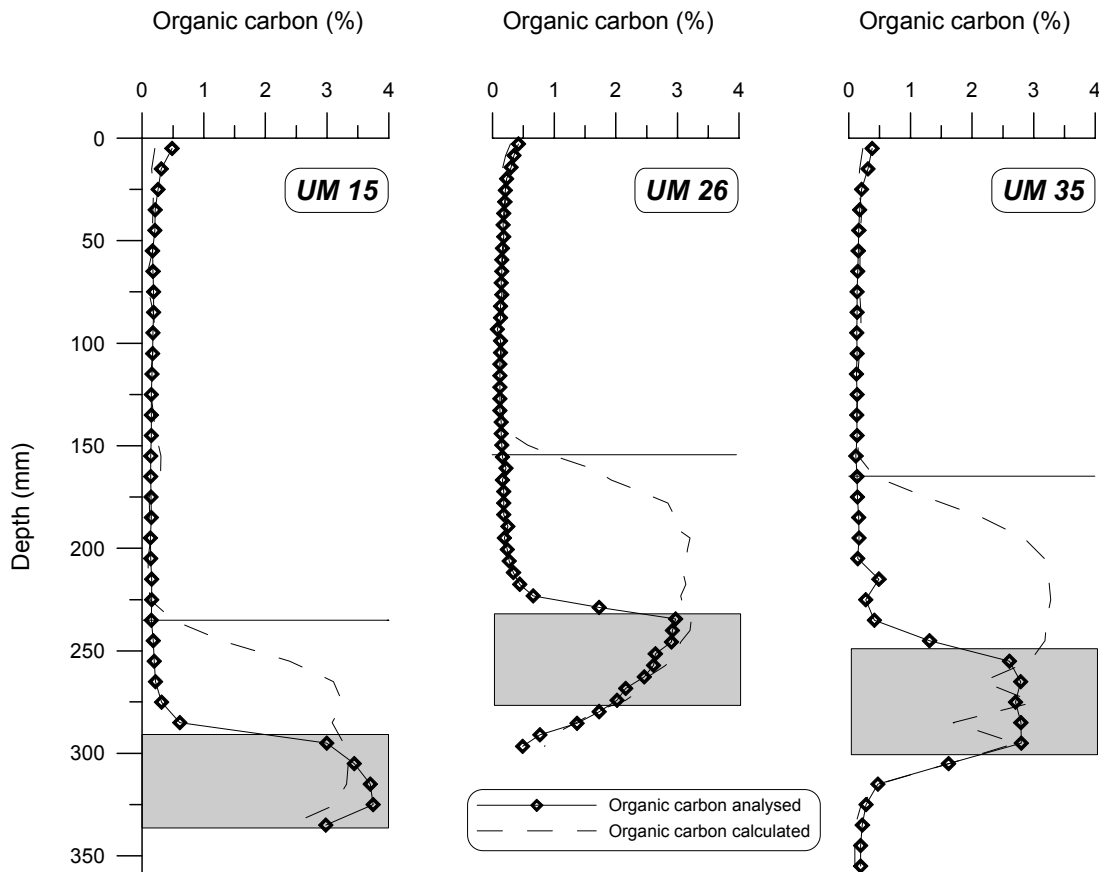


Figure 4.8 Concentration vs. depth profiles of measured (symbols) and calculated (dashed line) organic carbon using the Ba proxy method. Calculations are based on the fit obtained by the relationship for Ba and organic carbon derived from set 3 data (Figure 4.7). The dashed line indicates the initial organic carbon profile before oxidation of the upper S1 unit. The horizontal solid lines indicate the depths of the maxima of the upper Mn peaks.

Using the polynomial function obtained from the set 3 data of Figure 4.7 as a proxy, organic carbon profiles for the cores can be reconstructed from the Ba concentrations (Figure 4.8). As expected, the fit for the sapropel samples and the samples above the upper Mn peak is good with few exceptions. In the interval between the two Mn peaks, however, the calculated profile describes the initial organic carbon content of the sediment. The organic carbon concentration returns to low pelagic values at the level of the upper Mn peak maximum. Based on these profiles, it seems clear that this interval originally was part of the sapropel unit. Since the oxidation front is now located just below the lower Mn peak (at the top of the visible sapropel), the conclusion that the upper part of

the sapropel, between the two Mn peaks, has been completely oxidised, is confirmed by the calculated initial organic carbon profiles.

Following the reasoning above, the upper Mn peak is located at the top of the original S1 sapropel. Therefore, the formation of this peak by precipitation of dissolved Mn^{2+} from the bottom water or fixation of the peak in the sediment upon re-ventilation of the eastern Mediterranean deep water seems most probable. It can be concluded that the formation of sapropel S1 ceased more recently (5.2 kyr ago) than radiocarbon dating of the present S1 top indicates.

Table 4.1 Measured and calculated parameters for the different stations. Accumulation rates have been calculated assuming an age of the sapropel base of 9.0 kyr and a constant sedimentation rate since then. The accumulation rate for UM15 is estimated using the age of the upper solid phase Mn peaks of the two other cores. The dissolved Mn and Fe fluxes are calculated from their respective profiles (Figures 4.3c, 4.4c, 4.4d, 4.5c, 4.5d). The diffusion coefficients used for Mn and Fe are $88.4 \text{ cm}^2 \text{ yr}^{-1}$ and $91.5 \text{ cm}^2 \text{ yr}^{-1}$, respectively (from Li and Gregory, 1974; corrected for temperature and tortuosity). The iron flux is calculated using pore waters obtained by squeezing (UM26) or by the gel technique (UM35). The peak areas of the solid phase peaks were obtained using a dry sediment content of 0.75 g yr^{-3} , corresponding to a water content of $\sim 70\%$ of the sediment. The average S_{excess} in the sapropels is calculated by subtracting the pore water contribution from the total S value. The difference between the calculated and measured organic carbon concentrations (Figure 4.8) gives the amount of oxidised organic carbon for each core.

	UM15	UM26	UM35
Depth sapropel base (cm)	???	27.5	30.0
Depth upper Mn peak (cm)	23.5	15.5	16.5
Depth lower Mn peak (cm)	28.5	22.3	23.5
Accumulation rate (cm kyr^{-1})	~ 5	3.1	3.3
Manganese flux ($\text{moles cm}^{-2} \text{ yr}^{-1}$)			
<i>Squeezed</i>	$4.7 \cdot 10^{-8}$	$4.7 \cdot 10^{-8}$	$4.2 \cdot 10^{-8}$
<i>Gel</i>	$6.5 \cdot 10^{-8}$	$6.5 \cdot 10^{-8}$	$5.4 \cdot 10^{-8}$
Iron flux ($\text{moles cm}^{-2} \text{ yr}^{-1}$)	???	$8.9 \cdot 10^{-8}$	$1.5 \cdot 10^{-7}$
Peak area lower Mn peak (moles cm^{-2})	$1.3 \cdot 10^{-4}$	$1.4 \cdot 10^{-4}$	$2.0 \cdot 10^{-4}$
Peak area Fe peak (moles cm^{-2})	$4.0 \cdot 10^{-4}$	$8.0 \cdot 10^{-4}$	$1.1 \cdot 10^{-3}$
Average S_{excess} in sapropel (%)	2.6	1.1	1.2
Organic carbon oxidised (moles cm^{-2})	$6.5 \cdot 10^{-3}$	$1.0 \cdot 10^{-2}$	$1.2 \cdot 10^{-2}$

4.3.3 Amounts of post-depositionally oxidised organic carbon

The reconstructed organic carbon profiles allow a calculation of the amounts of oxidised organic carbon in the different cores. Furthermore, fluxes of dissolved Fe and Mn and the peak areas of the solid phase Fe and lower Mn peak can be calculated using the high-resolution data. It appears that the core with the highest accumulation rate (UM15) has the lowest amount of post-depositional organic carbon oxidised (Table 4.1). In addition, the solid phase Fe and lower Mn peaks are smallest in this core. The accumulation rate for UM15 is estimated using the age of the solid phase Mn peaks of the other two cores. The diffusion path for oxygen in this core is much longer and therefore the oxygen flux reaching the organic-rich sediment is much smaller than in the other cores. Another important factor that controls the burn down rate is the amount of reduced sulphur species,

given as average S_{excess} in Table 4.1. Average S_{excess} is calculated by subtracting the pore water contribution (sulphate) from the total S value as obtained by total dissolution of the sample. The sulphides are a result of sulphate reduction and these high concentrations can be reached because sulphate reduction takes place in an open system, i.e. there is a continuous supply of sulphate from the bottom water to the pore water (Passier et al., 1996). The concentration of sulphides in S1 is approximately twice as high in UM15 as in both other cores, so that less oxygen is available to oxidise the organic material.

Using the same reasoning as for UM15, the amount of organic carbon oxidised is expected to be higher in UM26 due to the lower accumulation rate. Values in Table 4.1, however, show that the solid phase diagenetic parameters (amount of post-depositionally oxidised organic carbon, Fe and lower Mn peaks and reduced sulphur species in the sapropel) are quite similar for both cores. A possible explanation for this is that the surficial sediments at station UM35 are more bioturbated than at station UM26 leading to an increased downward oxygen flux. Observations during the sampling of both cores seem to confirm this: the sapropel in UM35 showed clear fine bioturbation marks, while they were (almost) absent in the UM26 sapropel. Thomson et al. (1995) found bioturbation depths of max. 3 cm in their cores which is much shallower than the generally observed depths in deep-sea sediments of 6-10 cm (Cochran, 1985). This could mean that differences in the oxygen fluxes caused by different bioturbation intensities are only of minor importance.

Although the peak area of the lower Mn peak is larger in UM35, the pore water Mn flux is smaller. This may indicate that the present pore water fluxes are not representative of the fluxes since the end of sapropel formation. Calculating the age which would be needed to build up the Mn peaks using the present fluxes gives results of 2-4 kyr, a (much) shorter period than would be expected if formation started immediately after sapropel deposition. In contrast, the present Fe fluxes are too low to have built up the solid phase peak in 5.2 kyr, using the observed present fluxes, 7-9 kyr would be needed. Part of this contradiction originates from the mobilisation of Mn^{2+} through the reduction of MnO_2 by Fe^{2+} . The contrasting values for the solid phase parameters on the one hand and the pore water fluxes on the other, imply that pore water fluxes must have changed during the post-depositional period.

Calculations, as listed in Table 4.1 and discussed above, show that post-depositional oxidation of organic carbon, and therefore the penetration depth of the oxidation front, seems to be mainly controlled by the sediment accumulation rate. The depth of bioturbation in the sediment, which is very low compared to deep-sea sediments, plays a minor role, while the other parameters (dissolved Fe and Mn fluxes and reduced sulphur species in the sapropel) appear to be even less important.

4.4 Conclusions

Pore water profiles in combination with solid phase analyses have shown that the active oxidation front is located at the level of the lower Mn peak, immediately above the present-day S1 sapropel top. There is no Mn recycling at present associated with the upper Mn peak. Oxygen and nitrate fall to their background concentrations at this depth, pore water Mn and Fe increase below the lower Mn peak, and the peak marks an Eh transition from oxic conditions above to post-oxic below the front. Furthermore, the I and Se peaks at the top of the S1 sapropel and just below the lower Mn peak support this conclusion.

It is shown that the Ba-organic carbon relationship can be used to estimate the initial organic carbon profiles. The calculated organic carbon profiles indicate that the original sapropel unit was bounded by the upper Mn peak. This implies that the interval between the two manganese peaks was part of the initial S1 sapropel, but is now completely oxidised. The end of the formation of sapropel S1 is situated in more recent sediments (approximately 5.2 kyr old) than is conventionally accepted from radiocarbon dating of the visible top of S1. A basinwide event of bottom water re-ventilation and subsequent precipitation of dissolved Mn, or fixation of the solid phase Mn peak, marks the end of sapropel formation. The amount of post-depositional oxidised organic carbon and the penetration depth of the oxidation front seems to be mainly controlled by the accumulation rate and, less important, the bioturbation depth.

Acknowledgements. - We thank the crew and scientific parties of the 'Marion Dufresne' 1991 and 'Urania' 1994 cruises. H. de Waard, G. Nobbe, D. van der Meent, P. Anten, N.C. Higgs and I.W. Croudace are thanked for analytical assistance. We acknowledge the help of W. Davison for providing facilities during testing of the gel probe technique. We thank C.H. van der Weijden and J.J. Middelburg for critically reading the manuscript. Reviews by Dr. A. Mangini, Dr. T. Shaw and one anonymous reviewers and editorial work by Dr. T.F. Pedersen greatly improved the original version. This work was supported by the European Union Marine Science and Technology programme, contract numbers 900022C (MARFLUX) and MAS2-CT93-0051 (PALAEOFLUX). Part of this work was funded by UK-NERC grant GR9/1320. NSG paper no. 960408.

Chapter 5

Geochemical and paleomagnetic evidence for the occurrence of “missing” sapropels in eastern Mediterranean sediments¹

Abstract - The cyclic occurrence of sapropels appears to be associated with maxima in the 65°N summer insolation target curve. Studies of the most recent sapropel have revealed extensive oxidation of organic matter or even the complete removal of this unit. Geochemical and magnetic signals allow for the detection of such a “missing” sapropel. In older sediments, these signals are altered by ongoing diagenetic processes. An important parameter to reveal missing sapropels is Ba. Elevated concentrations of Ba are always found in visible sapropels, and even after oxidation of part of the sapropel, the initial Ba profile remains visible. We use this tool to trace down missing sapropels in KC01B, a 37-m Kullenberg core from the Calabrian Ridge, eastern Mediterranean. At least 8 of 11 sampled intervals around insolation maxima contain evidence of a completely oxidized sapropel: Ba, trace metal distributions, and magnetic parameters are similar to those observed around visible sapropels.

5.1 Introduction

Eastern Mediterranean sediments are characterized by an alternation of organic-poor hemipelagic, (light) brown sediments and organic-rich (> 2% organic carbon), dark olive-green sapropels. Sapropels are not only found in sediments below the present-day sea floor but also in uplifted marine sections on-land which date back to the Miocene (e.g. Hilgen, 1991; Hilgen et al., 1993, 1995; Lourens, 1994; Lourens et al., 1996; Van Os et al., 1994; Krijgsman, 1995). The cyclic occurrence of sapropels appears to be associated with climatic changes. All versions of the orbital hypothesis of climatic change predict that the obliquity of the Earth's axis and the precession of the equinoxes are the underlying controlling variables that influence climate through their impact on planetary insolation (Berger and Loutre, 1992). Initially, the occurrence of sapropels was inferred to be related to minima in the precession index (Rossignol-Strick, 1983, 1985; Prell and Kutzbach, 1987; Hilgen, 1991). Lourens et al. (1996) used the 65°N summer insolation target curve, calculated from the astronomical solution La90 (Laskar, 1990; Laskar et al., 1993) with present-day values for the dynamical ellipticity of the Earth and tidal dissipation by the Sun and Moon. A 3 kyr time lag between maxima in summer insolation and sapropel midpoints is introduced for the construction of climatic proxy time series. This results in the best fit with the geological record.

Sapropels are not found at each maximum in the insolation target curve. The absence may be caused by climatic conditions during maxima that were of different intensities which therefore did not always lead to sapropel formation. Alternatively, it is

¹ This paper has been published as: P.J.M. van Santvoort, G.J. de Lange, C.G. Langereis, M.J. Dekkers and M.Paterne, 1997, *Paleoceanography*, 12, 773 – 786. Copyright 1997 American Geophysical Union. Reproduced by permission of American Geophysical Union.

possible that a sapropel was deposited initially but has subsequently disappeared. Studies of the most recent sapropel have shown that extensive oxidation of organic material resulted in thinning (De Lange et al., 1989; Pruyssers et al., 1993; Van Santvoort et al., 1996²) or even complete removal of this sapropel unit (Higgs et al., 1994; Thomson et al., 1995). Such “missing” sapropels are most readily detected by studying geochemical parameters like Ba and other redox-sensitive elements like Fe and Mn.

Postdepositional changes in the sediment also cause the mobilization and precipitation of Fe-minerals and influences therefore the magnetic parameters in the sediment (e.g. Van Hoof et al., 1989; Verosub and Roberts, 1995). Mineral magnetic parameters, including intensity anhysteretic remanent magnetization (ARM), natural remanent magnetization (NRM), and initial magnetic susceptibility (χ_{in}), display a distinct signature with respect to sapropels (Dekkers et al., 1994; Langereis et al., 1997). Consequently, these parameters can be used as indicators of missing sapropels, even if sapropelic lithology is no longer visible.

In this paper, we present the results of a study of sediments from a 37-m eastern Mediterranean Kullenberg core (KC01B) with a maximum age of 1.1 Myr. On the basis of results from samples taken at 10-cm intervals (Dekkers et al., 1994; Langereis et al., 1997), eleven intervals that coincide with maxima in the insolation target curve have been sampled in detail. The diagenetic features around the most recent and an older sapropel are discussed, and a combination of geochemical and magnetic parameters has been used to trace missing sapropels in the sediments of core KC01B.

5.2 Material and methods

5.2.1 Sapropel Nomenclature

Under the conventional sapropel nomenclature system, sapropels are continuously numbered from S1 in the Holocene, continuing with increasing S numbers down the sequence (e.g. Ryan, 1972). This method gives problems in case of discovery of new sapropels between already classified ones. Since it was noticed that sapropels were correlated to peaks in the precession index, Hilgen (1991) proposed a numbering scheme based on naming sapropels after their correlative peak of the precession index beginning from the Holocene. Lourens et al. (1996) demonstrated that it was better to use the insolation curve rather than precession index for the correlation of sapropels and the climate cycle. In this paper we will follow the method of Langereis et al. (1997) who adapted the Hilgen (1991) method to the Lourens et al. (1996) findings: Maxima in the insolation curve are even-numbered, starting from the Recent, while minima are odd-numbered. Observed sapropels are denoted by an uppercase “S” and missing sapropels are denoted by a lowercase “s”. Sapropel S4, for example, becomes Si10, and a missing sapropel near maximum 14 becomes si14. When new sapropels are identified, only the lowercase “s” needs to be changed, and renumbering of existing sapropels is not necessary.

5.2.2 Sediment, Sampling, and Chronology

Kullenberg core KC01B (37 m) was recovered on the Pisano Plateau, Calabrian Ridge (Figure 5.1), during the 1991 Mast-I cruise with the R/V Marion Dufresne. Twelve sapropels are recognized, starting with Si10 (S4), and several tephra layers were also

² Van Santvoort et al. (1996) is chapter 4 of this thesis.

found. In some cases it is difficult to visually distinguish a tephra layer from a sapropel because color and texture can be similar. Initial sampling, both for geochemical and paleomagnetic purposes, took place at 10-cm intervals. On the basis of the Ba profile and the insolation target curve (Figure 5.2), 11 intervals have been sampled in more detail (0.5 to 1.5-cm resolution).

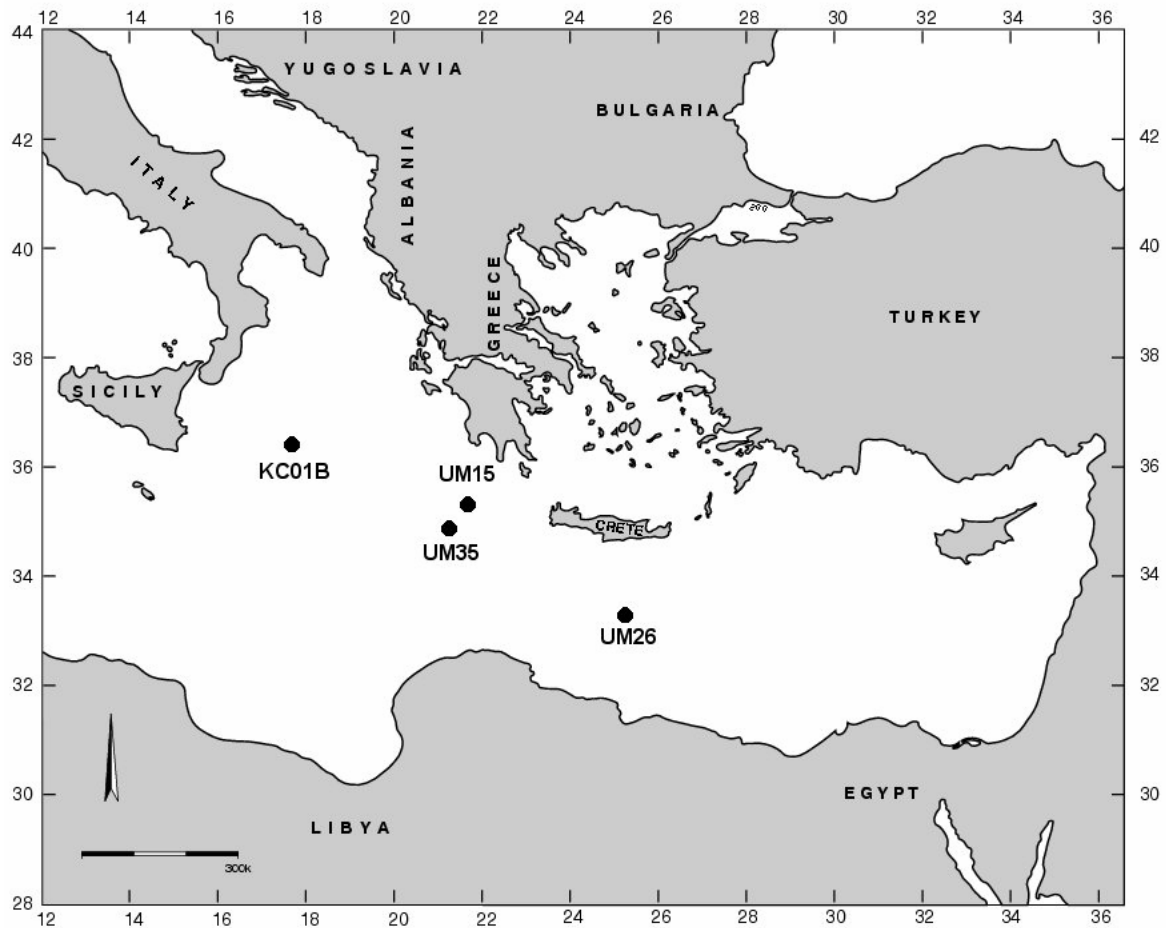


Figure 5.1 Locations of the cores used in this study. Core KC01B was taken at 36°15.2' N, 17°44.3' E, 3643 m water depth; station UM15 is at 35°17.4' N, 21°24.8' E, 3307 m; UM26 is at 33°23.6' N, 25°00.9' E, 2160 m; and UM35 is at 35°11.0' N, 21°12.5' E, 2670 m.

Similar studies were conducted on box cores UM15, UM26, and UM35 (Figure 5.1) that were collected during the 1994 Palaeoflux cruise of R/V Urania. The latter cores contain sequences that are typical for the eastern Mediterranean: oxic sediments on top, and a dark brown marker bed that is underlain by a sapropel (Si2). It should be noted that UM15 does not contain a complete sapropel sequence.

In accordance with Langereis et al. (1997), sapropels and some proposed missing sapropels are used in the correlation to the insolation curve. The oxygen isotope record was tuned to the ice sheet model of Imbrie and Imbrie (1980). The differences between the oxygen isotope curve (tuned to the ice sheet model) and the sapropel pattern (tuned to the La90 65°N summer insolation curve) are generally small, typically ranging from 0 to 5 kyr

and averaging 2 kyr. We emphasize that both results have been independently derived. A more elaborate discussion is given by Langereis et al. (1997).

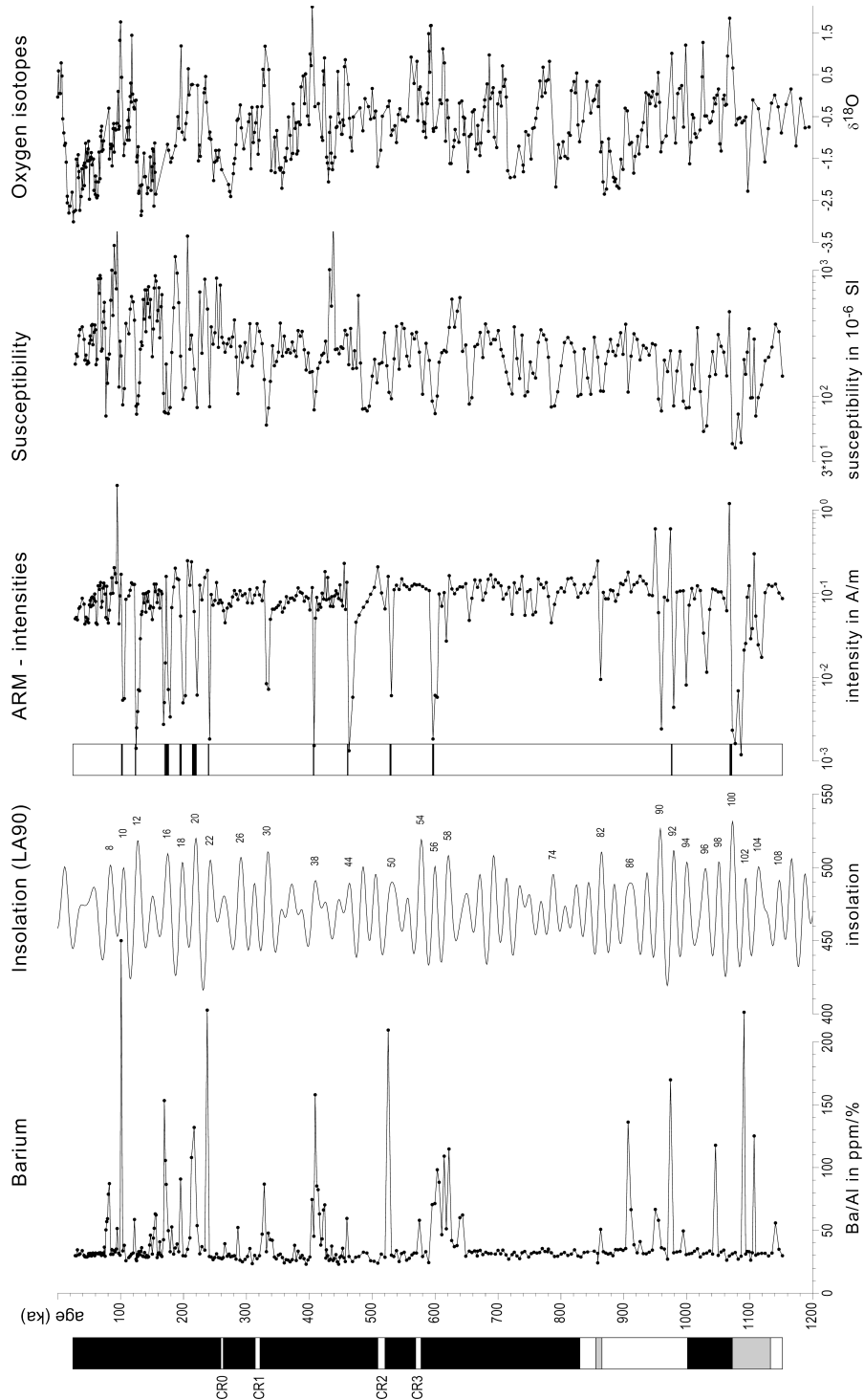


Figure 5.2 Mineral magnetic records (anhysteretic remanent magnetization (ARM) and susceptibility (χ_{in}), Ba (normalized to Al) and $\delta^{18}O$ of core KC01B compared with the insolation target curve of Laskar (1990). Visible sapropels are indicated in the stratigraphic column. No natural remanent magnetization (NRM) data are plotted because the profile is identical to the ARM plot.

5.2.3 Chemical Analyses

Samples were freeze-dried and finely ground in an agate mortar. After digestion in a mixture of hydrofluoric, nitric, and perchloric acids, final solutions were made up in 1 N HCl and were analyzed by inductively coupled plasma emission spectrometry (ICPES) on a Perkin Elmer Optima 3000. The quality of the ICPES analyses was monitored by the inclusion of laboratory and international standards. The error in the analyses was < 3% for major elements and < 7% for the trace elements. All measured concentrations, for both major and trace elements, are well above the limit of detection. Selenium was measured by hydride generation atomic absorption spectrometry (AAS) using a Perkin Elmer 3100 AAS in combination with a Perkin Elmer flow injection analyses system (FIAS) mercury/hydride chemifold and an autosampler. The analytical error is < 5% for concentrations > 3 ppb and up to 50% at the 0.1-ppb level.

Organic carbon was measured on a Fisons Instruments nitrogen carbon sulphur (NCS) NA1500 analyzer using dry combustion at 1030°C. Inorganic carbon, as carbonate, was removed before analysis by shaking the sample for 24 hours in 1 N HCl. This procedure was repeated once to ensure that all inorganic carbon had been removed. After drying at 80°C, the sample was ground in an agate mortar. International and in-house standards were used to check the accuracy of the method. Standard deviations of standards and sample duplicates were always < 1.5%.

To obtain the reducible fraction of the samples, a solution of 1 M hydroxylamine hydrochloride in 25% acetic acid was used with 1 g of powdered sediment (Chester and Hughes, 1967). The leachate was analyzed by ICPES.

Two powdered samples were analysed by X-ray diffraction (Philips PW1700) to obtain the mineralogical composition of the sediment. To correct concentrations, obtained by ICPES and AAS, for carbonate dilution, the measured concentrations were normalized by the Al concentration and were subsequently multiplied by the average Al content of the sediment. All elements reported here, except Ca, are corrected in this way.

5.2.4 Paleomagnetic Analyses

The magnetic variables used in the present study are NRM, ARM, and χ_{in} . It was not possible to use the high-resolution samples for paleomagnetic analyses due to the small amount of sample available. The presented magnetic data are the results from samples taken at 10-cm intervals, which will be compared with the high-resolution geochemical results.

An ARM was imparted by subjecting samples to an alternating field (AF) which decays from 100 mT to zero, while a bias field of 30 μ T is imposed. The ARM value is an estimate of the amount of magnetizable material present in the sample (e.g. Levi and Banerjee, 1976). In particular, fine-grained single domain magnetite has a strong ARM signal and will mainly determine the ARM value of the sample. The NRM intensity reported is that after AF demagnetization at 20 mT. At this demagnetization level, the unstable "viscous" part of the NRM has been demagnetized in these samples. Note that the NRM intensity depends not only on the concentration and type of magnetic minerals present but also on the intensity of the geomagnetic field at the time of NRM lock-in. The low-field magnetic susceptibility is the magnetic moment of a sample measured in a small magnetic field. In contrast to remanent magnetizations that are carried by ferrimagnetic or imperfect ferromagnetic minerals (e.g. ARM or NRM), paramagnetic (iron-bearing silicates like clay minerals, micas, amphiboles, and pyroxenes) and diamagnetic minerals (quartz, carbonates, feldspars) contribute to χ_{in} . NRM and ARM intensities were measured

with a vertical 2G Enterprises superconducting SQUID magnetometer or with a digital Geofizica Brno JR3 spinner magnetometer. Low-field magnetic susceptibility was measured with a Geofizica Brno KLY-2 susceptibility bridge (operating frequency 980 Hz, peak field 0.3 mT).

5.3 Results and discussion

5.3.1 Oxidation of the Most Recent Sapropel, Si2

Sapropels are geochemically characterized by high concentrations of organic carbon, Ba, and S. Barium is mainly present as barite (e.g. Thomson et al., 1995) and displays a “quasi-Gaussian” curve (Figure 5.3). This means that the Ba concentration displays a gradual increase starting at 32 cm and a gradual decrease at ending at 14 cm depth. Iron sulphides, with pyrite as the main sulphur phase, and organically bound S contribute to the high sulphur concentrations in the sapropels (Pruysers et al., 1993; Passier et al., 1996) (Figure 5.3). Reduced S-species are formed during, or briefly after, deposition of a sapropel, when anoxic conditions (i.e., sulphate reduction) prevail. In reaction with Fe-oxyhydroxides or dissolved Fe^{2+} , these can form Fe-sulphides, not only in, but also below, the sapropel (Passier et al., 1996). Note that in this paper, Fe-oxyhydroxides are a general term for Fe-oxides, Fe-hydroxides, and everything in between these two end-members.

Studies of the most recent sapropel have shown that extensive oxidation of organic material has resulted in thinning of this sapropel unit (De Lange et al., 1989; Pruyssers et al., 1993; Higgs et al., 1994; Thomson et al., 1995; Van Santvoort et al., 1996). The oxidation of the sapropel can be described by a progressive downward moving oxidation front (De Lange et al., 1989; Pruyssers et al., 1993; Thomson et al., 1993, 1995; Van Santvoort et al., 1996), that was developed by Wilson et al. (1985, 1986) to explain the formation of metal-rich layers in turbidites. Immediately after sapropel formation ceases, oxygen starts to diffuse down into the sediment. Oxygen is consumed in the oxidation process of organic material and reduced species of the solid phase, such as pyrite, as well as in oxidizing reduced Fe- and Mn-species in the pore water. Below the level where oxygen is present, decomposition of organic material takes place by reduction of nitrate and solid phase Fe- and Mn-oxyhydroxides. The latter process releases Fe^{2+} and Mn^{2+} to the pore water. After upward diffusion, these species are reprecipitated as oxyhydroxides when oxic pore waters are reencountered. Dissolved Fe precipitates at slightly lower oxygen concentrations than Mn so that the solid phase Fe peak is always located below the Mn peak (Figure 5.3). The Fe peak is found just below the transition of organic-poor to organic-rich sediment, while the Mn peak is found just above this level. When the downward flux of oxygen is larger than the upward flux of reductants, the oxidation front (the level at which oxygen becomes depleted) will move down, thus oxidizing more of the sapropel. The initially rapid downward movement of the front decelerates with time and forms Fe- and Mn-oxyhydroxide peaks of characteristic shape (e.g. Wilson et al., 1985, 1986) (Figure 5.3).

In addition to the Mn peak that is formed by the downward moving oxidation front (maximum at 223 mm in UM26), another peak is observed, a few centimeters above this diagenetic peak, at 155 mm (Figure 5.3). The upper peak is thought to mark the end of sapropel formation when the bottom water was reoxygenated (Higgs et al., 1994; Thomson et al., 1995; Van Santvoort et al., 1996). Either an upward moving Mn peak was fixed in its position or dissolved Mn precipitated from the water column. Mackensen et al. (1993)

observed a fluffy, organic-rich layer in the South Atlantic Ocean, in which organic material was readily oxidized, leading to large concentration gradients over the sediment-water interface. In this way, pore water gradients would be independent from the redox state of the bottom water, and oxygen depletion in the deep water is unnecessary. However, we consider the low-oxygen scenario to be the most likely option.

Depending on the oxygen concentration of the deep eastern Mediterranean water, the organic carbon flux to the seafloor, the sediment accumulation rate, and the bioturbation depth, some part of a sapropel will usually be oxidized. When the diffusion path of oxygen becomes too long (e.g. due to a high sedimentation rate) or when the organic carbon flux increases, the oxidation front stops moving downward and the remaining part of the sapropel will be preserved. In extreme cases, the entire sapropel can be oxidized, leaving no visible traces of the sapropel (Higgs et al., 1994; Thomson et al., 1995). Only the use of geochemical and magnetic parameters can reveal the former presence of such a sapropel.

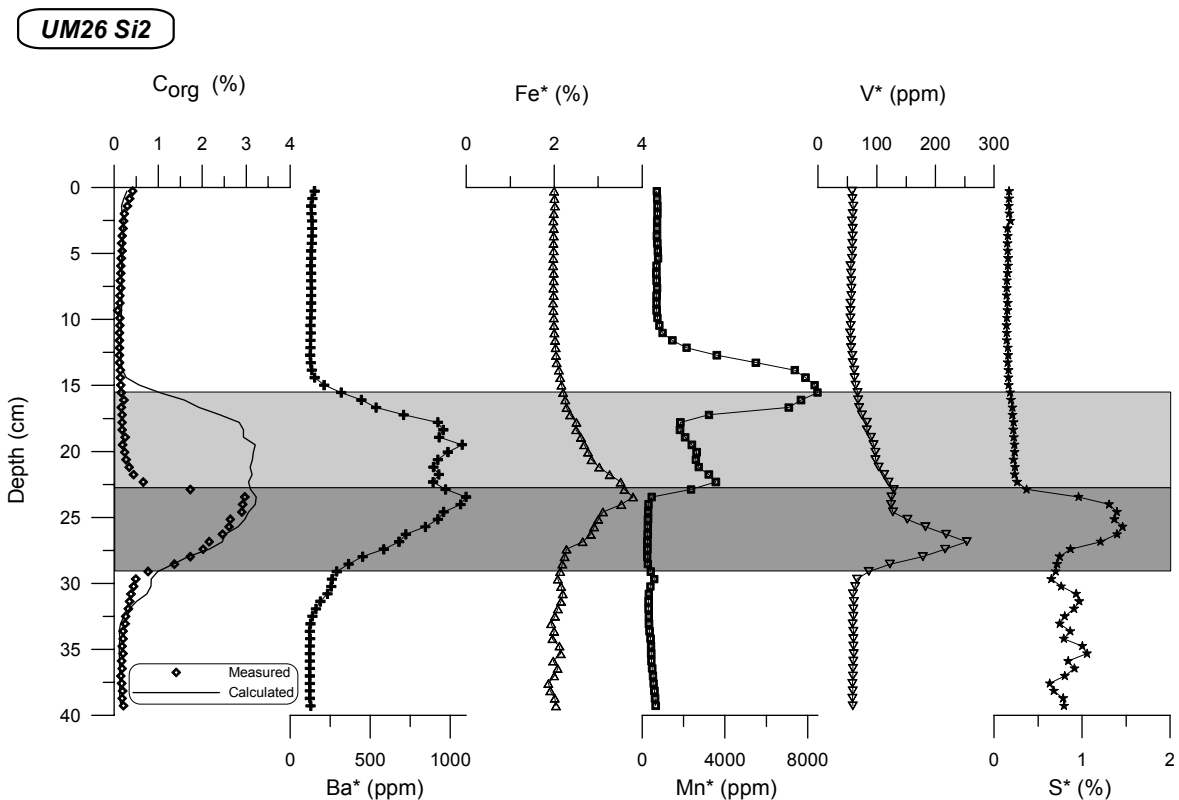


Figure 5.3 Concentration vs. depth profiles of measured (diamonds) and calculated (solid line) organic carbon, and measured Ba, Fe, Mn, V, and S for Si2 from core UM26. Solid phase Ba, Fe, Mn, and V are normalized to Al and multiplied by the average Al content to minimize the dilution effect by CaCO₃ (indicated by an asterisk). The part of the sapropel that is visible at present is indicated by the darker shaded area. The oxidized part of the initial sapropel, obtained from the calculated organic carbon values, is indicated by the lighter shaded area.

Sediments with a high organic carbon content, including sapropels, generally are reported to contain higher concentrations of trace metals relative to the surrounding sediments (Calvert, 1983; Sutherland et al., 1984; Calvert et al., 1985; Ten Haven et al., 1988; Pruyers et al., 1991). Most of these elements are associated with the organic

material, but Fe-oxyhydroxides may also contain considerable amounts of trace metals. On oxidation of the organic-rich layers, some metals, including Ni, Zn, and As, become associated with Fe- and Mn-oxyhydroxides, either by adsorption or by coprecipitation (e.g. Hem et al., 1989). Therefore, a positive correlation between the Fe- and Mn-content on one side and trace metal concentrations on the other is often found in the oxic sediments above sapropels.

Se, Cu, V, Sb, and Zn are continuously remobilized in the oxic environment and maintain concentration maxima in the vicinity of the oxidation front (Thomson et al., 1993). Because V has been analyzed in all intervals, this element, which represents the group mentioned above, will be discussed in more detail. Under oxic conditions, V behaves in a way that is similar to Fe, and is adsorbed as H_2VO_4^- (Trefry and Metz, 1989). A second, often larger V peak is generally observed within the sapropel and consists of a reduced, relatively immobile species (Figure 5.3). The formation of this peak could be related to the oxyanion that diffused from the seawater into the anoxic pore water. Reduction results in the formation of a reduced V-species that is immobilized by a yet unknown mechanism (Emerson and Husted, 1991).

A good correlation between organic carbon and Ba is often observed in organic rich sediments (Calvert 1983; Calvert and Fontugne, 1988; Klinkhammer and Lambert, 1989) and in sediment trap data (Dymond et al., 1992). This led to the assumption that Ba, which is present as biogenic barite, can be used as a paleoproductivity proxy (Dymond et al., 1992; De Lange et al., 1994; Thomson et al., 1995). However, barite may dissolve under sulphate-reducing conditions if the pore water becomes SO_4^{2-} depleted (e.g. Brumsack and Gieskes, 1983; Van Os et al., 1991; Gingele and Dahmke, 1994). In that case, dissolved Ba diffuses away and reprecipitates on encountering pore waters with sufficiently high sulphate concentrations. In sediments, this remobilization and subsequent precipitation is reflected by the presence of additional, mostly sharp Ba peaks (e.g. Van Os et al., 1991). The profile of Si2 (Figure 5.3) does not contain any indication of extensive remobilization of Ba. Because oxidation of organic matter does not influence the barite content of the sediment, the Ba profile reflects the initial organic carbon profile. The expected Ba-organic carbon relationship was used by Van Santvoort et al. (1996) to reconstruct the initial organic carbon profile for the oxidized part of the sapropel in the three box cores (Figure 5.3).

The high S-concentrations in sapropels can be explained by two mechanisms. First, organic-rich sediments contain more pore water and therefore more pore water sulphate. Second, owing to the anoxic conditions in the sapropel during and after deposition, the available sulphate is used in the degradation of organic material. In reaction with Fe-oxyhydroxides or, more likely, dissolved Fe^{2+} , the reduced S-species can form Fe-sulphides. When anoxia prevail long enough, more reduced S-species are produced than can be removed by the reactive Fe. In that case a downward diffusion of reduced S-species is observed, and precipitation of Fe-sulphides below the sapropel takes place (Passier et al., 1996). This leads to an S profile that shows high concentrations not only in, but also below, the sapropel (Figure 5.3).

Reduction of Fe-oxyhydroxides in and below the sapropel, followed by diffusion and re-precipitation at the oxidation front, changes the magnetic signal of the sediments. The ARM and NRM intensities dominantly are controlled by the amount of magnetic minerals in the sediment and, in particular, by fine-grained single domain magnetite. It is obvious that these signals decrease at levels where Fe-oxyhydroxides have been dissolved, while much higher values may be found at depths of (re-)precipitation. Recent research

(Roberts et al., 1996) revealed higher concentrations of magnetic minerals (probably a magnetic Fe-sulphide) in sapropels. It is yet unknown which mineral is formed when the sapropel is oxidized and how this mineral contributes to the magnetic values of the sediment. Paramagnetic and ferrimagnetic minerals contribute to χ_{in} . Therefore, the differences in χ_{in} are less distinct than for ARM and NRM. Oxidation of a sapropel may lead to high values for especially ARM in the interval that initially contained the sapropel and may therefore be a good indicator of missing sapropels.

In summary, the profiles in the interval of Si2 are “ideally” developed. This means that the oxidation process is taking place at this moment, resulting in the formation of trace metal peaks and in the removal of organic material and reduced Fe-compounds. The observations in this interval are not influenced or overprinted by other diagenetic processes, and therefore we will use these profiles as a reference in the next sections where we will discuss older intervals.

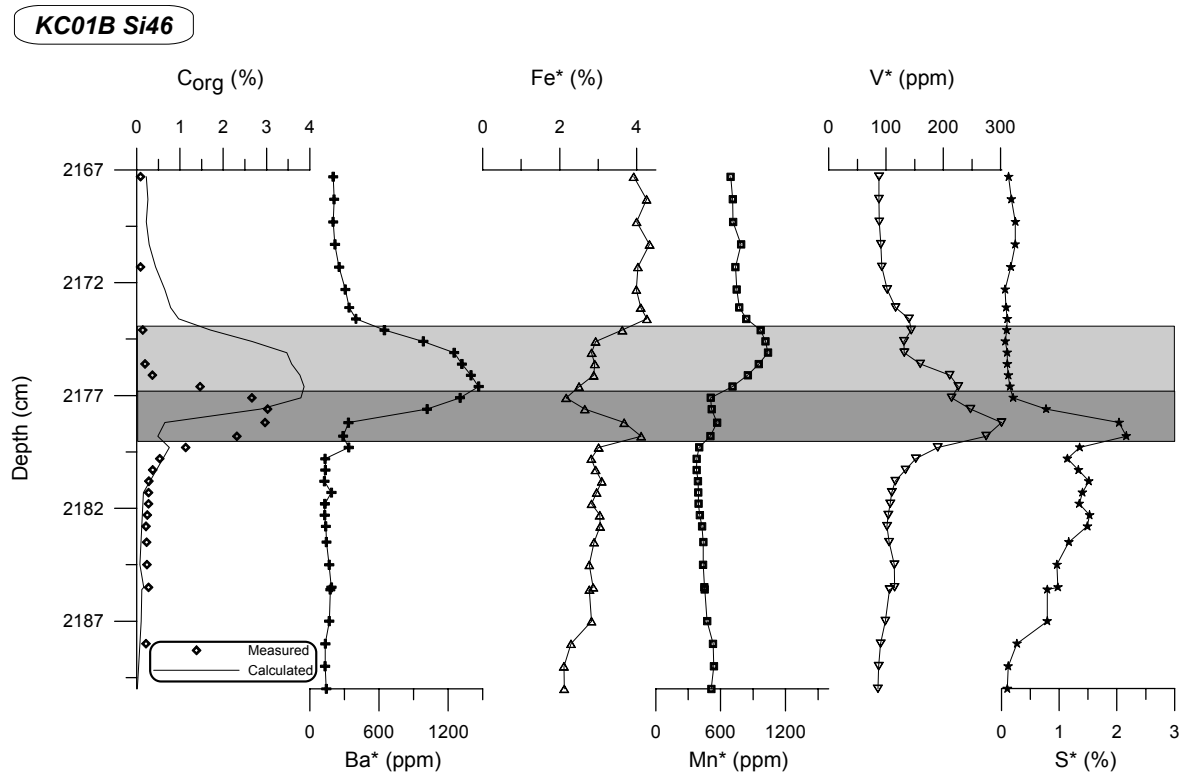


Figure 5.4 Concentration vs. depth profiles of measured (diamonds) and calculated (solid line) organic carbon, and measured Ba, Fe, Mn, V, and S for Si46 from core KC01B. Concentration normalization and shadings are similar to those for Figure 5.3.

5.3.2 Oxidation of an Older Sapropel, Si46

After the oxygen supply to a sapropel is cut off, for example, by an increased organic carbon flux, nitrate and Fe- and Mn-oxyhydroxides act as electron acceptors in the decomposition of organic matter. In addition, under more reducing conditions, pore water sulphate is reduced, which may lead to dissolution of barite, i.e., to mobilization of Ba. As a consequence of these postoxic and anoxic early diagenetic processes, the profiles of redox-sensitive elements may change significantly (Figure 5.4).

The Ba profile of sapropel si46 is similar to that around Si2: The curve has a semi-Gaussian shape. Using the same Ba-organic carbon relationship as in the calculations for the upper sapropel (Van Santvoort et al., 1996), the initial organic carbon profile is calculated. Part of Si46 must have been oxidized in a way similar to that for Si2, namely, the interval from 2174 to 2177 cm (the light shaded area in Figure 5.4): In this interval, high Ba concentrations are found, indicating that the initial organic carbon content of the sediment must have been higher. Furthermore, in the lowermost part of the profile, the measured organic carbon concentrations increase a few centimeters below the level where the initial concentrations (calculated from Ba) start to increase. This points to mobilization of Ba in the lowermost part of the sapropel. The strong sulphate-reducing conditions that at some time must have occurred in the lower part of the sapropel are reflected by the high sulphide (up to 2.5%) contents in that interval (Figure 5.4).

The downward movement of the oxidation front causes the formation of Fe- and Mn-layers with maxima just below and just above the visible sapropel top, respectively. Near the base of Si46, the Fe-profile in Figure 5.4 has a maximum that is thought to consist of reduced Fe-minerals like pyrite and Fe-monosulphides. The oxidation front has caused the removal of these minerals in the oxidized upper part of the sapropel, as reflected by the S profile (Figure 5.4). In Si2, solid phase Fe-concentrations are enhanced in the oxidized part of the sapropel and reach a maximum at the oxidation front near the present top of the sapropel (Figure 5.3). In the same interval in Si46, Fe has been removed. A similar shift in depth is observed in the Mn profile: A maximum is expected just above the visible sapropel top (oxidation front), but for Si46, the highest Mn values are found 4 cm above the expected depth. A decrease in the oxygen flux to the sediment (for example, caused by an increased organic carbon flux) may cause an upward movement of the oxidation front. The sediments that contain the recently precipitated Fe- and Mn-oxyhydroxides become postoxic again, which results in reduction of the oxyhydroxides. The oxygen supply may also be stopped by a new period of (near) anoxia of the bottom water (or by the earlier mentioned fluffy layer), with similar results. The only difference may be that in case of a complete oxygen cutoff, the dissolved species can diffuse over larger distances.

The trace metals that are closely correlated to the Fe content of the sediment, like Zn and Ni (not shown), have similar profiles as Fe (Figure 5.4). The profile of V, which should contain high concentrations at the oxic-postoxic interface (oxidation front) and in the sapropel, demonstrates the expected enrichments (Figure 5.4). The paleomagnetic parameters show the expected signals: Low values of NRM, ARM, and χ_{in} are recorded below the sapropel where Fe-oxyhydroxides are nearly completely used during oxidation of organic matter, and higher concentrations of magnetic minerals occur above the sapropel where Fe-bearing minerals have precipitated (Figure 5.2). Sampling at 10-cm intervals was too coarse to observe the detailed effects of remobilization processes on the magnetic variables. Note that NRM data are not shown in this paper because they are identical to the ARM profile, with the difference that the NRM peaks are less distinct.

In summary, we can state that some of the initial geochemical and magnetic signals within sapropels may change or even disappear on postdepositional oxidation and subsequent postoxic conditions. The combination and sequence of geochemical and magnetic signals, however, may give an indication of the partial, or even complete, oxidation of a sapropel.

5.3.3 “Missing” Sapropels

The main criterion for sampling certain potential sapropel intervals at high resolution was the presence of high Ba concentrations in the 10-cm-resolution samples coinciding with a low organic carbon content and a peak in the insolation target curve (Figure 5.2). The organic carbon contents of samples from 11 selected intervals were all < 0.2%.

To test whether the high Ba concentrations in the intervals with no visual signs of sapropel are in the form of barite (the principal form of Ba in visible sapropels) or sorbed onto oxyhydroxides and/or carbonates (and therefore of diagenetic origin), samples were treated with a reductive acid (Chester and Hughes, 1967). In all samples, less than 2% of the Ba was removed in this way, and in most cases, less than 1% was removed. We therefore conclude that the Ba found in these intervals is mainly present in the form of barite and is likely to be of the same origin as the Ba enrichments found in visible sapropels (i.e., increased surface-water productivity). We also conclude on the basis of this evidence that these zones of Ba enrichment represent missing sapropels.

On the basis of results from these high-resolution samples, the 11 intervals can be ranked in three groups: (1) missing sapropels, (2) partially overprinted missing sapropels, and (3) completely overprinted missing sapropels.

5.3.3.1 *Missing sapropels (si26, si30, si90, and si102)*

The first group of intervals that contains inferred missing sapropels is characterized by a quasi-Gaussian shaped Ba profile (Figure 5.5). The profiles do not contain evidence of Ba remobilization, except for a minor peak that lies above the main peak in si90, which means that the redox conditions never became extremely sulphate-reducing. Therefore the Ba profiles are thought to reflect the initial Ba concentrations, and these data can be used to calculate the initial organic carbon profile from the Ba-organic carbon relationship that is observed in the UM box cores (Van Santvoort et al., 1996) (Figure 5.5). The four calculated organic carbon profiles differ considerably from each other: Maxima range from 0.8% in si26 to 4.3% in si30. According to the definition of Kidd et al. (1978), a sapropel must at least contain 2% organic carbon which would mean that si26 would not have been classified as a sapropel. In this paper, however, we will use the term “sapropel” for a distinct sediment layer, which has an organic carbon content that is significantly higher than that of the surrounding hemipelagic sediment, and which is deposited in an open marine environment and is correlated with an insolation maximum. By comparing these data with those from sapropels that are visible today (Table 5.1), it appears that thickness and calculated maximum organic carbon concentrations are similar for visible sapropels and those inferred for the missing sapropels.

Iron- and Mn-rich layers are alternative indicators for the possible paleo-occurrence of a sapropel. Manganese peaks are located above the Fe peaks in all intervals. For a completely oxidized sapropel, it is expected that both peaks would be found near the base of the former sapropel. The downward movement of the oxidation front is determined by the amount of reduced species that can be oxidized and by the oxygen flux. As soon as the oxidation front reaches sediment with low organic carbon concentrations, the front will move down faster, resulting in lower solid phase concentrations of Fe and Mn. It is clear that the maxima are located well above the inferred base of the sapropels, similar to the Fe and Mn peaks in Si46. The Mn peak is always located close to the inferred top of the initial sapropel and may therefore reflect, similar to Si2, the end of sapropel formation. Ongoing diagenesis, after oxidation of the sapropel, is clearly evident in si30 by the double Fe-peak. In the missing sapropel interval, Mn in si30 is partly incorporated in or adsorbed onto

carbonates, which results in a good correlation between Ca and Mn. Under postoxic to anoxic conditions, the maximum dissolved Mn concentration in pore water is typically limited by the precipitation of Mn carbonate (e.g. Suess, 1979; De Lange, 1986). Overgrowth of Mn-carbonates on foraminifera tests was reported by Boyle (1983) who stated that these coatings can account for a significant proportion of the Mn in reduced (deep-sea) sediments. Reaction of dissolved Fe with Mn-oxyhydroxides results in dissolved Mn and solid-phase Fe-oxyhydroxides. A considerable amount of the Mn-oxyhydroxides can thus be reduced, and Mn^{2+} may subsequently have diffused to other levels or be incorporated into carbonates.

Table 5.1 Measured and calculated parameters for the different (“missing”) sapropels.

	Maximum C_{org} concentration measured (%)	Maximum C_{org} concentration calculated (%) ^a	Thickness (cm) ^b	Total C_{org} (10^{-2} mol cm^{-3}) ^c
UM15 Si2	3.7	3.8	???	???
UM26 Si2	3.0	3.2	12.0	2.10
UM35 Si2	2.8	3.6	13.5	2.10
Si10 (S4)	2.7	4.9	15.5	1.96
Si12 (S5)	3.4	6.3	7.0	1.91
Si18 (S7)	5.9	4.9	10.1	0.45
Si22 (S9)	2.0	4.3	7.3	0.97
Si46 (S12)	3.0	8.8	8	4.08
Si92	2.3	4.1	6.8	0.59
si8	missing sapropel	0.9	???	1.35
si14	missing sapropel	1.0	???	0.86
si26	missing sapropel	0.7	5.0	0.12
si30	missing sapropel	4.4	7.0	1.33
si40	missing sapropel	1.6	???	0.73
si58	missing sapropel	2.5	???	1.23
	missing sapropel	2.2	???	1.29
si60	missing sapropel	0.6	???	0.28
si86	missing sapropel	0.8	???	0.72
si90	missing sapropel	3.5	16.0	1.49
si98	missing sapropel	2.8	???	0.67
si102	missing sapropel	2.2	5.0	0.42

^a Organic carbon is calculated using the equation derived from the $Ba-C_{org}$ relationship derived from the UM-box cores (Van Santvoort et al., 1996).

^b Thickness of the interval with calculated organic carbon values above 0.3%.

^c Total C_{org} is calculated over the interval with values above 0.3%, using a dry sediment content of 0.75 g cm^{-3} , corresponding to a water content of $\sim 70\%$ of the sediment. Note that UM15 does not contain a complete sapropel interval, and therefore no thickness and total organic carbon value can be calculated.

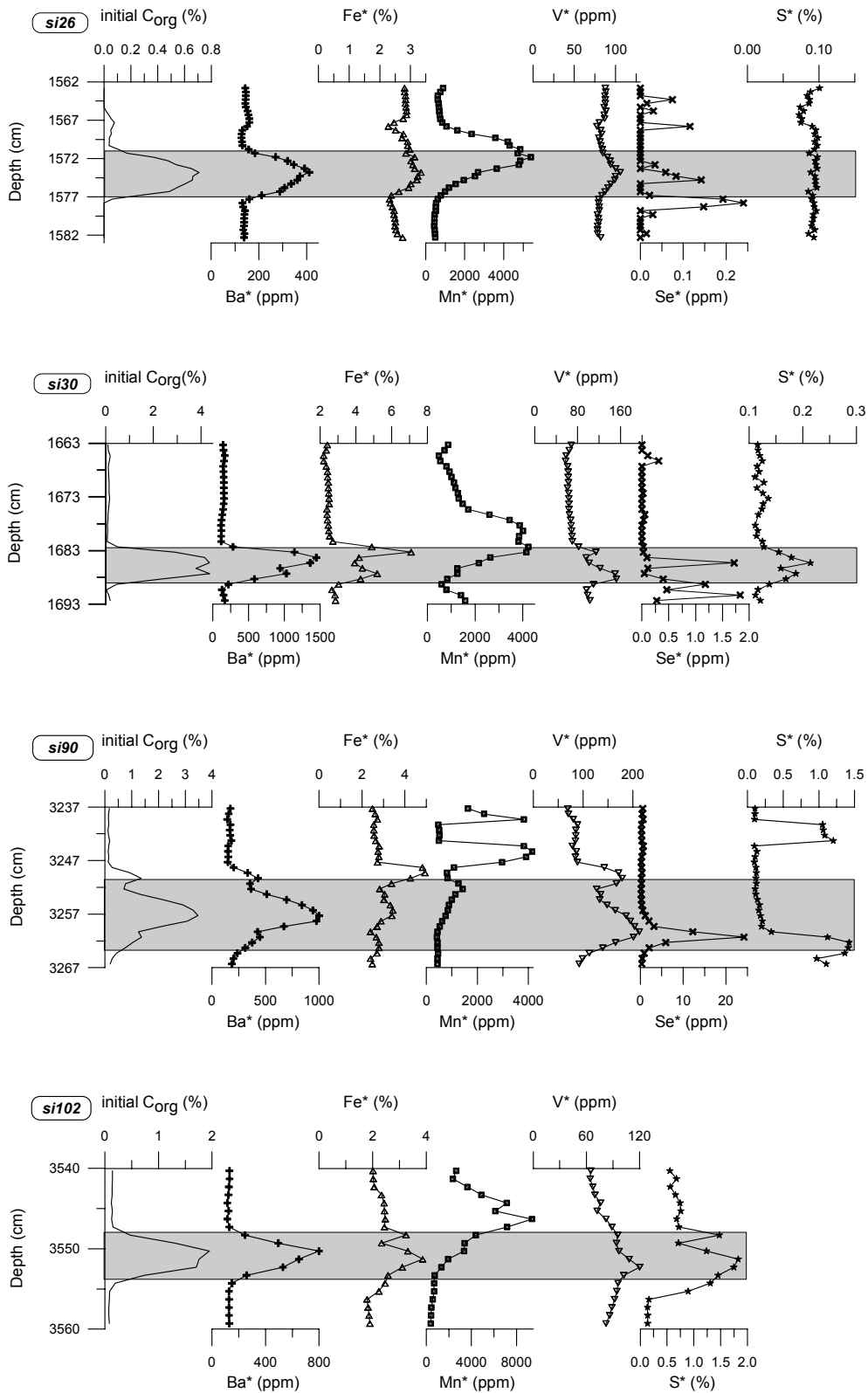


Figure 5.5 Concentration vs. depth profiles of calculated initial organic carbon, and measured Ba, Fe, Mn, V, Se, and S for si26, si30, si90, and si102 from core KC01B. Concentrations are normalized in the same way as for Figure 5.3. The initial sapropel, obtained from the calculated initial organic carbon values, is indicated by the shaded area. No Se was analyzed in si102.

Sulphur contents are low in the oxidized intervals, except for si102 and the lower part of si90 where total-S concentrations of up to 2% are found (Figure 5.5). The peak around si102 is thought to originate from sapropel Si100, according to the sulphidise down mechanism described by Passier et al. (1996). The S peak in si90, at the base of the initial sapropel, may indicate the last remnant of this sapropel. The origin of the peak above si90 is yet unknown.

Ongoing diagenesis is also responsible for the different profiles of redox-sensitive elements such as Se and V. In si30 and si90, peaks of both elements are found near the base of the missing sapropel (Figure 5.5), indicating that this was the depth of the ancient oxidation front and that oxygen did not diffuse deeper than this level. For si26, the Se concentrations are very low and therefore highly unreliable. However, the main (lowermost) peak does not coincide with a V peak. Consequently, it is likely that the oxidation front moved deeper into the sediment, below the sampled interval. The relatively low concentration of organic carbon in the missing si26 sapropel (Table 5.1) indicates that this sapropel has been easy to oxidize.

In the four missing sapropels of this group, the ARM, NRM, and χ_{in} values are similarly low underneath the inferred sapropel base and are high in and above the former sapropel (Figure 5.2). The magnetic signals, as observed in these intervals, are similar to those observed near sapropels that are visible today (compare Figure 5.2).

On the basis of geochemical and magnetic data, we conclude that the intervals around si26, si30, si90, and si102 initially contained sapropels that have subsequently been completely oxidized. Ongoing diagenesis has altered the distribution of redox-sensitive elements considerably. In two intervals, si30 and si90, Se peaks indicate the position of the ancient oxidation front. Redox conditions never became extremely anoxic because the Ba profiles contain only minor traces of remobilization.

5.3.3.2 *Partially overprinted missing sapropels (si58, si60, si86, and si98)*

Partially overprinted missing sapropels all have Ba profiles that contain multiple peaks: two in si60, si86 and si98, and four in si58 (Figure 5.6). Mobilization of Ba probably occurred in these intervals due to dissolution of barite under sulphate-reducing conditions. Such mobilization prohibits the calculation of the initial organic carbon profile since it is unknown to which extent the initial Ba concentrations changed at each depth level. It is also impossible to deduce the exact thickness of the initial sapropel from these profiles because it is likely that the Ba is distributed over a wider interval now than it has been during formation of the sapropel. However, the distance over which dissolved Ba may have diffused is likely to be small, because sulphate-reducing conditions were probably present only in a restricted part of the sediment column. During sapropel formation, there is a continuous supply of bottom water sulphate to the pore water, as demonstrated by Passier et al. (1996). In such situations, Ba cannot diffuse over large distances but will reprecipitate as barite on encountering pore water with sufficient sulphate. Ongoing sulphate reduction after deposition of the sapropel is also unlikely. In almost all sapropels that are still visible now, including the Si2, active sulphate reduction is absent (e.g. Pruyers et al., 1993).

Missing sapropel si58 is a special case which contains a quadruple Ba peak which can have three possible origins. (1) The Ba profile represents the initial Ba signal: Four separate periods of sapropel formation must have occurred. Noncontinuous sapropel formation (e.g. Si16 or S6) may be caused by short periods of bottom water renewal or by decreases in primary production. (2) The Ba profile is the result of mobilization and

reprecipitation of barite at different levels. (3) The Ba profile is the result of two missing sapropels, each having an initial peak and a mobilization peak. The peaks at 2505 and 2525 cm would then be the initial Ba peaks, since they still show a gradual increase and decrease at the base and top of the missing sapropel. The peaks at 2495 and 2515 cm, however, have a relatively sharp transition from high to low Ba concentrations in the upper part of the peak, which may be an indication of diagenetic formation (compare the upper peak in si86; Figure 5.6). This is our preferred interpretation, because it is easier to completely oxidize two thin sapropels than to oxidize a single thick sapropel (as required by option 1) and it does not need special diagenetic conditions as required by option 2.

Assuming that the amount of Ba above background concentrations is representative for the total amount of Ba that has been deposited initially during sapropel formation, it is possible to calculate the total amount of initial organic carbon (Table 5.1). Calculated values are of the same magnitude as those of non-overprinted missing sapropels and as sapropels that are still visible in the present-day sediment column.

The sulphur concentrations in the oxidized intervals are low (Figure 5.6) and indicate no other sulphur source than pore water sulphate. All reduced sulphur minerals have been oxidized by the oxidation front.

The profiles of solid phase Fe and Mn are more complex than in the non-overprinted missing sapropels: The Fe profiles are different, with only minor peaks. Owing to the more reducing conditions, more Fe has been remobilized and has diffused outside the sampled intervals. This remobilization is reflected by the relatively constant values of the paleomagnetic parameters, ARM, NRM, and χ_{in} (Figure 5.2). The Mn concentrations are relatively high in the interval with high Ca values (not shown) and are thought to be associated with carbonates.

In all intervals (except si58) a clear V peak is visible. The position of the peak is mostly in the interval which we interpret to represent remobilized Ba. In case of a completely oxidized sapropel this peak was expected to appear at the base of the Ba-enrichment. It seems therefore that the present-day V peak no longer indicates the depth of the ancient oxidation front.

In conclusion, these intervals contain missing sapropels, though the evidence is less clear than for the nonoverprinted missing sapropels. The combination of the observed Ba profile with remobilization peaks and the peaks in redox-sensitive elements in, or close to, these intervals point to a former sapropel that has been completely oxidized. The total Ba may still represent the total organic carbon flux but does not necessarily indicate the precise sapropel boundaries.

5.3.3.3 *Completely overprinted missing sapropels (si8, si14, and si40)*

Overprinted missing sapropels are characterized by Ba profiles that indicate severe mobilization of Ba (Figure 5.7). All profiles contain higher than background (> 200 ppm) Ba values over a wide depth interval, often with several minor Ba peaks. The quasi-Gaussian shaped Ba peak observed in si40 is located on top of a relatively high Ba background and is therefore probably not representative of the original profile. In these intervals, severe sulphate reduction is inferred to have taken place where the reduction rate was (much) faster than the diffusion rate of sulphate from the bottom water. As a result, pore water sulphate concentrations decreased to a level that barite was dissolved. Similar to the profiles of the partially overprinted missing sapropels, these profiles cannot be used to calculate the initial organic carbon profile, nor can the initial sapropel boundaries be indicated.

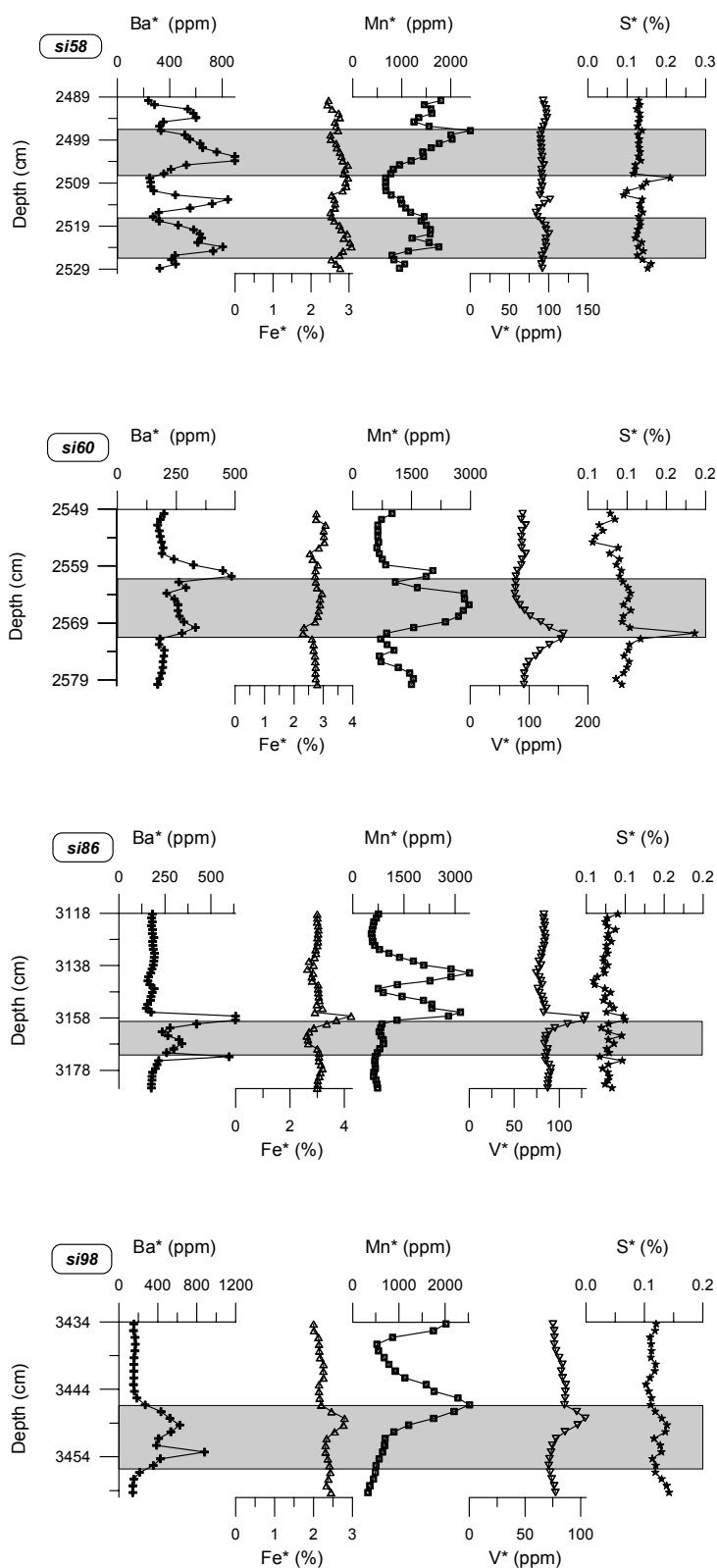


Figure 5.6 Concentration vs. depth profiles of Ba , Fe , Mn , V , and S for *si58*, *si60*, *si86*, and *si98* from core KC01B. Concentrations are normalized in the same way as for Figure 5.3; the initial sapropel is indicated by the shaded area.

The reduced sulphur minerals that formed during sapropel formation have all been subsequently oxidized. Pore water sulphate makes up the present S concentrations. The sharp Ba peak at 683 cm in si8 is not of diagenetic origin. A peak at this depth is also found in the profiles of Al, Ce, Co, Fe, Na, P, S, and Ti. At the same level, Be, Cr, K, Li, Mg, Sc, and V show (strong) negative peaks. Note that not all elements are shown in Figure 5.7. Simultaneously, the Ca concentration drops to values below 6%, which is extremely low for eastern Mediterranean sediments. The suite of elemental concentrations at this level points to a volcanic origin. The age of the sediment is 79 kyr, as calculated by Langereis et al. (1997), which is similar to the age of about 82 kyr of tephra layer X-2 (Cita et al., 1977). For the top few meters of this core, the dating methods of Langereis et al. (1997) and Cita et al. (1977) give similar ages: For Si12 (sapropel S5), ages of 124 and 125 kyr respectively are obtained. Therefore it is likely that this layer represents tephra layer X-2. This tephra layer contains sanidine, augite, biotite, occasional plagioclase, hornblende (uncommon), apatite, and sphene (Vezzoli, 1991) and is completely different to the surrounding sediments, which results in sharp (negative) peaks. The tephra is fine-grained and has a color similar to that of the surrounding sediment. Therefore this layer was not previously identified. X-ray diffraction (XRD) analyses of the two samples that were taken in this layer confirm that it is of volcanic origin. Both samples contain considerable amounts of anorthite (> 25%) and smaller amounts of albite, augite, phlogopite, and kaolinite. Consequently, the high Ba in this interval is not sapropel-related.

When focusing on the interval above this tephra layer and the intervals around si14 and si40, no distinct Fe and Mn peaks are found. On the basis of the Ba profiles, we conclude that redox conditions must have been more anoxic for these intervals than for the previously discussed intervals. Most Fe- and Mn-oxyhydroxides have probably been reduced and have diffused away from this interval. In addition, no clear spikes that point to missing sapropels have been found from other redox-sensitive elements. Because Fe-oxyhydroxides have been mobilized, no clear signals are observed in the paleomagnetic variables; only relatively constant values remain (Figure 5.2).

In conclusion, these intervals may contain a missing sapropel, but the evidence for this (i.e., occurrence of a Ba enrichment at an insolation maximum) is ambiguous. The deposition of subsequent sapropels near these intervals may be responsible for the extensive diagenetic changes observed around si14 and si40. The cause of the extensive remobilization in si8 is less clear. Sapropel Si10 (S4) is found below this interval, but it is unlikely that this layer, which does not show any evidence of sulphate reduction, could have been directly responsible for the complete removal of most traces of a missing sapropel in si8.

5.3.4 Insolation Maxima Without a Corresponding Ba Peak

Not all distinct maxima in the insolation target curve have a corresponding Ba peak (Figure 5.2). This may be related to four possible reasons. The first of these is the initial sampling resolution of 10 cm that is too coarse to reveal all Ba enrichments.

Second, if sapropels do not form at every insolation maximum, there may never have been a Ba-enrichment at that level. This could indicate that climate changes, which lead to higher paleoproductivity and subsequent sapropel formation, do not always occur or that they occur at an intensity that is too low to initiate higher productivities. There is no straightforward relationship between the relative value of the insolation maximum and the height of the Ba peak (Figure 5.2). With the present state of knowledge of sapropel formation, and its expression in sediments, it is not possible to decide if sapropel formation

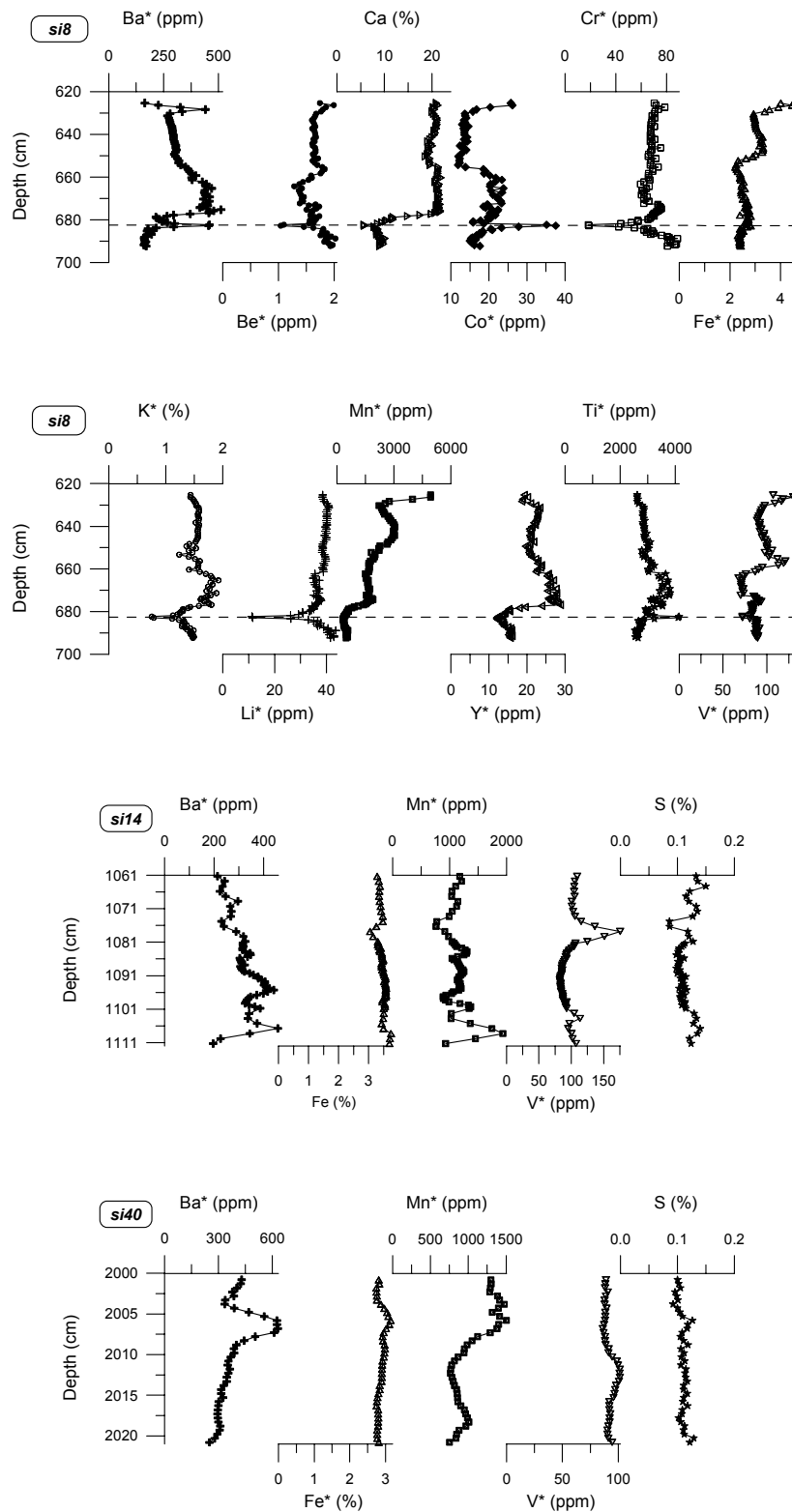


Figure 5.7 Concentration vs. depth profiles of Ba, Be, Ca, Co, Cr, Fe, K, Li, Mn, Y, Ti, and V for *si8* and Ba, Fe, Mn, V, and S for *si14* and *si40* from core KC01B. All elements, except Ca and S, are normalized to Al and multiplied by the average Al content to minimize the dilution effect by CaCO_3 (indicated by the asterisk). The dashed line in the *si8* profiles indicates the position of the tephra layer.

has occurred at every insolation maximum. We have shown that initially more sapropels have been deposited than are presently observed and have supplied potential tools to detect such initial presence.

The third reason is, although all sapropels that are preserved in sediments always have elevated Ba concentrations, sapropel formation may also have occurred without a change in the Ba content of the sediment. This is only possible if the higher organic carbon concentrations in sapropels result strictly from enhanced preservation due to anoxic bottom water conditions. This option does not seem to be realistic, however, because no sapropel that is found at present is of this type. Sapropels that formed by enhanced preservation may only have a relatively low organic carbon concentration, which would easily result in their rapid oxidation. Consequently, such hypothetical sapropels would no longer be visible.

The fourth is that oxidation of sapropels leads to diagenetic signals in the sediment. If a new, larger sapropel is deposited above an oxidized sapropel, however, the diagenetic processes in the new sapropel can (partially) overprint older ones, as was demonstrated above. Further diagenesis cannot only remobilize the metal-rich layers, but it may also dissolve the Ba peaks which subsequently precipitate at a different level or become part of the new diagenetic signal. This means that (almost) no signs of the older sapropel are left in the sediment and that a missing sapropel is no longer chemically detectable at that level.

With respect to these complicating factors, it is difficult to demonstrate that a sapropel was originally deposited at every insolation maximum. Furthermore, it is unknown to what extent and by what mechanism(s) the climate changes and how this corresponds to sapropel formation. It is unlikely that the present combination of geochemical and paleomagnetic data alone can solve this problem. However, we have clearly demonstrated that there were initially more sapropels than those observed today in the sediments of the last 1.1 Myr in the eastern Mediterranean Sea. This is an important finding for the study and interpretation of sedimentary paleoclimatic signals found in this area. Furthermore, inorganic geochemical and, to a lesser extent, magnetic signals can be used to reveal major changes in paleoclimatology and paleoceanography. In this way, a large number of samples can easily be processed, allowing for a much more detailed data set.

5.4 Conclusions

Sapropels always display high Ba concentrations, and they always appear at maxima in the insolation target curve. After oxidation of a sapropel, the Ba profile is preserved. Barium, present as barite, may only be mobilized under strongly sulphate reducing conditions. Early diagenesis produces a downward moving oxidation front, which causes the formation of Fe- and Mn-rich layers of characteristic shape, as well as typical distributions of other redox-sensitive elements. In the 1.1-Ma sediment column of core KC01B, a large number of Ba spikes have been found that are not related to visible sapropels. Most of these Ba peaks lie near maxima in the insolation target curve, which suggested the former presence of additional, now “missing” sapropels.

Four of the sampled intervals (si26, si30, si90, and si102) contain chemical signals that indicate the complete oxidation of sapropels. The distribution of Ba and (trace) elements is similar to that observed in a partly oxidized sapropel (Si46). The magnetic properties of missing sapropels show a pattern similar to that of visible sapropels, which

supports the conclusion that these intervals are the remnants of completely oxidized sapropels.

In four other intervals (si58, si60, si86, and si98), ongoing diagenesis has partially overprinted the signals that formed during oxidation of the sapropel. However, the combination of elevated Ba concentrations and peaks in the redox-sensitive elements are useful indicators for missing sapropels. The profiles of si8, si14, and si40 are more strongly overprinted and contain only faint traces of missing sapropels.

There is no direct relation between the relative value of the insolation maximum and the height of the Ba peak found at that level: Visible sapropels, which have high Ba concentrations, are not always found at the most pronounced insolation maxima. Furthermore, Ba peaks are not observed at each insolation maximum. This may be caused by (1) the sampling resolution which was too coarse to recover all Ba enrichments; (2) sapropel formation by enhanced preservation rather than by increased primary production; (3) overprinting by more recent diagenesis and, (4) the absence of sapropel formation.

We have demonstrated that the 1.1-Ma sediment record of core KC01B initially contained more sapropels than are visible today. Geochemical and magnetic parameters are useful tools to reveal the occurrence of these missing sapropels and therefore major changes in paleoclimate and paleoceanography, even though observations may be complicated by postoxidative diagenetic alterations of the sediment.

Acknowledgements. - We thank the crews and scientific parties of the Marion Dufresne 1991 and Urania 1994 cruises. H. de Waard, E. Koning, M. Klein-Tank, D. van der Meent, R. Alink, and P. Anten are acknowledged for their assistance with geochemical analyses. Paleomagnetic and rock magnetic measurements were carried out by J. Meijer and P.-J. Verplak. M.B. Cita and staff and students are acknowledged for the laborious picking of the microfossils for stable isotope analysis. We thank C.H. van der Weijden for critically reading the manuscript. Reviews by R. Zahn, A. Roberts, and one anonymous reviewer and editorial work by M.L. Delaney greatly improved the original version. This work was supported by the European Union Marine Science and Technology program, contract numbers 900022C (MARFLUX) and MAS2-CT93-0051 (PALAEOFLUX). M.J.D. acknowledges support of the Royal Netherlands Academy of Sciences and Arts in the form of a fellowship. This is NSG paper 96.1213.

Chapter 6

Components of eastern Mediterranean sediments¹

Abstract - A 37 m long eastern Mediterranean piston core (KC01B) is used to study different components in eastern Mediterranean sediments. In addition, this core is used to improve the age model of the last 1.1 Myr. As a result, sapropels S12 to Sb have been dated in previous papers one to two precession cycles younger than proposed now in the new age model. Twenty seven tephra layers have been identified in this core. Some of the layers could be related to known tephra layers, but the majority of layers has not been described before. As no distinct tephra samples have been taken for geochemical analyses, it is for only 15 layers that a geochemical composition can be given. Core KC01B also contains numerous turbidites, comprising a total of more than 2 m of sediment. The composition of these turbidites does not deviate from the sediments in which they are embedded. The source area must, therefore, be relatively local. One layer that was previously described as a turbidite now appears to be a, possibly displaced, sapropel with a relatively low organic carbon content. This sapropel is partly oxidized and corresponds with a maximum in the insolation curve. A comparison between sapropel and normal sediments (turbidites, tephra layers and diagenetically altered sediments are excluded) show that these are on average remarkably similar. This indicates that sedimentological signals were not very different during periods of sapropel formation and therefore climatic variations do not have a great impact on the composition of sediment on this location. Clear climate related cyclic variations have not been found in core KC01B.

6.1 Introduction

The eastern Mediterranean sedimentary column contains different types of sediment. The most abundant type is light-brown, organic-poor hemipelagic sediment, reflecting normal sedimentation. Intercalated are several distinctive olive-green to black organic-rich sapropels (e.g. Cita et al., 1977; Kidd et al., 1978; Shaw and Evans, 1984). A special type of sediments are tephra layers with very different texture and grain size. Most studies have focused on volcanic deposits over the last 200 to 400 kyr (e.g. Keller et al., 1978; Vezzoli, 1991; Narcisis and Vezzoli, 1999) and have shown that the occurrence of tephra layers may be basin wide or rather restricted to a more local area. Apart from these sediments, turbidites may be present. A well described example is the turbidite caused by a tsunami wave that was initiated by the collapse of the Santorini caldera 3500 yr ago (e.g. Cita et al., 1984, 1996; Cita and Aloisi, 2000).

In this paper we present the results from a high-resolution study of a 37 m long Kullenberg core (KC01B) with a maximum age of ~1.1 Myr. This is one of the longest cores recovered in the eastern Mediterranean and contains the oldest sapropels sampled so far in a piston core. It narrows the gap between the piston core sapropels and those found in land-based sections. Langereis et al. (1997) used this core to construct an astronomical time scale for the last 1.1 Myr. Comparison of high resolution color reflectance records of KC01B and a more recent ODP core has led to an improvement of this age model

¹ Authors: P.J.M. van Santvoort, G.J. de Lange, L.J. Lourens and J. Thomson (to be submitted).

(Lourens, in prep.). The consequences for the dating of core KC01B will be discussed. Furthermore, this core provides an excellent opportunity to study the composition of older tephra and sapropel layers.

Turbidites make up a substantial part of the sediment in this core. The amount, thickness, composition and distribution are discussed. The composition of these turbidites may provide information on their source area and possibly on the type of events that triggered them. Therefore, a comparison is made between the geochemical composition of turbidites and normal sediments.

The cyclic occurrence of sapropels appears to be associated with climatic changes and related to maxima in the summer insolation target curve (e.g. Rossignol-Strick et al., 1982; Rossignol-Strick, 1985, 1987; Lourens, 1996). Climatic changes may also be responsible for the variation in the terrestrial contribution to eastern Mediterranean sediments (Dominik and Stoffers, 1978). If climate changes are cyclic, as suggested by the periodical occurrence of sapropels, and if they cause variations in the terrestrial contribution to the sediment, then a cyclicity in the terrestrial component of the sediment is expected. Such cyclicity had indeed been observed in ODP cores (Wehausen and Brumsack, 1998; Nijenhuis et al., 2001) where changes in paleoenvironmental or climatic conditions are reflected by variations in major- and minor-element geochemistry. In addition, cyclic variations in carbonate content and detrital-matter composition are observed. In the present study we will unravel turbidites and tephra intervals from pelagic sediments and we will assess potential (cyclic) variations in geochemical composition within the pelagic intervals.

6.2 Material and methods

Kullenberg core KC01B was recovered during the 1991 MARFLUX-I cruise of R.V. Marion Dufresne (Figure 6.1). Initially, KC01B was sampled every 10 cm, extended to every 5 cm later on. In and around sapropels and in intervals where a 'missing' sapropel was suspected samples were taken with a 0.5 cm resolution, resulting in over 3000 sediment samples.

The sediment samples were freeze-dried and finely ground in an agate mortar, then digested in a mixture of hydrofluoric, nitric and perchloric acids. Final solutions were analysed in 1 M HCl by ICP-AES on a Perkin Elmer Optima 3000 at Utrecht University and at IOS (UK). The quality of the analyses was monitored by the inclusion of laboratory and international standards. The error in the analyses was < 4% for all elements.

Organic carbon was determined on a Fisons Instruments NCS NA 1500 analyser using dry combustion at 1030°C. Inorganic carbon, as carbonate, was removed before analysis by shaking the sample for 24 hours in 1 M HCl. This procedure was repeated to ensure that all inorganic carbon had been removed. The sample was rinsed twice with distilled water and dried at 80°C. After drying, the sample was ground in an agate mortar. International and in-house standards were used to check the accuracy of the method. Standard deviations were always < 2%. Tests showed that the amount of organic carbon hydrolysed by the HCl treatment was negligible.

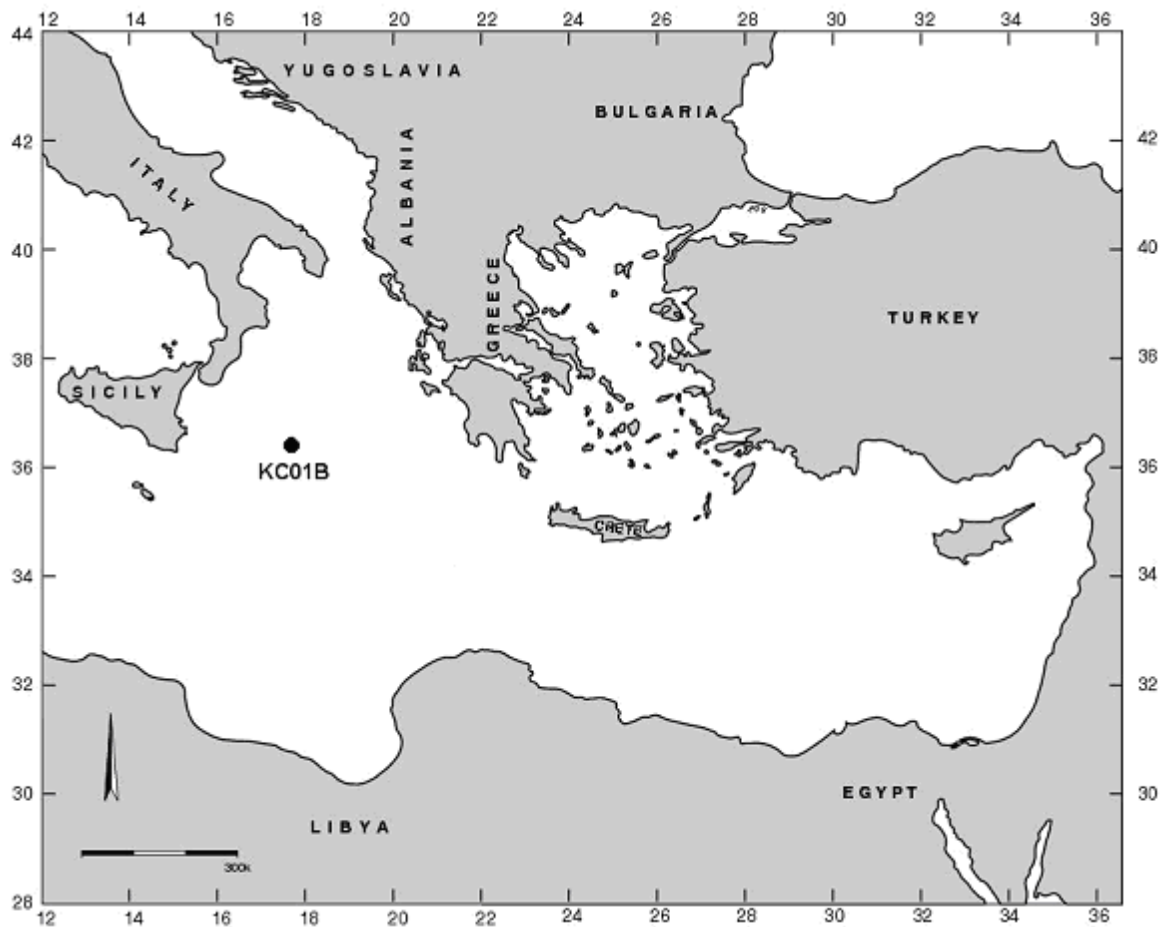


Figure 6.1 Location of core KC01B; the core was taken at $36^{\circ}15.2' N$, $17^{\circ}44.3' E$ (Calabrian Ridge, Pisano Plateau), at a water depth of 3643 m.

6.3 Results and discussion

6.3.1 Age model

Two age models have been proposed for KC01B. The first age model was based on tuning the actual sapropels as well as a number of “ghost-sapropels”, that were indicated by specific geochemical and rock magnetic properties of the sediment to the $65^{\circ}N$ summer insolation time series (Langereis et al., 1997). Rossignol-Strick et al. (1998) constructed concomitantly an independent age model through tuning the oxygen isotope record of KC01B to the ice sheet model of Imbrie and Imbrie (1980). Differences in the order of 0 to 5 kyr occur between both age models, due to the choice of two different target curves and the adopted time lags between insolation forcing and climate response. Largest differences (in the order of kyr) between both age models occur at 618 and at 785 kyr.

Recently, Lourens (in prep.) evaluated both age models by using a detailed comparison of high-resolution color reflectance records between KC01B, KC01 and ODP Site 964, all located at the same site. This comparison revealed that intensive tectonic deformation occurred at several intervals in KC01B. The most characteristic deformation features are found at ~ 25 and 27.5 m piston depth, where normal and reverse faulting caused tectonic reduction and multiplication of sediments, respectively. Using the ODP

Site 964 composite sedimentary record as a guide, these tectonic problems in KC01B could be restored and hence an evaluation of the time scale could be carried out. For this purpose, the sapropel chronology of Langereis et al. (1997) for KC01B was compared with that of Emeis et al. (2000) for ODP Site 964. In addition, both age models were compared with a new age model based on a more gradual change in sedimentation rate and/or compaction with depth. Lourens (in prep.) concluded that the oxygen isotope chronology of KC01B based on the latter age model fits well with open ocean oxygen isotope records as well as with the astronomical precession and obliquity time series. It is this age model we have used for calculating the age of the sediment in the samples.

As a consequence of the multiplication of sediments, a total of 1.5 m of sediment is omitted from the geochemical dataset.

6.3.2 Sediments

Four different sediment types can be distinguished in KC01B: normal hemipelagic sediment, organic-rich hemipelagic sediment (sapropels), tephra layers and turbidites. Each type will be discussed; a general composition of normal sediment and sapropels will be given.

6.3.2.1 *Normal, hemipelagic sediment*

This sediment type comprises most of the sedimentary column and reflects the normal sedimentation conditions that prevail in the eastern Mediterranean. The sediments are characterized by low organic carbon content (< 0.2 wt.%) and are mostly brown-creamish in color. These sediments are deposited in oxygenated water and consist of a marine (carbonates and organic carbon) and a terrestrial (mainly aluminosilicates) component.

The marine primary productivity related contribution is determined by the amount of available nutrients in the surface waters. The anti-estuarine circulation, with the inflow of Atlantic, nutrient-depleted surface water and outflow of nutrient-enriched Mediterranean Intermediate Water, results in low nutrient values in eastern Mediterranean surface water. At present, the top of the sediment contains 0.35–0.50 wt.% organic carbon (Van Santvoort et al., 2002²). The most reactive part is rapidly oxidized in the upper 5 cm and concentrations lower than 0.2 wt.% remain.

The terrestrial component consists of fluvial and eolian input. Fluvial sources are the Nile, but also rivers entering the Black Sea, the Po and other rivers of the northern borderlands. The composition of material is different for the different rivers. The Nile material is dominated by smectite, while other rivers transport more illite and chlorite (Dominik and Stoffers, 1978). Rivers do not only transport aluminosilicates, but also organic carbon. This land-derived organic matter is more resistant to oxidation and finally makes up approximately 30% of the organic material in the hemipelagic non-sapropel sediment below 5 cm depth (Van Santvoort et al., 2002).

The amount and composition of terrestrial material that is transported through eolian and fluvial pathways is determined by climatological factors: a wet climate causes higher fluvial runoff while a dry climate is responsible for a higher eolian contribution. At present, the climate is dry and the Sahara is an important contributor to the sedimentation (Guerzoni et al., 1997). Climatic changes may change the composition of the sediments; and since climatic changes are thought to occur in cycles, the sediment composition should reflect these cycles.

² Van Santvoort et al. (2002) is chapter 2 of this thesis.

6.3.2.2 *Sapropels*

Usually a sapropel is defined as a dark-olive green to black sediment layer that contains more than 2 wt.% organic carbon (Kidd et al, 1978). More recently, Van Santvoort et al. (1997)³ redefined a sapropel as a distinct sediment layer, which has an organic carbon content that is significantly higher than that of the surrounding hemipelagic sediment, and which is deposited in an open marine environment and is correlated with an insolation maximum.

The occurrence of sapropels appears to be cyclic and corresponds closely with minima in the precessional index when perihelion occurred in the northern hemisphere summer (e.g. Rossignol-Strick, 1983, 1985; Prell and Kutzbach, 1987; Hilgen, 1991). Numerous studies exist on the formation of sapropels and many scenarios have been written. All models proposed on the origin of sapropels can be classified in the following groups:

(1) Anoxia in the bottom water causes a better preservation of organic material. Anoxia is produced by water column stratification that is due to the introduction of low saline surficial waters. Several sources are suggested: the Black Sea, where melting waters from northern European glaciers were stored (e.g. Olausson, 1961; Ryan, 1972; Thunell et al., 1977); the Nile river, following an intensification of the monsoonal regime in Africa (e.g. Rossignol-Strick et al., 1982; Rossignol-Strick, 1985, 1987; Howell and Thunell, 1992). Evidence for a low salinity layer is given by $\delta^{18}\text{O}$ depletions in planktonic foraminiferal shells within sapropels, which can be related to the $\delta^{18}\text{O}$ signature of fresh water input (e.g. Vergnaud-Grazzini et al., 1977; Thunell et al., 1983, Gudjonsson and Van der Zwaan, 1985; Vergnaud-Grazzini et al., 1986).

(2) Enhanced primary production in the photic zone is the cause of an increased organic matter accumulation in the sediments. Some models focus on the formation of particular sapropels (e.g. De Lange and Ten Haven, 1983; Howell and Thunell, 1992), others propose this mechanism as the cause of formation for all sapropels (e.g. Pedersen and Calvert, 1990; Calvert et al., 1992).

(3) Mixed models in which an increase in production of organic matter is accompanied by suboxic to anoxic bottom waters (e.g. Rohling and Gieskes, 1989; Rohling and Hilgen, 1991; Higgs et al., 1994). The introduction of a low salinity layer could have led to reduced deep water circulation, limiting the amount of oxygen in the deeper parts of the water column. Eventually this could have led to anoxic bottom water conditions, resulting in enhanced preservation of organic material (Cita et al., 1977; De Lange et al., 1989; Nolet and Corliss, 1990).

The most distinct feature of sapropels is the high organic carbon content. The initial organic carbon profile has been inferred from the preserved barite as having a quasi-Gaussian shape (e.g. Thomson et al., 1995). However, the actually observed profiles are commonly different from their initial deposition: the upper part of a sapropel may be oxidized which means that the organic carbon presently observed, usually has an abrupt change to normal Mediterranean background values. Breakdown of organic material takes place after deposition when the bottom water is re-oxygenated at the end of sapropel formation. Oxygen and nitrate are available again in the bottom and pore waters and diagenetic processes are responsible for the oxidation (burn down) of organic matter. An

³ Van Santvoort et al. (1997) is chapter 5 of this thesis.

extensive description of this process can be found in Higgs et al. (1994) and Van Santvoort et al. (1996, 1997)⁴.

Another characteristic of sapropel sediments is the high S concentration. Most of this S is present as pyrite (Passier et al., 1996), but organic sulphur is also relatively enriched within the sapropels because pyrite formation was Fe-limited for certain periods of time (Passier et al., 1999). During this period, the surplus of sulphide diffused out of the sapropel, causing pyrite formation below the sapropels and sulphide reoxidation in the water column. The combination of high S and organic carbon concentrations will usually classify a sample as a sapropel.

A good correlation between Ba (present as biogenic barite) and organic carbon is often observed in organic-rich sediments (Calvert and Fontugne, 1988; Klinkhammer and Lambert, 1989) as well as in sediment trap data (Dymond et al., 1992). Therefore, Ba is considered to be a paleoproductivity indicator (De Lange et al., 1994, Francois et al., 1995, Thomson et al., 1995). This feature has been used to calculate the position of sapropels before they were (partially) oxidized (Van Santvoort et al., 1996, 1997).

Finally, sediments with a high organic carbon content, including sapropels, are reported to contain higher concentrations of trace metals relative to the surrounding sediments (e.g. Calvert, 1983; Calvert et al., 1985; Pruyssers et al., 1991; Nijenhuis et al., 2001). These elements are not only associated with organic material, but Fe-oxyhydroxides and pyrite may also contain considerable amounts of trace metals.

In core KC01B 16 sapropels are observed (Table 6.1), ranging in thickness from 1 to 40 cm. Sapropels S*, S'' and Sd have not been identified onboard and have therefore not been sampled. The amount of organic carbon in this core varies from 0.3 up to almost 6.1 wt.%.

Table 6.1 Sapropel layers in core KC01B. The age is calculated using the improved age model of Lourens (in prep.).

	Depth (m)	Thickness (cm)	Age (kyr)
S4	7.77 – 7.84	3	100.4 – 101.8
S5	8.76 – 8.80	4	123.5 – 124.3
S6	11.75 – 12.15	40	168.8 – 177.0
S7	12.83 – 12.91	8	193.8 – 196.3
S8	13.37 – 13.54	17	212.18 – 218.9
S9	14.03 – 14.04	1	238.3 – 238.7
S'	15.73 – 15.74	1	287.6 – 288.1
S10	16.81 – 16.86	5	330.1 – 331.7
S11	19.25 – 19.27	2	406.4 – 407.1
S12	21.70 – 21.72	2	501.2 – 502.0
Sa	22.82 – 22.87	5	551.7 – 553.7
S*	23.98 – 24.04	6	594.9 – 597.7
Sb	24.38 – 24.43	5	617.3 – 619.3
S''	32.44 – 32.47	3	953.3 – 954.8
Sc	32.88 – 32.90	2	975.0 – 976.4
Sd	34.85 – 35.02	17	1065.5 – 1072.8

⁴ Van Santvoort et al. (1996) is chapter 4 of this thesis.

6.3.2.3 Tephra layers

Two major source regions for tephra can be distinguished in the eastern Mediterranean: the Italian volcanic provinces (Sicilian, Aeolian, Campanian, Roman and Tuscan) and the Aegean provinces. Since the composition of the products from both provinces is quite diverse, the eastern Mediterranean is a very suitable region for tephrochronological studies. The use of deep-sea drilling cores allowed for the development of a tephrostratigraphy for the last 200 kyr (e.g. Ryan, 1972; Cita et al., 1977; Keller et al., 1978). There has been little focus on the description and distribution of older tephra layers thus far.

In KC01B, a total of at least 33 tephra layers have been distinguished, varying in thickness from 1 to 20 cm, making up a total of 121.5 cm (Table 6.2). The layers are numbered according to the numbering of Lourens (in prep.). The age of the layers is in the range from 17 to 1110 kyr. These layers are not evenly distributed throughout the core, but seem to appear more or less in clusters (Figure 6.2).

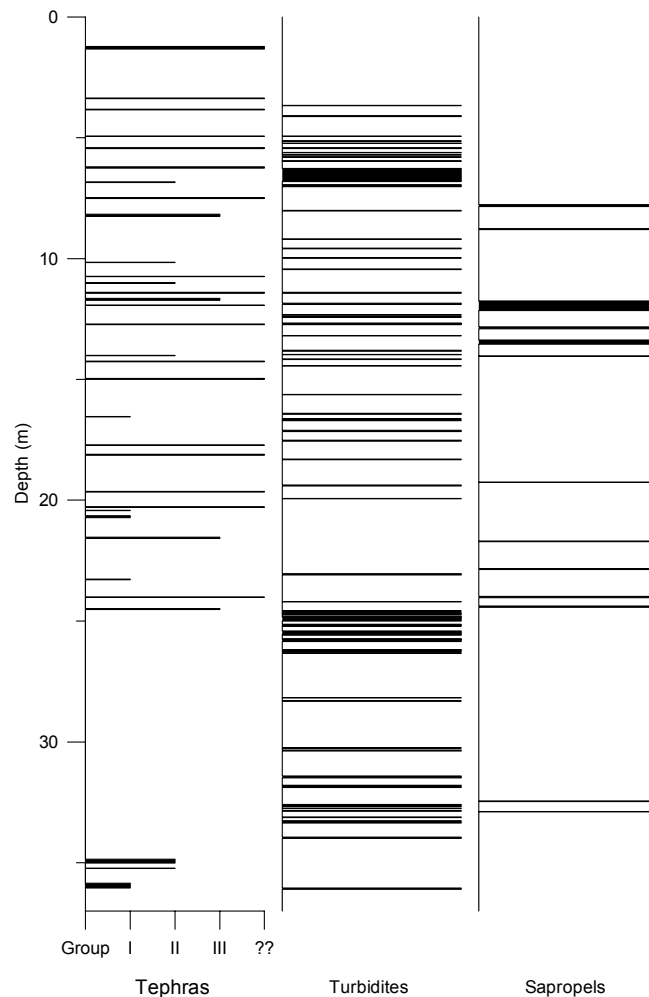


Figure 6.2 Distribution of the different type of layers in the core. The group according to Figure 6.3 is given for each tephra layer. ?? indicates that the layer has not been sampled and analysed, so the group is not known. Note that the amount of turbidites is actually bigger than can be seen in the plot. Since some layers are too close together to be separated, they appear as a thicker layer in the plot. See Table 6.1, 6.2 and 6.3 for the exact depths of the sapropels, tephra layers, and turbidites, respectively.

From the total of 33 tephra layers, 15 layers have been identified onboard and have been sampled for bulk geochemical analyses. It should be noted that the common method used for digestion of the samples does not permit Si to be analysed. Usually, it is only the glass fraction of the tephra that is used for geochemical analyses (Keller et al., 1978). In this study, however, the analyzed samples are a mixture of tephra and clay. The most important reason to use only the glass fraction is that the proportion of minerals to glass changes as a function of distance from the source area as tephra is transported by wind.

Some of the tephra layers can be identified as layers described before in the literature and have been labeled accordingly (Table 6.2). Identification is based on mineralogical composition and age of the tephra. The calculated composition range of these layers is given in the Appendix and is in concordance with literature values (e.g. Keller et al., 1978). It should be taken into account that re-sedimentation of volcanoclastic products, caused by turbiditic events, may be an important process, making it more difficult to identify distinct tephra layers (Narcisi and Vezzoli, 1999).

Table 6.2 *Tephra layers in KC01B. Mineralogy and identification have been provided by L. Vezzoli. The layers have been numbered according to Lourens (in prep.). If a tephra has been identified as a previously reported layer, this is indicated in the Layer column. Layers for which both sampling and analysis have been done are marked by a capital "A" in the Analysed column. The numbers in the Group column refer to the different groups shown in Figure 6.3.*

	Depth (m)	Age (kyr)	Analysed	Colour	Mineralogy	Layer	Group
i1	1.23-1.61	17		black	cpx, plg, bt, fld	Y1	
i2	3.36-3.38	34				Y3	
i3	3.82-3.85	39		dark yellow	cpx, plg, bt	Y5	
i4	4.93- 4.94	53				Y7	
i5	5.41-5.45	59					
i6	6.21-6.26	72				X2	
i7	6.83-6.85	83	A	olive grey	cpx, hrn, plg, fld, bt		ii
i8	7.47-7.51	95		black	cpx, hrn, plg, bt, fld	X3 and X4?	
i9	8.16-8.25	111	A	olive brown	cpx, plg, fld, bt	X6	III
i10	10.15-10.17	143	A	grey	cpx, hrn, plg, fld	W2	II
i11	10.74-10.75	151		grey	cpx, bt	W1?	
i12	11.00-11.02	154	A			W1	II
i13	11.39-11.43	162					
i14	11.65-11.73	167	A	olive black	plg, bt	V0	III
i15	11.92-11.94	172				V2	
i16	12.71-12.73	191					
i17	14.005-14.025	238	A	black	cpx, hrn, plg		II
i18	14.245-14.265	245		olive black	cpx, hrn, plg, fld		
i19	14.965-14.995	266		pale grey	cpx, hrn	V4?	
i20	16.535-16.55	320	A	brown black	cpx		I

	Depth (m)	Age (kyr)	Analysed	Colour	Mineralogy	Layer	Group
i21	17.715-17.725	359		dark grey	cpx, hpr, hrn, plg		
i22	18.105-18.145	371		grey	cpx, plg, fld	Mt	
i23	19.635-19.655	422		black	bt, cpx		
i24	20.275-20.295	446		black	cpx, hpr, hrn, plg, fld		
i25	20.415-20.435	452	A	black	cpx, plg, fld		I
i26	20.645-20.715	462	A				I
i27	21.525-21.575	497	A	grey	cpx, hpr, plg, fld		III
i28	23.265-23.295	569	A	grey	cpx, plg, fld, bt		I
i29	24.005-24.015	596				VdD3	
i30	24.485-24.525	622	A	yellow grey	cpx, plg, fld, bt		III
i31	34.855-35.015	1066	A	olive black	cpx, plg, fld		II
i32	35.225-35.245	1083	A				II
i33	35.845-36.05	1112	A				I

Abbreviations in mineralogy: *cpx*=clinopyroxene; *plg*=plagioclase; *bt*=biotite; *fld*=feldspar; *hrn*=hornblende.

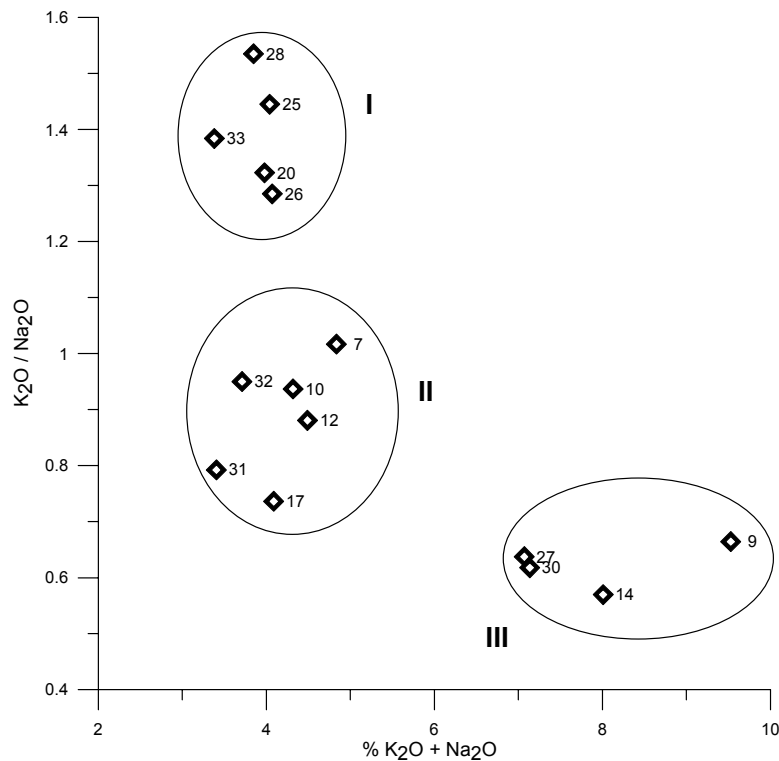


Figure 6.3 Distinctive groupings of various tephras as determined by ratios of potassium to sodium oxide. Numbers in the figure correspond to the numbers of the layers in Table 6.2.

It should be noted that the actual composition of the pure tephra will be somewhere in between the two extreme values listed in the Appendix. An attempt is made to distinguish between different source areas for the tephtras. This can be done by plotting (K_2O / Na_2O) versus ($\% Na_2O + K_2O$) (Figure 6.3). The plot suggests three different source areas, which is in good agreement with the findings by Keller et al. (1978) who, based on a much larger number and wider spatial distribution of cores, have distinguished four source areas. Higher values for the sum of Na_2O and K_2O are usually found in layers with a Roman or Campanian origin (group III). Ash layers with an Aeolian or Hellenic origin both have lower values for the sum, but the K_2O/Na_2O ratio is generally lower for the Aeolian layers (group II). The groupings in Figure 6.3 do not seem to correspond directly with these differences in geographical origin. Group III contains tephra layers X5 or X6 (i9) with a reported Campanian origin and V1 (i14) that is the result of a Santorini eruption (Keller et al., 1978; Narcis and Vezzoli, 1999). The same for group II where layer W1 (i12) has a Roman origin, layer W2 (i10) is the result of another Santorini eruption while layer X2 (i7) has a Campanian source. Group I contains no identified layers with known composition. In summary we conclude that, although similar chemical groups are distinguished, these do not seem to be related to tephtras reported by e.g. Keller et al. (1978). Possible explanations are that the layers described in literature are different from the layers found in KC01B, or that the location of the core is (much) further away from the source which can lead to a different composition of the deposited tephtra.

The plot as shown in Figure 6.3 does not change much if the compositions are moved between the lowest and highest values. The three different groupings remain and the layers are classified in the same group. The tephtra layers identified in this core provide a good opportunity for more detailed studies on the composition and origin of older tephtra layers.

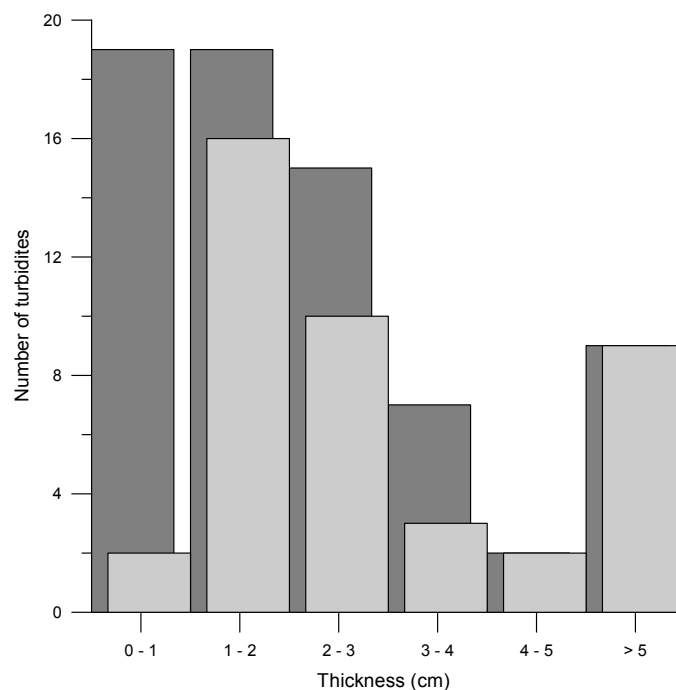


Figure 6.4 Histogram showing the number of turbidites in relation to their thickness. The darker bars show the number of observed turbidites in each class, the lighter bars the analyzed turbidites.

6.3.2.4 Turbidites

Turbidites may occur due to slope instability or to events that lead to enhanced instability. Such events may be sea-level fluctuations (Weaver and Kuijpers, 1983) or seismic activity (e.g. Cita et al., 1984, 1996). In core KC01B, 71 turbidite layers have been distinguished, varying in thickness from 0.5 to 54 cm (Table 6.3). Figure 6.4 shows the thickness of the layers, all layers (darker bars) as well as the analysed layers (lighter bars). These turbiditic layers comprise 222 cm of sediment. Figure 6.2 shows that the distribution of turbidites is not random and they seem to appear partly in clusters.

Figure 6.5 shows a comparison of the intensity of deposition of tephra layers and turbidites. The thickness of tephra and turbidites is calculated for each 2 kyr interval, and then a moving average of 10 kyr is applied to the data. In most cases, tephra layers seem to appear predominantly in periods with a low turbiditic activity. Or the other way around, most turbidites are formed in periods with low volcanic activity. If turbidites were formed as the result of volcanic activity then a correlation in the intensity of deposition is expected. However, only a few intervals in Figure 6.5 support this hypothesis. Weaver and Kuijpers (1983) suggested that the occurrence of turbidites is correlated with global climate changes, in particular glaciations and related eustatic sea-level fluctuations. This, and the fact that the eastern Mediterranean is a known seismic active area, may be a more feasible explanation for the distribution of turbidites.

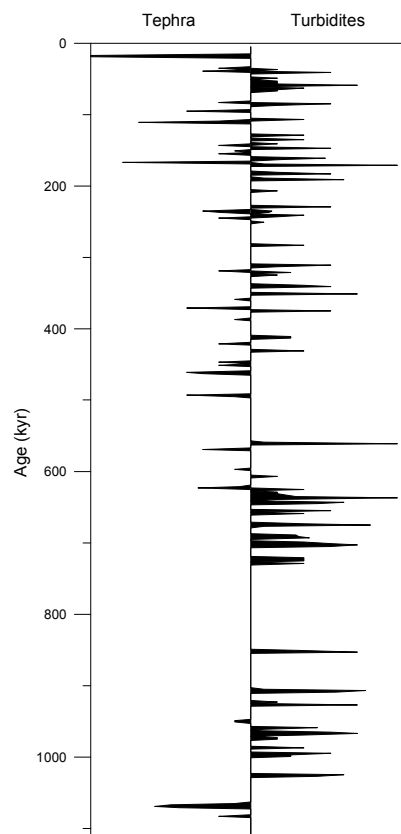


Figure 6.5 Comparison of the intensity of deposition of tephra layers and turbidites. The intensity is defined as the total thickness of each sediment type is calculated in a 2 kyr interval. Subsequently, a moving average of 10 kyr is applied to the dataset.

Three types of turbidites can be distinguished: (1) turbidites that have a similar composition as the surrounding sediment; (2) turbidites that have similar concentrations for most elements as the surrounding sediment; (3) turbidites that have a different composition.

Ad. (1). Most of the analyzed turbiditic layers (25 out of 42) are geochemically indistinguishable from the sediments in which they are embedded (Figure 6.6). It was only by sedimentological features such as distinctly different colors or grain size that these layers are interpreted as turbidites. This group (1) contains the thinnest intervals. It may be concluded that these turbidites are local and the distance from the source to the coring location is relatively small.

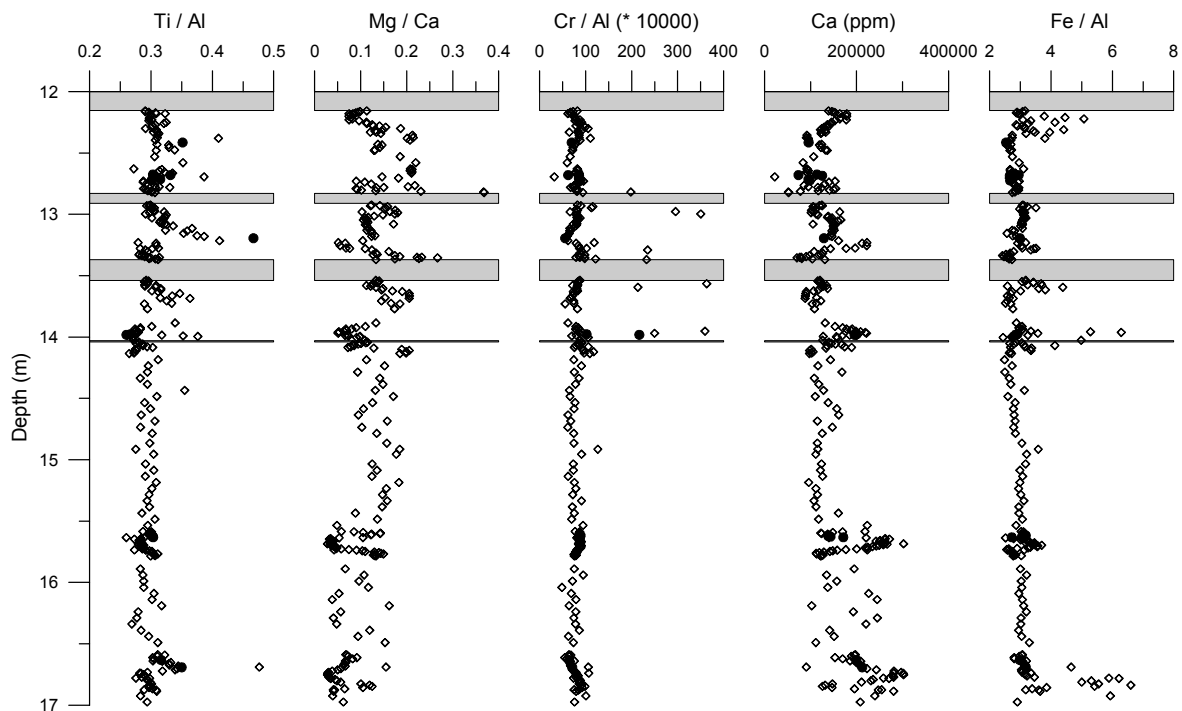


Figure 6.6 Profiles of Ti/Al , Mg/Ca , Cr/Al , Ca and Fe/Al versus depth (12 – 17 m). The small diamonds are normal hemipelagic sediment samples, the larger dots are turbidite samples. The profiles show that the composition of the turbidites is very similar to the normal sediments.

Ad. (2). One third of the turbidites display similar concentrations for most elements as the surrounding sediment. However, one to three (various) elements show a clear offset from the background sediment. These deviations occur in trace elements in almost all cases, but offsets in major elements like Ca and Ti are also observed. An example of this can be seen for the Ti/Al plot in Figure 6.6. The turbidite at a depth of 13.19 – 13.20 m has a higher Ti/Al ratio than the sediments above and below it. This type of turbidites (2) is mostly thicker than the turbidites in the former group (1), up to 10 cm. Since the differences with the surrounding sediment are relatively small, these turbidites (2) are also considered to be local. The events that caused these turbidites were probably more intense since more material was displaced.

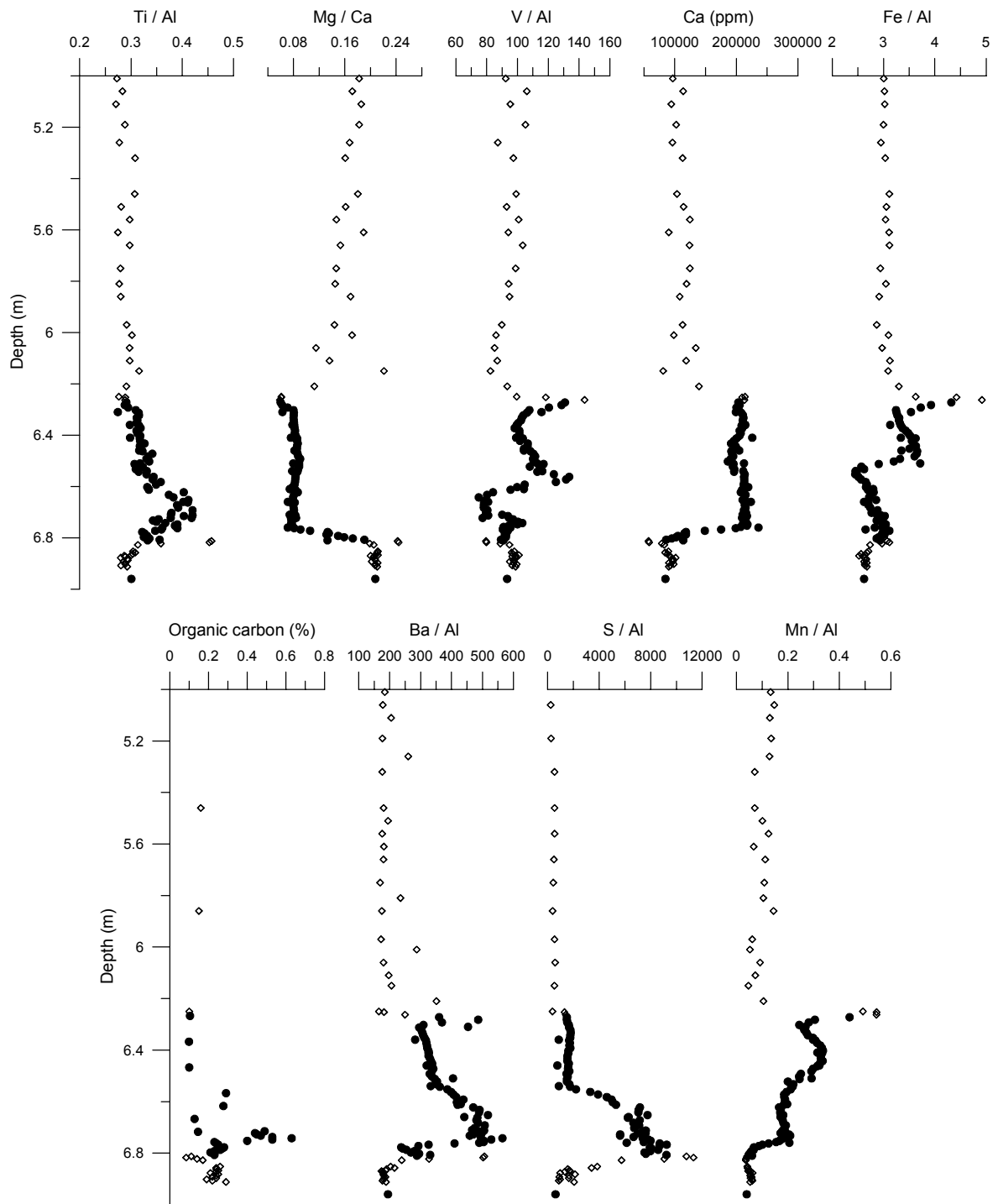


Figure 6.7 Concentration vs. depth profiles of Ti/Al , Mg/Ca , V/Al , Ca , Fe/Al , Organic carbon, Ba/Al , S/Al , and Mn/Al (5 – 7 m). The small diamonds are normal hemipelagic sediment samples, the larger dots are turbidite samples. The thick turbidite 11 is located between 6.27 and 6.81 m.

Table 6.3 *Turbiditic layers in KC01B: depth in the core and thickness. Not all layers have been sampled and analysed for geochemical purposes. The sampled layers are marked with a capital "A" in the Analysed column.*

	Depth (m)	Thickness (cm)	Analysed	Remarks
1	3.66 – 3.67	1		
2	4.09 – 4.12	3	A	
3	4.93 – 4.94	1		May be tephra layer i4
4	5.13 – 5.14	1		
5	5.23 – 5.24	1		
6	5.41 – 5.45	4		May be tephra layer i5
7	5.61 – 5.62	1		
8	5.70 – 5.71	1		
9	5.79 – 5.80	1		
10	5.96 – 5.97	1		
11	6.27 – 6.81	54	A	
12	6.95 – 6.97	2	A	
13	7.00 – 7.02	2	A	
14	8.01 – 8.03	2	A	
15	9.19 – 9.20	1		
16	9.57 – 9.59	2		
17	9.97 – 9.98	1		
18	10.43 – 10.46	3		
19	11.39 – 11.43	4		May be tephra layer i13
20	11.84 – 11.90	6	A	
21	12.33 – 12.34	1		
22	12.40 – 12.43	3	A	
23	12.67 – 12.69	2	A	
24	12.71 – 12.73	2	A	May be tephra layer i16
25	13.19 – 13.20	1	A	
26	13.80 – 13.83	3		
27	13.97 – 13.985	1.5	A	
28	14.145 – 14.175	3		
29	14.435 – 14.44	0.5		
30	15.615 – 15.635	2	A	
31	16.40 – 16.44	4		
32	16.625 – 16.64	1.5	A	
33	16.69 – 16.70	1	A	
34	17.105 – 17.155	5	A	
35	17.515 – 17.555	4	A	
36	18.295 – 18.325	3	A	
37	19.375 – 19.405	3	A	
38	19.925 – 19.945	2		
39	23.035 – 23.095	6	A	
40	24.195 – 24.205	1		
41	24.575 – 24.595	2	A	
42	24.665 – 24.675	1		
43	24.705 – 24.715	1		

	Depth (m)	Thickness (cm)	Analysed	Remarks
44	24.795 – 24.815	2	A	
45	24.845 – 24.945	10	A	
46	24.945 – 25.005	6	A	
47	25.135 – 25.165	3	A	
48	25.195 – 25.215	2	A	
49	25.415 – 25.525	11		
50	25.555 – 25.585	3		
51	25.725 – 25.765	4		
52	25.775 – 25.845	7		
53	26.175 – 26.205	3		
54	26.225 – 25.255	3		
55	26.315 – 26.335	2		
56	28.165 – 28.185	2		
57	28.295 – 28.315	2		
58	30.24 – 30.26	2		
59	30.34 – 30.38	4		
60	31.41 – 31.49	8		
61	31.80 – 31.81	1		
62	31.85 – 31.89	4		
63	32.59 – 32.62	3		
64	32.66 – 32.69	3		
65	32.745 – 32.755	1		
66	32.845 – 32.865	2		
67	33.115 – 33.135	2		
68	33.265 – 33.295	3		
69	33.335 – 33.365	3		
70	33.94 – 34.00	6		
71	36.05 – 36.10	5		

Ad. (3). There is only one turbidite with a composition that is distinctly different from that of the nearby sediments, turbidite 11 (54 cm thick) at a depth of 6.27 – 6.81 m (Figure 6.7). The elements shown have a clear offset from the surrounding sediments, as well as from most other sediments. It is obvious that this is not a homogeneous layer: Ca is rather high in the top 50 cm of the turbidite and rapidly drops at the bottom. Mg/Ca shows a similar pattern as $1 / Ca$, indicating that Mg is mainly associated with aluminosilicates rather than carbonates. The organic carbon content is relatively high (0.4 – 0.6%) just above the level where Ca drops and Ba shows a maximum at the same level. Fe and Mn display two peaks.

These signals indicate that this layer is a (possibly displaced) sapropel layer with low organic carbon content that is partly oxidized. The upper Fe and Mn peaks are located at 6.45 m depth, and may reflect the reventilation event that ended the sapropel formation (Van Santvoort et al., 1996). After this event oxygen was available for the oxidation of the sapropel. While diffusion of dissolved Fe and Mn continued from below, new peaks were built up. Since oxidation may have been rather fast because of the relatively low organic carbon concentrations, these peaks are not very pronounced. The oxidation front has moved to a depth of 6.71 m, which means that 25 cm of the original sapropel has been

oxidized. At this time, 8 cm of the original sapropel remains, so that the thickness of this sapropel must have been approximately 35 cm. This is very thick, compared to most sapropels, whether still visible at present or completely oxidized (Van Santvoort et al., 1997). The position of this sapropel in the core is consistent with the occurrence of a maximum in the LA90 summer insolation curve at this level (Van Santvoort et al., 1997).

Normally, Ti / Al shows a decrease in a sapropel. Figure 6.7 shows that Ti / Al has an increase in the supposed sapropel interval which could point to slumping. The values for some elements at the top of this layer for example are clearly deviating from normal values and may indicate a thin tephra layer. Ca remains constant, but Ti/Al drops and elements like Fe, Mn, Ba and V show sharp increases. Lourens (in prep.) identified this layer as the tephra layer i6. Therefore, this initial 'turbidite' is now rather interpreted as a possibly displaced or even slumped sapropel.

6.3.2.5 *Composition of pelagic sediments*

Sapropels and normal sediment are thought to be deposited under different environmental conditions, most probably caused by climatic changes. This means that the composition of the sediments, in particular the terrestrial component, may be different. Before a comparison can be made, it must be taken into account that the sediment composition may have changed after deposition, in particular for redox-sensitive elements.

In normal oxic sediments the major diagenetic process is the degradation of organic material by oxygen. Trace elements that are released by this process are immediately immobilized by the adsorption to Fe- and Mn-oxyhydroxides. This means that only the organic carbon content changes in the sediment. When conditions change to suboxic or anoxic, solid phase Fe- and Mn-oxyhydroxides may dissolve, releasing adsorbed trace elements. Precipitation may occur at levels where oxygen is present.

Generally, the transition from oxic to anoxic conditions is found in or near sapropels. Therefore, trace element enrichments are supposed to be found near the top of the sapropels. Since sapropels can be completely oxidized, it is possible to find sapropel-related enrichments without the corresponding visual sapropel evidence (Van Santvoort et al., 1997). Trace element enrichments can also be caused by leaching of tephra or turbidites.

When redox conditions become even more anoxic, sulphate is used to oxidize organic matter. This may lead to the mobilization of Ba (e.g. Van Os et al., 1991). Another effect is the formation of sulphides that will form pyrite when Fe^{2+} is available (Passier et al., 1996). Due to excess sulphide formation within a sapropel, Fe-sulphides will not only form within, but also below the sapropel. When a sapropel is not completely oxidized, these sulphide enrichments are still visible today. Complete oxidation will remove the sulphur, but the iron remains as oxyhydroxides.

Diagenetic processes mainly affect the distribution of trace metals in the sediment. If there is some redistribution of major elements (for example Ca due to carbonate dissolution), this is negligible compared to the concentrations in the sediment.

When the composition of the two types of pelagic sediment is compared, it is necessary to minimize the effect of diagenesis on the calculated average values. Therefore, some of the samples have been removed from the dataset: (1) samples within 15 cm above the top of a visible sapropel; (2) samples in the interval of missing sapropels (Van Santvoort et al., 1997) and (3) samples where more than two trace elements show concentrations at least five times the base level. Furthermore, the median value is used

instead of the average value to reduce the influence of a few samples with higher concentrations.

Table 6.4 Composition of hemipelagic non-sapropel sediment and sapropels. Data for sediment with clear diagenetic signals have been omitted from the calculation.

	Normal sediment		Sapropel	
	Median	St. dev.	Median	St. dev.
C _{org} (%)	0.14	0.07	2.10	1.21
δ ¹³ C (‰)	-24.1	0.7	-23.4	0.9
Al (%)	6.0	1.3	5.4	0.9
Ba (ppm)	202	61	323	388
Be (ppm)	2.00	0.62	1.95	0.34
Ca (%)	13.9	5.7	14.0	2.9
Ce (ppm)	70	22	91	14
Co (ppm)	23	9	43	33
Cr (ppm)	83	24	103	133
Cu (ppm)	37	19	68	92
Fe (%)	3.2	0.7	3.7	0.8
K (%)	1.6	0.4	1.5	0.3
Li (ppm)	47	11	44	11
Mg (%)	1.7	0.3	1.4	0.2
Mn (ppm)	926	365	796	199
Na (%)	1.2	0.3	1.6	0.3
Ni (ppm)	56	16	98	99
P (ppm)	479	135	488	159
S (ppm)	1274	4917	21252	11434
Sc (ppm)	11	3	20	48
Sr (ppm)	605	265	580	126
Ti (ppm)	3274	737	2789	487
V (ppm)	99	24	183	267
Y (ppm)	18	3	18	25
Zn (ppm)	80	23	84	24
Zr (ppm)	87	38	91	31

Results are listed in Table 6.4. As expected, the difference in organic carbon content is obvious. Most trace elements are slightly higher in the sapropel. Major elements show similar values for both sediment types. Sodium is slightly enriched in the sapropel because of the higher water content of the sediment. The sulphur enrichment in the sapropel is very distinct. Barium, being a paleoproductivity indicator, is expected to display a higher average concentration in the sapropel. However, it is only slightly enriched, which may indicate severe sulphate reduction and redistribution of Ba from sapropels into the overlying sediments. Normally, Ti (or Ti/Al) is reported to be lower in sapropels. In KC01B, the sapropel Ti concentration is only slightly lower than in normal sediment. Following the approach of Rutten et al. (2000), the Ti/Al ratio for oxic, hemipelagic sediment is calculated as 54 mg g⁻¹ and for sapropels 51 mg g⁻¹. For rivers this ratio is reported to be between 48.2 and 59.6 mg g⁻¹, and dust has a ratio between 57.8 and

69.6 mg g⁻¹. This indicates that there is no single source of terrestrial material, but that there is a shift towards more fluvial input during periods of sapropel formation.

As a conclusion, the sediment composition of sapropel and normal sediment is remarkably similar. This can only be seen by removing the samples from the dataset that are diagenetically influenced. Therefore, it seems that climatic variations do not have a great impact on the composition of the sediment on this location. This is in contrast to data reported for other sites in the eastern Mediterranean where clear cycles in the sediment composition occur (Wehausen and Brumssack, 1998, Nijenhuis et al., 2001).

6.3.3 Cyclicality

Most sapropel studies have focussed on upper Pleistocene sapropels, but results can easily be applied to older (lower Pleistocene and Pliocene) sapropels as well, such as in land-based marine successions (e.g. Gudjonsson and Van der Zwaan, 1985; Rio et al., 1991; Van Os et al., 1994). It was observed first in these land sections that sapropels occur in distinct intervals of large scale carbonate cycles (Hilgen, 1987). The carbonate cycles have been studied using different techniques and methods: micropaleontological (De Visser et al., 1989), magnetostratigraphic (Langereis and Hilgen, 1991; Hilgen, 1991) and geochemical (Van der Weijden, 1993; Van Os et al., 1994). Consensus is that formation of the carbonate cycles closely corresponds with variations in the precessional index.

Wehausen and Brumsack (1998) observed cyclic variations in carbonate content and detrital-matter composition, caused by precession-induced climatic variations, in two ODP cores. One core was recovered from Pisano Plateau, Calabrian Ridge (CR), the same location as KC01B, the other one from the lower northern slope of Eratosthenes Seamount (ES), south of Cyprus. It should be noted that the cyclic variations were much more clear in the ES than in the CR core. The authors explained this by the fact the ES sediments are influenced by changes in discharge from the Nile: sapropels are formed during periods of enhanced discharge and lower Ti/Al, Mg/Al, K/Al and Zr/Al ratios. Furthermore, accumulation rates of carbonate and terrigenous detrital matter were 30% lower during such episodes. The Nile influence is absent at the CR site. Terrigenous detrital matter chemistry reflects periods of longer Saharan dust input alternating with fluvial input from the northern borderlands. Apparently, this results in less distinct extremes in the cycles of the CR core.

Sapropels are the result of cyclic climatic variations. Other climate related cycles are supposed to be found in the intervals in the core where sapropels are found. The best interval for this in KC01B is one with four consecutive sapropels (170 – 240 kyr). Profiles from this interval are shown in Figure 6.8. To exclude differences in accumulation rates the depth axis is replaced by a time axis. The bases of the four sapropels have ages of 177 – 196 – 219 – 239 kyr, resulting in cyclic intervals of 19 to 23 kyr. This is in good agreement with the 23 kyr interval of the precession curve. The Ca profile seems to display some form of periodicity. A closer look at the age of the maxima in Ca (197 – 208 – 222 – 236 – 256 – 286 – 304 – 328 kyr) reveals intervals ranging from 11 to 30 kyr. These intervals are shorter or longer than the 23 kyr interval and they all have different lengths. Iron shows a similar pattern although some maxima have shifted a little, possibly due to diagenetic processes. Ti/Al and Mg/Ca show a minimum where Ca has a maximum. The Cr/Al profile is probably diagenetically altered and does not show any cycles.

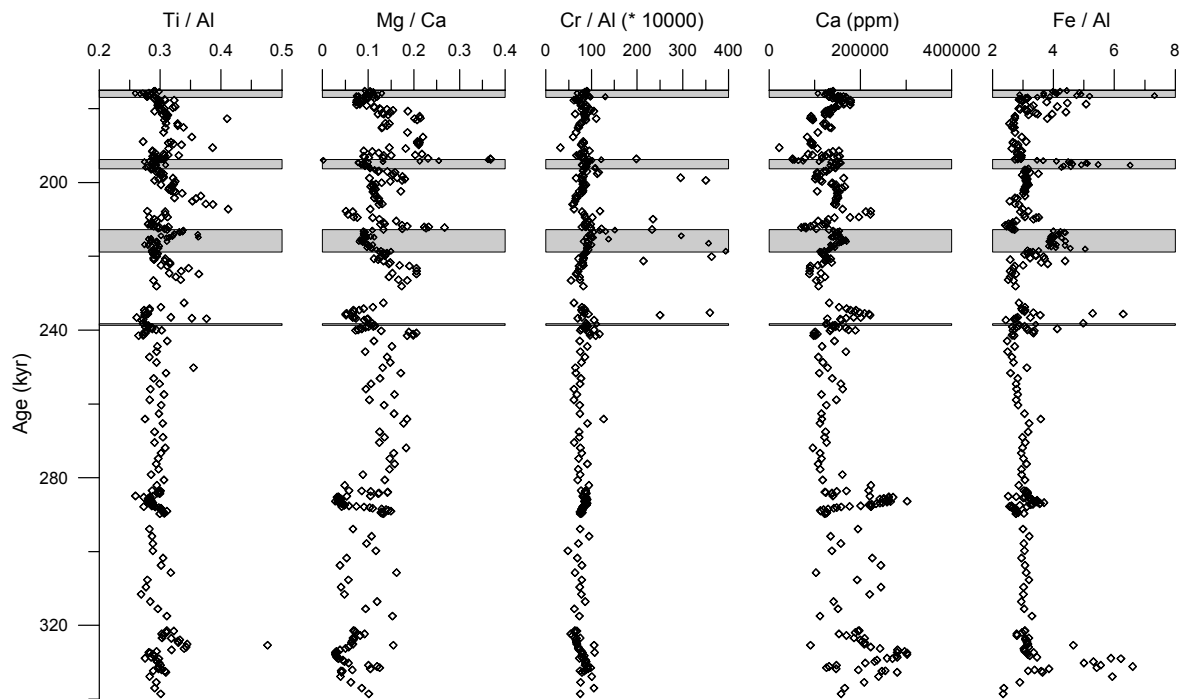


Figure 6.8 Concentration vs. age profiles of Ti/Al , Mg/Ca , Cr/Al , Ca , and Fe/Al (170 – 340 kyr). Plotted are the normal hemipelagic sediments. Sapropels are indicated by the shaded intervals.

Thus, an unambiguous precessional cycle is not observed for the geochemical data of this study. Apparently, climatic variations are not clearly reflected in the sediments of KC01B, apart from the sapropels. Possible causes are:

(1) Climatic variations do not have a measurable cyclic effect on the main sediment composition in this part of the Mediterranean due to source areas having similar geochemical compositions. An exception is the distinct sapropels. Wehausen and Brumsack (1998) actually observed climate related cycles in the ODP core from this site. An important difference is that the cycles observed by Wehausen and Brumsack (1998) are older than the sediments in KC01B. Furthermore, the analytical precision of Wehausen and Brumsack (1998) was better than for the samples used in this study ($< 1\%$ and $< 4\%$, respectively). It should be noted that the present dataset is a combination of samples that are analysed in two different labs which can further decrease the analytical precision. In this way, possible cycles may be obscured by analytical imperfections.

(2) Possibly, the amplitude of the insolation curve is a determining factor: only high maxima result in clear climatic cycles. The interval shown in Figure 6.8 covers the most dramatic extremes for the last 1 Myr in the insolation curve (e.g. Van Santvoort et al., 1997, Figure 5.2). If the amplitude is important, cycles should be seen in the interval of 170 – 240 kyr. Since they are not, the height of the insolation maximum is not a key factor here.

(3) Homogenisation of the sediment, due to bioturbation may weaken or even completely remove it. It was shown by Van Santvoort et al. (2002) that the surface mixed layer at present was only 2 cm for three different boxcores, among the thinnest reported for marine sediments. As a result of the oligotrophic conditions in the area, organic matter fluxes reaching the seafloor are low. As a consequence of the low food supply and its rapid remineralisation, the intensity of bioturbation is low and the bioturbation depth is small.

Since there is no indication that in the periods between sapropel formation the organic matter fluxes were very different from today, it is assumed that bioturbation was as low as it is today. In addition, there are no indications that the intensity of bioturbation was much different at sites where clear cycles have been found. Therefore, this process cannot be responsible for the disturbance of a cyclic pattern.

(4) Core KC01B contains a large number of detected tephra layers. However, it is possible that this core contains even more tephra layers that have not been identified. Bioturbation may have caused mixing of such, probably thin, layers with the regular sediment, resulting in a sediment with a different composition. This will disturb the cyclic pattern in the profiles. In this case, the observed profiles would display small intervals with deviating concentrations since bioturbation is relatively shallow. Apart from the identified tephra layers, such additional intervals have not been found in KC01B.

(5) The initial cycles have been overprinted by diagenetic processes. It was shown before that diagenesis may influence the distribution of trace elements in the sedimentary column. However, it is unlikely that large scale remobilization of major elements like Ca has occurred after deposition. It may be possible that some dissolution of carbonates occurred, but then the profile would not have been as gradual as it is now. It should be noted that it will be difficult to distinguish between sediments that are diagenetically altered and sediments that are mixed with volcanic material.

(6) The location of this core is relatively far away from the rivers of the northern borderlands and the southern Sahara. Therefore, the influence of the fluvial and eolian signals may not be strong enough at the location of core KC01B, resulting in a more or less climate independent sediment composition. It can also explain the remarkable similarity in composition of sapropel and normal sediments in this core. Sapropel formation (increased productivity and enhanced preservation) is triggered by events elsewhere in the basin and the sediment composition remains the same. This hypothesis is the most likely one. To test this, the age model would have to be applied to other eastern Mediterranean cores.

6.4 Conclusions

The age model for the last 1.1 Myr has been improved using core KC01B and other cores. It was observed that 1.5 m of sediment was the result of soft-sediment slumping. For further work, this interval should be omitted from the dataset. Furthermore, dating of sapropels S12 to Sb has changed: in the new model these layers are dated one or two precession cycles older than before.

Thirty three tephra layers have been identified in core KC01B. Some of these layers could be related to known tephra layers. The older layers have not been described before. These layers show three distinct compositions that could not directly be related to areas of origin.

Almost 2 m of sediment in this core consists of turbidites. Most layers are 1–2 cm thick and the composition of the sediment does not deviate from the sediments in which they are embedded. It may be concluded that the source area of the turbidites is very local and the distance from the source to the coring location is relatively small. This does not provide information on the events that triggered these turbidites. Only a few turbidites have a slightly different composition, mostly the thicker ones, and these may be transported over larger distances. One layer that was at first identified as a thick turbidite appears to be a, possibly displaced and slumped, sapropel with low organic carbon content. The age of the

sapropel corresponds with a maximum in the insolation curve which suggests that this is not a slumped sapropel. This is confirmed by the geochemical profiles that show clear and undisturbed signals of sapropel oxidation.

A comparison between sapropel and normal sediments (turbidites and tephra layers excluded) show that these are remarkably similar. The only major differences are organic carbon and sulphur content. And since the amount of organic material is higher, trace metals are slightly enriched in the sapropels, but not as much as expected. Usually, this picture may not be very clear due to diagenetic overprint of the original signals. It seems, therefore, that climatic variations do not have a great impact on the composition of the sediment on this location.

Climate related cyclic variations in major elements have not been found in core KC01B. Four consecutive sapropels were deposited at 19 – 23 kyr intervals, confirming the relation with the 23 kyr period in the precession and insolation curve. No such cycle could be distinguished in the major elements in this interval. The most likely explanation for this is that this core is too far away from Sahara, northern borderlands and Nile to be distinctly influenced by the variations in eolian and fluvial contributions. Alternatively, only subtle geochemical differences may occur between material originating from different source areas. This can also explain the similarity between normal and sapropel sediments. A similar approach as was chosen for KC01B (age model, sediment composition) should be applied to other cores to discriminate between the different components that contribute to the sediment composition.

Acknowledgements - We thank the crew and scientific party of the 'Marion Dufresne' 1991 cruise. H. de Waard, G. Nobbe, D. van der Meent and P. Anten are thanked for analytical assistance. L. Vezzoli kindly provided mineralogical data. C.H. van der Weijden is thanked for critically reading the manuscript. This work was supported by the European Union Marine Science and Technology programme, contract numbers MAS2-CT93-0051 (PALAEOFLUX), MAS3-CT97-0137 (SAP) and EVK3-2000-00042 (BIODEEP).

References

- Anastasakis G.C. and Stanley D.J. (1986) Uppermost sapropel, Eastern Mediterranean: paleoceanography and stagnation. *Nat. Geogr. Res.*, **2**, 179–197.
- Anderson R. and Kirkland D. (1980) Dissolution of salt deposits by brine density flow. *Geology*, **8**, 66-69.
- Antoine D., Morel A. and André J.-M. (1995) Algal pigment distribution and primary production in the eastern Mediterranean as derived from coastal zone scanner observations. *J. Geoph. Res.*, **100**, 16193–16209.
- Belderson R.H., Kenyon N.H. and Stride A.H. (1978) Local submarine salt-karst formation on the Hellenic Outer Ridge, Eastern Mediterranean. *Geology*, **6**, 716-720.
- Bender M.L., Fanning K.A., Froelich P.N., Heath G.R. and Maynard V. (1977) Interstitial nitrate profiles and oxidation of sedimentary organic matter in the eastern equatorial Atlantic. *Science*, **198**, 605-609.
- Bender M.L. and Heggie D.T. (1984) Fate of organic carbon reaching the deep sea floor: a status report. *Geochim. Cosmochim. Acta*, **48**, 977-986.
- Berger A. and Loutre M.F. (1992) Astronomical solutions for paleoclimate studies over the last 3 million years. *Earth Planet. Sci. Lett.*, **111**, 369-382.
- Berner R.A. (1980) Early diagenesis: a theoretical approach. Princeton University Press.
- Berner R.A. (1981) A new geochemical classification of sedimentary environments. *J. Sediment. Petrol.*, **51**, 359-365.
- Béthoux J.P. (1979) Budgets of the Mediterranean Sea. Their dependence on the local climate and on the characteristics of the Atlantic waters. *Oceanol. Acta*, **2**, 157-163.
- Betzer P.R., Showers W.J., Laws E.A., Winn D., DiTullio G.R. and Kroopnick P.M. (1984) Primary productivity and particle fluxes on a transect of the equator at 153°W in the Pacific Ocean. *Deep Sea Res.*, **31**, 1–11.
- Boudreau B.P. (1986) Mathematics of tracer mixing in sediments: I Spatially dependent, diffusive mixing. *Am. J. Sci.*, **286**, 161-198.
- Boudreau B.P. (1994) Is burial velocity a master parameter for bioturbation? *Geochim. Cosmochim. Acta*, **58**, 1243–1249.
- Boudreau B.P. (1997) Diagenetic models and their implementation. Modelling transport and reactions in aquatic sediments. Springer. 414p.
- Boyle E.A. (1983) Manganese carbonate overgrowths on foraminifera tests. *Geochim. Cosmochim. Acta*, **47**, 1815-1819.

- Bray C.J. and Karig D.E. (1985). Porosity of sediments in accretionary prisms and some implications for dewatering processes. *J. Geoph. Res.*, **90**, 768-778.
- Brumsack J.H. and Gieskes J.M. (1983) Interstitial water trace element chemistry of laminated sediments from the Gulf of California, Mexico. *Mar. Chem.*, **14**, 89-106.
- Bryden H.L. and Kinder T.H. (1991). Steady two-layer exchange through the Strait of Gibraltar. *Deep-Sea Res.*, **38**, S445-S463.
- Bryden H.L. and Stommel H.M. (1984) Limiting processes that determine basic features of the circulation in the Mediterranean Sea. *Oceanol. Acta*, **7**, 289-296.
- Burdige D.J. and Gieskes J.M. (1983) A pore water/solid phase diagenetic model for manganese in marine sediments. *Amer. J. Sci.*, **283**, 29-47.
- Cai, W.-J., Reimers, C.E. and Shaw, T. (1995) Microelectrode studies of organic carbon degradation and calcite dissolution at a California Continental rise site. *Geochim. Cosmochim. Acta*, **59**, 497-511.
- Calvert S.E. (1983) Geochemistry of Pleistocene sapropels and associated sediments from the eastern Mediterranean. *Oceanol. Acta*, **6**, 255-267.
- Calvert S.E. and Fontugne M.R. (1988) Geochemistry and origin of Mediterranean sapropels. *EOS*, **69**, 1234.
- Calvert S.E., Mukherjee S., and Morris R.J. (1985) Trace metals in fulvic and humic acids from modern organic-rich sediments. *Oceanol. Acta*, **8**, 167-173.
- Calvert S.E., Nielsen B. and Fontugne M.R. (1992) Evidence from nitrogen isotope ratios for enhanced productivity during the formation of eastern Mediterranean sapropels. *Nature*, **359**, 223-225.
- Camerlenghi A. (1988) Sub-surface dissolution of evaporites in the Eastern Mediterranean sea. *Thesis, A & M University, Texas*.
- Camerlenghi A. and Cita M.B. (1987) Setting and tectonic evolution of some Eastern Mediterranean deep-sea basins. *Mar. Geol.*, **75**, 31-55.
- Camerlenghi A., Cita M.B., Hieke W. and Ricchiuto T. (1992) Geological evidence for mud diapirism on the Mediterranean Ridge accretionary complex. *Earth Planet. Sci. Lett.*, **109**, 493-504.
- Chapman R.E. (1974) Clay diapirism and overthrust faulting. *Geol. Soc. Am. Bull.*, **85**, 1597-1602.
- Chester R. and Hughes M.J. (1967) A chemical technique for the separation of ferromanganese minerals, carbonate minerals and adsorbed trace elements from pelagic sediments. *Chem. Geol.*, **2**, 249-262.

- Cita M.B., Aghib F.S., Arosio S., Folco E., Sarto L., Erba E. and Rizzi A. (1989) Bacterial colonies and manganese micronodules related to fluid escape on the crest of the Mediterranean Ridge. *Riv. It. Paleont. Strat.*, **95**, 315-336.
- Cita M.B. and Aloisi G. (2000) Deep-sea tsunami deposits triggered by the explosion of Santorini (3500y BP), eastern Mediterranean. *Sed. Geol.*, **135**, 181-203.
- Cita M.B., Camerlenghi A., Kastens K.A. and McCoy F.W. (1984) New findings of Bronze Age homogenites in the Ionian Sea. Geodynamic implications for the Mediterranean. *Mar. Geol.*, **5**, 47-62.
- Cita M.B., Camerlenghi A. and Rimoldi B. (1996) Deep-sea tsunami deposits in the eastern Mediterranean: new evidence and depositional models. *Sediment. Geol.*, **104**, 155-173.
- Cita M.B., Vergnaud-Grazzini C., Chamley H., Ciaranfi N. and D'Onofrio S. (1977) Paleoclimatic record of a long deep sea core from the eastern Mediterranean, *Quat. Res.*, **8**, 205-235.
- Cochran, J.K. (1985) Particle mixing rates in sediments of the eastern equatorial Pacific: Evidence from ^{210}Pb , $^{239,240}\text{Pu}$ and ^{137}Cs distributions at MANOP sites. *Geochim. Cosmochim. Acta*, **49**, 1195-1210.
- Cochran J.K., McKibbin-Vaughan T., Dornblaser M.M., Hirschberg D., Livingston H.D. and Buessler K.O. (1990) ^{210}Pb scavenging in the North Atlantic and North Pacific Oceans. *Earth Planet. Sci. Lett.*, **97**, 332-352.
- Colley S., Thomson J., Wilson T.R.S. and Higgs N.C. (1984) Post-depositional migration of elements during diagenesis in brown clay and turbidite sequences in the North East Atlantic. *Geochim. Cosmochim. Acta*, **48**, 1223-1235.
- Cussen H., Braithwaite A.C. and Wilson T.R.S. (1994) A robust, pressure-tolerant, low oxygen demand, dissolved oxygen electrode for profiling into deep ocean sediment. *Underw. Techn.*, **20**, 3-7.
- Dählmann A. and De Lange G.J. (2003) Fluid-sediment interactions at Eastern Mediterranean mud volcanoes: a stable isotope study from ODP Leg 160. *Earth. Planet. Sci. Lett.*, **212**, 377-391.
- Davison W., Grime G.W., Morgan J.A.W. and Clarke K. (1991) Distribution of dissolved iron in sediment pore waters at submillimetre resolution. *Nature*, **352**, 323-325.
- De Lange G.J. (1986) Chemical composition of interstitial water in cores from the Nares abyssal plain (Western North Atlantic). *Oceanol. Acta*, **9**, 159-168.
- De Lange G.J. (1986). Early diagenetic reactions in interbedded pelagic and turbiditic sediments in the Nares Abyssal Plain (western North Atlantic): Consequences for the composition of sediment and interstitial water. *Geochim. Cosmochim. Acta*, **50**, 2543-2561.

- De Lange G.J. (1992). Shipboard routine and pressure-filtration system for pore-water extraction from suboxic sediments. *Mar. Geol.*, **109**, 77-81.
- De Lange G.J., Catalano G., Klinkhammer G.P. and Luther III G.W. (1990a). The interface between oxic seawater and the anoxic Bannock brine; its sharpness and the consequences for the redox-related cycling of Mn and Ba. *Mar. Chem.*, **31**, 205-217.
- De Lange G.J., Middelburg J.J. and Pruyzers P.A. (1989) Discussion: Middle and Late Quaternary depositional sequences and cycles in the eastern Mediterranean. *Sedimentology*, **36**, 151–158.
- De Lange G.J., Middelburg J.J., Van der Weijden C.H., Catalano G., Luther III G.W., Hydes D.J., Woittiez J.R.W. and Klinkhammer G.P. (1990b) Composition of anoxic hypersaline brines in the Tyro and Bannock Basins, Eastern Mediterranean. *Mar. Chem.*, **31**, 63-88.
- De Lange G.J. and Ten Haven H.L. (1983) Recent sapropel formation in the Eastern Mediterranean. *Nature*, **305**, 797-798.
- De Lange G.J., Van Os B., Pruyzers P.A., Middelburg J.J., Castradori D., Van Santvoort P., Müller P.J., Eggenkamp H. and Prahl F.G. (1994) Possible early diagenetic alteration of palaeo proxies. *NATO ASI*, **I 17**, 225-258.
- De Lange G.J., Van Santvoort P.J.M., Langereis C., Thomson J., Corselli C., Michard A., Rossignol-Strick M., Paterne M. and Anastasakis G. (1999) Palaeo-environmental variations in eastern Mediterranean sediments: a multidisciplinary approach in a prehistoric setting. *Progress in Oceanography*, **44**, 369-386.
- De Visser J.P., Ebbing J.H.J., Gudjonsson L., Hilgen F.J., Jorissen F.J., Verhallen P.J.J.M. and Zevenboom D. (1989) The origin of rhythmic bedding in the Pliocene Trubi Formation of Sicily, southern Italy: *Palaeogeogr., Palaeoclimatol., Palaeoecol.*, **69**, 45–66.
- Degens E.T. (1969) Biogeochemistry of stable carbon isotopes. In: *Organic geochemistry* (ed. G. Eglinton and M.T.J. Murphy), Springer Verlag, New York, pp. 304–329.
- Dekkers M.J., Langereis C.G., Vriend S.P., Van Santvoort P.J.M. and De Lange G.J. (1994) Fuzzy *c*-means cluster analysis of early diagenetic effects on natural remanent magnetisation acquisition in a 1.1 Myr piston core from the Central Mediterranean. *Phys. Earth Planet. Int.*, **85**, 155–171.
- Dominik J. and Stoffers P. (1979) The influence of Late Quaternary stagnations on clay sedimentation in the eastern Mediterranean Sea. *Geol Rundsch.*, **68**, 302 – 317.
- Dugdale R.C. and Wilkerson F.P. (1988) Nutrient sources and primary production of the South-Eastern Mediterranean. *Oceanologica Acta* **9**, 179–184.
- Dymond J., Suess E. and Lyle M. (1992) Barium in deep-sea sediment: A geochemical proxy for palaeoproductivity. *Paleoceanography*, **7**, 163-181.

- Emeis K.-C., Sakamoto T., Wehausen R. and Brumsack H.-J. (2000) The sapropel record of the eastern Mediterranean Sea – results of Ocean Drilling Program Leg 160. *Paleogeogr., Palaeoclimatol., Palaeoecol.*, **158**, 371-395.
- Emerson S., Fischer K., Reimers C. and Heggie D. (1985) Organic carbon dynamics and preservation in deep-sea sediments. *Deep-Sea Research*, **32**, 1–12.
- Emerson S. and Hedges J.I. (1988) Processes controlling the organic carbon content of open ocean sediments. *Paleoceanography*, **3**, 621–634.
- Emerson S.R. and Husted S.S. (1991) Ocean anoxia and the concentrations of molybdenum and vanadium in seawater. *Mar. Chem.*, **34**, 177-198.
- Fisher N.S., Cochran J.K., Krishnaswami S. and Livingston H.D. (1988) Predicting the ocean flux of radionuclides on sinking biogenic debris. *Nature*, **335**, 622–625.
- Flynn W.W. (1968) The determination of low levels of polonium-210 in environmental materials. *Anal. Chim. Acta*, **43**, 221–227.
- Fontugne M., Arnold M., Labeyrie L., Calvert S.E., Paterne M. and Duplessy J.-C. (1992) Hydrology of the Eastern Mediterranean during sapropel formation. In: *Fourth International Conference on Paleoceanography (Kiel, Germany, 21-25 September 1992), Program and Abstracts: GEOMAR Report*, **15**, 114.
- Francois R., Honjo S., Manganini S.J. and Ravizza G.E. (1995) Biogenic barium fluxes to the deep sea: Implications for paleoproductivity reconstruction. *Glob. Biogeochem. Cycles*, **9**, 289-303.
- Froelich P.N., Klinkhammer G.P., Bender M.L., Luedtke N.A., Heath G.R., Cullen D., Dauphin P., Hammond D., Hartman B. and Maynard V. (1979) Early oxidation of organic matter in pelagic sediments of the Eastern Equatorial Atlantic: Suboxic diagenesis. *Geochim. Cosmochim. Acta*, **43**, 1075-1090.
- Gacia E., Duarte C.M. and Middelburg J.J. (2002) Carbon and nutrient deposition in a Mediterranean seagrass (*Posidonia oceanica*) meadow. *Limnol. oceanogr.*, **47**, 23-32.
- Gingele F. and Dahmke A. (1994) Discrete barium particles and barium as tracers of paleoproductivity in South Atlantic sediments. *Paleoceanography*, **9**, 151-168.
- Glud R.N., Gundersen J.K., Jorgensen B.B., Revsback N.P. and Schulz H.D. (1994) Diffusive and total uptake of deep-sea sediments in the eastern South Atlantic Ocean: in situ and laboratory measurements. *Deep-Sea Res.*, **41**, 1767–1788.
- Goldberg E.D. and Koide M. (1962) Geochronological studies of deep-sea sediments by the ionium/thorium method. *Geochim. Cosmochim. Acta*, **26**, 417-450.
- Goñi M.A., Ruttenger K.C. and Eglinton T.I. (1998) A reassessment of the sources and importance of land-derived organic matter in surface sediments from the Gulf of Mexico. *Geochim. Cosmochim. Acta*, **62**, 3055–3075.

- Grundmanis V. and Murray J.W. (1982) Aerobic respiration in pelagic marine sediments. *Geochim. Cosmochim. Acta*, **46**: 1101–1120.
- Gudjonsson L. and Van der Zwaan G.J. (1985) Anoxic events in the Pliocene Mediterranean stable isotope evidence of run-off. *Palaeontology*, **Proc. B 88**, 69-82
- Guerzoni S., Molinaroli E. and Chester R. (1997) Saharan dust inputs to the western Mediterranean Sea: depositional patterns, geochemistry and sedimentological implications. *Deep-Sea Res. II*, **44**, 631–654.
- Hammond D.E., McManus J., Berelson W.M., Kilgore T.E. and Pope R.H. (1996) Early diagenesis of organic material in equatorial Pacific sediments: Stoichiometry and kinetics. *Deep-sea Res. II*, **43**, 1365-1412.
- Hedges J.I., Cowie G.L., Richey J.E., Quay P.D., Benner R., Strom M. and Forsberg B.R. (1994) Origins and processing of organic matter in the Amazon River as indicated by carbohydrates and amino acids. *Limnol. Oceanogr.*, **39**, 743–761.
- Hedges J.I. and Keil R.G. (1995) Sedimentary organic matter preservation: an assessment and speculative synthesis. *Mar. Chem.*, **49**, 81–115.
- Hem J.D., Lind C.J. and Roberson C.E. (1989) Coprecipitation and redox reactions of manganese oxides with copper and nickel. *Geochim. Cosmochim. Acta*, **53**, 2811-2822.
- Henneke E. (1993) Anoxic hypersaline sediments from the Tyro area - salinity gradients. *Geologica Ultraiectina*, **109**, 5-20.
- Higgs N.C., Thomson J., Wilson T.R.S. and Croudace I.W. (1994) Modification and complete removal of eastern Mediterranean sapropels by postdepositional oxidation. *Geology*, **22**, 423–426.
- Hilgen F.J. (1987) Sedimentary rhythms and high-resolution chronostratigraphic correlations in the Mediterranean Pliocene. *Newsl. Stratigr.*, **17**, 109–127.
- Hilgen F.J. (1991) Astronomical calibration of Gauss to Matuyama sapropels in the Mediterranean and implication for the geomagnetic polarity time scale. *Earth Planet. Sci. Lett.*, **104**, 226-244.
- Hilgen F.J., Lourens L.J., Berger A. and Loutre M.F. (1993) Evaluation of the astronomically calibrated timescale for the late Pliocene and earliest Pleistocene. *Paleoceanography*, **8**, 549-565.
- Hilgen F.J., Krijgsman W., Langereis C.G., Lourens L.J., Santarelli A. and Zachariasse W.J. (1995) Extending the astronomical (polarity) time scale into the Miocene. *Earth Planet. Sci. Lett.*, **136**, 495-510.
- Hoffert M., Perseil A., Hekinian R., Choukroune P., Needham H.D., Francheteau J. and Le Pichon X. (1978) Hydrothermal deposits sampled by diving saucer in Transform Fault "A" near 37°N on the Mid-Atlantic Ridge, Famous Area. *Oceanol. Acta*, **1**, 74-86.

- Howell M.W. and Thunell R.C. (1992) Organic carbon accumulation in Bannock Basin: evaluating the role of productivity in the formation of Eastern Mediterranean sapropels. *Mar. Geol.*, **103**, 461–471.
- Hsü K.J., Montadert L., Bernoulli D., Cita M., Erickson A., Fabricus F., Garrison R., Kidd R., Melieres F., Muller C. and Wright R. (1978). Florence Rise: Sites 375/376. *Init. Rep. DSDP*, **42**, 219-304.
- Huang Y, Dupont L., Sarnthein M., Hayes J.M. and Eglinton G. (2000) Mapping of C₄ plant input from North West Africa into North East Atlantic sediments. *Geochim. Cosmochim. Acta*, **64**, 3505–3515.
- Hydes D.J. and Hill N.C. (1985) Determination of nitrate in seawater: Nitrate to nitrite reduction with copper-cadmium alloy. *Estuarine Coastal Shelf Sci.*, **21**, 127-130.
- Imbrie J., and Imbrie J.Z. (1980) Modeling the climatic response to orbital variations. *Science*, **207**, 943-953.
- Jasper J.P. and Hayes J.M. (1993) Refined estimation of marine and terrigenous contributions to sedimentary organic carbon. *Glob. Biogeochem. Cycles*, **7**, 451–461.
- Jongsma D., Fortuin A.R., Huson W., Troelstra S.R., Klaver S.T., Peters J.M., Van Harten D., De Lange G.J. and Ten Haven L. (1983) Discovery of an anoxic basin within the Strabo Trench, Eastern Mediterranean. *Nature*, **305**, 795-797.
- Jørgensen B.B. (1978) A comparison of methods for the quantification of bacterial sulfate reduction in coastal marine sediments. 2. Calculations from mathematical models. *J. Geomicrobiol.*, **1**, 29–51.
- Kastens K.A. and Spiess F.N. (1984) Dissolution and collapse features on the Eastern Mediterranean Ridge. *Mar. Geol.*, **56**, 181-193.
- Keller J., Ryan W.B.F., Ninkovich D. and Altherr R. (1978) Explosive volcanic activity in the Mediterranean over the past 200,000 yr as recorded in deep-sea sediments. *Geol. Soc. Am. Bull.*, **89**, 591-604.
- Kennedy H.A. and Elderfield H. (1987) Iodine diagenesis in pelagic deep-sea sediments. *Geochim. Cosmochim. Acta*, **51**, 2489-2504.
- Kessler M. (1973) Oxygen supply; theoretical and practical aspects of oxygen supply and microcirculation of tissue (ed. M. Kessler et al.), University Park Press, pp 312.
- Kidd R.B., Cita M.B. and Ryan W.B.F. (1978) Stratigraphy of eastern Mediterranean sapropel sequences recovered during DSDP Leg 42A and their paleoenvironmental significance. *Initial Rep. Deep Sea Drill. Proj.*, **42A**, 421-443.
- Klinkhammer G.P. and Lambert C.E. (1989) Preservation of organic matter during salinity excursions. *Nature*, **339**, 271-274.

- Krijgsman W., Hilgen F.J., Langereis C.G., Santarelli A., and Zachariasse W.J. (1995) Late Miocene magnetostratigraphy, biostratigraphy and cyclostratigraphy from the Mediterranean. *Earth Planet. Sci. Lett.*, **136**, 475-494.
- Krom M.D., Davison P., Zhang H. and Davison W. (1994) High-resolution pore-water sampling with a gel sampler. *Limnol. Ocean.*, **39**, 1967-1972.
- Langereis C.G., Dekkers M.J., Van Santvoort P.J.M., and De Lange G.J. (1997) Magnetostratigraphy and astronomical calibration of the last 1.1 Myr from a Eastern Mediterranean piston core and dating of short events in the Brunhes. *Geophys. J. Int.*, **129**, 75-94.
- Langereis C.G. and Hilgen F.J. (1991) The Rossello composite: a Mediterranean and global reference section for the Early to early Late Pliocene. *Earth Planet. Sci. Lett.*, **104**, 211-225.
- Laskar J. (1990), The chaotic motion of the solar system: A numerical estimate of the size of the chaotic zones. *Icarus*, **88**, 266-291.
- Laskar J., Joutel F. and Boudin F. (1993) Orbital, precessional, and insolation quantities for the Earth from -20 to +10 Myr. *Astron. Astrophys.*, **270**, 522-533.
- Legeleux F., Reyss J.-L. and Schmidt S. (1994) Particle mixing rates in sediments of the northeast tropical Atlantic: Evidence from $^{210}\text{Pb}_{\text{xs}}$, ^{137}Cs , $^{228}\text{Th}_{\text{xs}}$ and $^{234}\text{Th}_{\text{xs}}$ downcore distributions. *Earth Planet. Sci. Lett.*, **128**, 545-562.
- Levi S. and Banerjee S.K. (1976) On the possibility of obtaining relative paleointensities from lake sediments. *Earth Planet. Sci. Lett.*, **29**, 219-226.
- Li Y.-H. and Gregory S. (1974). Diffusion of ions in sea water and in deep-sea sediments. *Geochim. Cosmochim. Acta*, **38**, 703-714.
- Longhurst A., Sathyendranath S., Platt T. and Caverhill C. (1995) An estimate of global primary production in the ocean from satellite radiometer data. *J. Plankt. Res.*, **17**, 1245-1271.
- Lourens L.J. (1994) Astronomical forcing of Mediterranean climate during the last 5.3 million years, Ph.D. Thesis, Utrecht University, Utrecht, Netherlands, 247 pp.
- Lourens L.J. (in prep.) Mediterranean sapropel and $\delta^{18}\text{O}$ chronologies of the past 1.1 Myr.
- Lourens L.J., Hilgen F.J., Zachariasse W.J., Van Hoof A.A.M., Antonarakou A. and Vergnaud-Grazzini C. (1996) Evaluation of the Plio-Pleistocene astronomical timescale. *Paleoceanography*, **11**, 391-413.
- Mackensen A., Hubberten H.-W., Bickert T., Fischer G. and Fütterer D.K. (1993) The $\delta^{13}\text{C}$ in benthic foraminiferal tests of *Fontbotia Wuellerstorfi* (Schwager) relative to the $\delta^{13}\text{C}$ of dissolved inorganic carbon in Southern Ocean deep water: Implications for glacial ocean circulation models. *Paleoceanography*, **8**, 587-610.

- Mangini A., Eisenhauer A. and Walter P. (1991) A spike of CO₂ in the atmosphere at glacial-interglacial boundaries induced by rapid deposition of manganese in the oceans. *Tellus*, **43B**, 97-105.
- Manzella G.M.R., Gasparini G.P. and Astraldi M. (1988) Water exchange between the Eastern and Western Mediterranean through the Strait of Sicily. *Deep-Sea Res.*, **35**, 1021-1035.
- McDuff R.E. and Gieskes J.M. (1976) Calcium and magnesium profiles in DSDP interstitial waters: diffusion or reaction? *Earth Planet. Sci. Lett.*, **33**, 1-10.
- McDuff R.E., Gieskes J.M. and Lawrence J.R. (1978) Interstitial water studies leg 42A. *Init. Rep. DSDP*, **42**, 561-569.
- Medinaut shipboard report (1998) *Unpublished report, Utrecht University*.
- Meysman F.J.R. (2001) Modelling the influence of ecological interactions on reactive transport processes in sediments. *PhD-thesis, University of Gent*. 213pp.
- Meysman F.J.R., Middelburg J.J., Herman P.M.J. and Heip C.H.R. (2003) Reactive transport in surface sediments. II. MEDIA: an object-oriented problem-solving environment for early diagenesis. *Comp. & Geosc.*, **29**, 301-318.
- Moorby S.A., Cronan D.S. and Glasby G.P. (1984) Geochemistry of hydrothermal Mn-oxide deposits from the S.W. Pacific Island Arc. *Geochim. Cosmochim. Acta*, **48**, 433-441.
- Moore W.S. and Dymond J. (1988) Correlations of ²¹⁰Pb removal with organic carbon fluxes in the Pacific Ocean. *Nature*, **331**, 541-544.
- Mucci A. and Edenborn H.M. (1992) Influence of an organic-poor landslide deposit on the early diagenesis of iron and manganese in a coastal marine sediment. *Geochim. Cosmochim. Acta*, **56**, 3909-3921.
- Müller P.J. and Suess E. (1979) Productivity, sedimentation rate, and sedimentary organic matter in the oceans - I. Organic carbon preservation. *Deep-Sea Research*, **26A**, 1347-1362.
- Murat A. and Got H. (1987) Middle and Late Quaternary depositional sequences and cycles in the eastern Mediterranean. *Sedimentology*, **34**, 885-899.
- Narcisi B. and Vezzoli L. (1999) Quaternary stratigraphy of distal tephra layers in the Mediterranean – an overview. *Glob. Plan. Change*, **21**, 31-50.
- Nautinil shipboard report (2003) *Ifremer, Brest, France* (ed. J.-P. Boucher).
- Nijenhuis I.A., Becker J.J. and De Lange G.J. (2001) Geochemistry of coeval marine sediments in Mediterranean ODP cores and a land section: implications for sapropel formation models. *Palaeogeogr. Palaeoclimat. Palaeo-ecol.*, **165**, 97-112.

- Nolet G.J. and Corliss B.H. (1990) Benthic foraminiferal evidence for reduced deep-water circulation during sapropel deposition in the eastern Mediterranean. *Mar. Geol.*, **94**, 109-130
- Nozaki Y., Cochran J.K., Turekian K.K. and Keller G. (1977) Radiocarbon and ^{210}Pb distribution in submersible-taken deep-sea cores from Project FAMOUS. *Earth Planet. Sci. Lett.*, **34**, 167-173.
- Olausson E. (1961) Studies of deep sea cores. Repts. *Swedish Deep-Sea Exped. 1947-1948*, **8**, 337-391.
- Passier, H.F., Böttcher, M.E. and De Lange G.J. (1999) Sulphur Enrichment in Organic Matter of Eastern Mediterranean Sapropels: A Study of Sulphur Isotope Partitioning. *Aquatic geochem.*, **1**, 99-118.
- Passier, H.F., Middelburg J.J., Van Os, B.J.H. and De Lange, G.J. (1996) Diagenetic pyritisation under eastern Mediterranean sapropels caused by downward sulphide diffusion. *Geochim. Cosmochim. Acta*, **60**, 751-763
- Pedersen T.F. and Calvert S.E. (1990) Anoxia versus productivity: what controls the formation of organic carbon rich sediments and sedimentary rocks? *AAPG Bull.*, **V.74**, 454-466.
- Pierre C. and Fontes J.C. (1978) Isotope composition of Messinian sediments from the Mediterranean Sea as indicators of paleoenvironments and diagenesis. *Init. Rep. DSDP*, **42**, 635-650.
- Prahl F.G., Bennet J.T. and Carpenter R. (1980) The early diagenesis of aliphatic hydrocarbons and organic matter in sedimentary particulates from Dabob Bay, Washington. *Geochim. Cosmochim. Acta*, **44**, 1967-1976.
- Prahl F.G., De Lange G.J., Lyle M. and Sparrow M.A. (1989) Post depositional stability of long-chain alkenones under contrasting redox conditions. *Nature*, **341**, 434-437.
- Prell W.L. and Kutzbach J.E. (1987) Monsoon variability over the past 150,000 years. *J. Geophys. Res.*, **92**, 8411-8425.
- Presley B.J., Petrowski C. and Kaplan I.R. (1973). Interstitial water chemistry: deep sea drilling project, leg 13. *Init. Rep. DSDP*, **13**, 809-821.
- Price N.B. and Calvert S.E. (1977) The contrasting geochemical behaviours of iodine and bromine in recent sediments from the Namibian shelf. *Geochim. Cosmochim. Acta*, **41**, 1769-1775.
- Pruysers P.A., De Lange G.J. and Middelburg J.J. (1991) Geochemistry of eastern Mediterranean sediments: Primary sediment composition and diagenetic alterations. *Mar. Geol.*, **100**, 137-154.

- Pruyters P.A., De Lange G.J., Middelburg J.J. and Hydes D.J. (1993) The diagenetic formation of metal-rich layers in sapropel-containing sediments in the eastern Mediterranean. *Geochim. Cosmochim. Acta*, **57**, 257–536.
- Reimers C.E., Fisher K.M., Merewether R. Smith Jr. K.L. and Jahnke R.A. (1986) Oxygen microprofiles measured in situ in deep ocean sediments. *Nature*, **320**, 741-746.
- Revsbech N.P., Jørgensen B.B. and Blackburn T.H. (1980). Oxygen in the sea bottom measured with a microelectrode. *Science*, **207**, 1355-1356.
- Rio D., Sprovieri R. and Thunell R. (1991) Pliocene-lower Pleistocene chronostratigraphy: a re-evaluation of the Mediterranean type sections, *Geol. Soc. Amer. Bull.*, **103**, 1049-1058.
- Roberts A.P., Stoner J.S. and Richter C. (1996) Coring-induced magnetic overprints and limitations of the long-core paleomagnetic measurements technique: Some observations from leg 160, eastern Mediterranean Sea. *Proc. ODP, Init. Repts.*, **160**, 497-505.
- Roether W. and Well R. (2001) Oxygen consumption in the Eastern Mediterranean. *Deep-sea Research I*, **48**, 1535-1551.
- Rohling E.J. (1991) Shoaling of the Eastern Mediterranean pycnocline due to reduction of excess evaporation: implications for sapropel formation. *Paleoceanography*, **6**, 747-753.
- Rohling E.J. and Gieskes W.W.C. (1989) Late Quaternary changes in Mediterranean Intermediate Water density and formation rate. *Paleoceanography*, **4**, 531-545.
- Rohling E.J. and Hilgen F.J. (1991) The eastern Mediterranean climate at times of sapropel formation: a review. *Geol. Mijnb.*, **70**, 253-264.
- Rossignol-Strick M. (1983) African monsoons, an immediate climatic response to orbital insolation. *Nature*, **303**, 46-49.
- Rossignol-Strick M. (1985) Mediterranean Quaternary sapropels, and immediate response of the African monsoon to variations of insolation. *Palaeogeogr., Palaeoclimatol., Palaeoecol.*, **49**, 237-263.
- Rossignol-Strick M. (1987) Rainy periods and bottom water stagnation initiating brine accumulation and metal concentrations: 1. The late Quaternary. *Paleoceanography*, **2**, 333-360.
- Rossignol-Strick M., Nesteroff W., Olive P. and Vergnaud-Grazzini C. (1982) After the deluge: Mediterranean stagnation and sapropel formation. *Nature*, **295**, 105-110.
- Rossignol-Strick M., Paterne M., Bassinot F., Emeis K.-C. and De Lange G.J. (1998) An unusual mid-Pleistocene monsoon period over Africa and Asia. *Nature*, **392**, 269-272.
- Rutten A., De Lange G.J., Ziveri P., Thomson J., Van Santvoort P.J.M., Colley S. and Corselli C. (2000) Recent terrestrial and carbonate fluxes in the pelagic eastern Mediterranean; a comparison between sediment trap and surface sediment. *Palaeogeogr., Palaeoclimatol., Palaeoecol.*, **158**, 197-213.

- Ryan W.B.F. (1972) Stratigraphy of Late Quaternary sediments in the Eastern Mediterranean. In: *The Mediterranean Sea - A natural sedimentation laboratory* (ed. D.J. Stanley), Dowden, Hutchinson and Ross, Stroudsburg, pp. 149-169.
- Sarmiento J.L., Herbert T. and Toggweiler J.R. (1988) Mediterranean nutrient balance and episodes of anoxia. *Glob. Biog. Cycles*, **2**, 427-444.
- Sarnthein M., Pflaumann, U., Ross, R., Tiedemann, R. and Winn K. (1992) Transfer functions to reconstruct ocean palaeoproductivity: a comparison. In: *Geol. Soc. Spec. Pub No 64* (ed. C.P. Summerhayes, W.L. Prell and K.C. Emeis), pp. 411-427.
- Sarnthein M., Tetzlaff G., Koopmann B., Wolter K. and Pflaumann U. (1981) Glacial and interglacial wind regimes over the eastern subtropical Atlantic and North-West Africa. *Nature*, **293**, 193-196.
- Scientific staff of Cruise Bannock 1984-12 (1985). Gypsum precipitation from cold brines in an anoxic basin in the Eastern Mediterranean. *Nature*, **314**, 152-154.
- Shaw H.F. and Evans G. (1984) The nature, distribution and origin of a sapropelic layer in sediments of the Cilicia Basin, northeastern Mediterranean. *Mar. Geol.*, **61**, 1-12.
- Sigl W., Charmely H., Fabricius F., D'Argoud G. and Müller J. (1978) Stratigraphy of Late Quaternary sediments in the Eastern Mediterranean. In: *Init. Repts. DSDP 42A* (ed. K.J. Hsü, L. Montadert et al.), pp. 445-465.
- Slomp C.P., Thomson J., De Lange G.J. (2002) Enhanced regeneration of phosphorus during formation of the most recent eastern Mediterranean sapropel. *Geochim. Cosmochim. Acta*, **66**, 1171-1184.
- Soetaert K., Herman P.M.J., Middelburg J.J., De Stigter H.S., Van Weering T.E.W., Epping E. and Helder W. (1996) Modelling of ²¹⁰Pb-derived mixing activity in ocean margin sediments: diffusive versus non-local mixing. *J. Mar. Res.*, **54**, 1207-1227.
- Soetaert K., Herman P.M.J., Middelburg J.J. and Heip C (1998) Assessing organic matter mineralization, degradability and mixing rate in an ocean margin sediment (Northeast Atlantic) by diagenetic modelling. *J. Mar. Res.*, **56**, 519-534.
- Strickland J.D.H. and Parsons T.R. (1968) A practical handbook of seawater analysis. *Fish. Res. B. Canada Bull.*, **164**.
- Suess E. (1979) Mineral phases formed in anoxic sediments by microbial decomposition of organic matter. *Geochim. Cosmochim. Acta*, **43**, 339-352.
- Suess E. (1980) Particulate organic carbon flux in the oceans - surface productivity and oxygen utilization. *Nature*, **288**, 260-263
- Sutherland H.E., Calvert S.E. and Morris R.J. (1984) Geochemical studies of the Recent sapropel associated sediment from the Hellenic outer ridge, eastern Mediterranean Sea, I Mineralogy and chemical composition. *Mar. Geol.*, **56**, 79-92.

Ten Haven H.L., De Lange G.J. and McDuff R.E. (1987) Interstitial water studies of Late Quaternary Eastern Mediterranean sediments with emphasis on early diagenetic reactions and evaporitic salt influences. *Mar. Geol.*, **75**, 119-136.

Ten Haven H.L., De Leeuw J.W., Schenk P.A. and Klaver G.T. (1987) Geochemistry of Mediterranean sediments. Bromine/organic carbon and uranium/organic carbon ratios as indicators for different sources of input and post-depositional oxidation, respectively. *Org. Geochem.*, **13**, 255-261.

Thomson J., Higgs N.C., Croudace I.W., Colley S. and Hydes D.J. (1993) Redox zonation of elements at an oxic/anoxic boundary in deep-sea sediments. *Geochim. Cosmochim. Acta*, **57**, 579-595.

Thomson J., Higgs N.C., Wilson T.R.S., Croudace I.W., De Lange G.J. and Van Santvoort P.J.M. (1995) Redistribution and geochemical behaviour of redox-sensitive elements around S1, the most recent Eastern Mediterranean sapropel. *Geochim. Cosmochim. Acta*, **59**, 3487-3501.

Thomson J., Mercone D., De Lange G.J. and Van Santvoort P.J.M. (1999) Review of recent advances in the interpretation of Eastern Mediterranean sapropel S1 from geochemical evidence. *Mar. Geol.*, **153**, 77-89.

Thunell R.C., Williams D.F. and Kennet J.P. (1977) Late Quaternary paleoclimatology, stratigraphy and sapropel history in Eastern Mediterranean deep-sea sediments. *Mar. Micropaleontol.*, **2**, 371-388.

Thunell R.C., Williams D.F. and Cita M.B. (1983) Glacial anoxia in the Eastern Mediterranean. *J. Foraminifera. Res.*, **13**, 283-290.

Trauth M.H., Sarntheim M. and Arnold M. (1997) Bioturbational mixing depth and carbon flux at the sea floor. *Paleoceanography*, **12**, 517-526.

Trefry J.H. and Metz S. (1989) Role of hydrothermal precipitates in the geochemical cycling of vanadium. *Nature*, **342**, 531-533.

Troelstra S.R., Ganssen G.M., Van der Borg K. and De Jong A.F.M. (1991) A Late Quaternary stratigraphic framework for Eastern Mediterranean sapropel S1 based on AMS ¹⁴C dates and stable oxygen isotopes. *Radiocarbon*, **33**, 15-21.

Turekian K.K., Nozaki Y. and Benninger L.K. (1977) Geochemistry of atmospheric radon and radon products. *Ann. Rev. Earth. Planet. Sci.*, **5**, 227-255.

Turley C.M. (1999) The changing Mediterranean Sea – a sensitive ecosystem? *Progress Oceanogr.*, **44**, 387-400.

Ullman W.J. and Aller R.C. (1982) Diffusion coefficients in nearshore marine sediments. *Limnol. Oceanogr.*, **27**, 552-556.

- Van der Weijden C.H. (1993) Geochemical signatures preserved in sediments of the Semaforo and Vrica sections (Calabria, Italy) and their relations with variations of the sedimentary regime. *Palaeogeogr., Palaeoclimatol., Palaeoecol.*, **103**, 203–221.
- Van Hoof A.A.M., Van Os B.J.H., Rademakers J.G., Langereis C.G. and De Lange G.J. (1989) A palaeomagnetic and geochemical record of the upper Cochiti reversal and two subsequent precessional cycles from Southern Sicily (Italy). *Earth Planet. Sci. Lett.*, **117**, 235-250.
- Van Os B.J.M., Lourens L.J., Hilgen F.J. and De Lange G.J. (1994) The formation of Pliocene sapropels and carbonate cycles in the Mediterranean: Diagenesis, dilution or productivity. *Paleoceanogr.*, **9**, 601-617.
- Van Os B.J.H., Middelburg J.J. and De Lange G.J. (1991) Possible diagenetic mobilisation of barium in sapropelic sediment from the eastern Mediterranean. *Mar. Geol.*, **100**, 125-136.
- Van Os B.J.H. and Rohling E.J. (1993) Oxygen isotope depletions in Eastern Mediterranean sapropels exclude estuarine circulation. *Geologica Ultraiectina*, **109**, 3-12.
- Van Santvoort P.J.M., De Lange G.J., Thomson J., Cussen H., Wilson T.R.S., Krom M.D. and Ströhle K. (1996) Active post-depositional oxidation of the most recent sapropel (S1) in sediments of the Eastern Mediterranean. *Geochim. Cosmochim. Acta*, **60**, 4007–4024.
- Van Santvoort P.J.M., De Lange G.J., Langereis C.G. and Dekkers M.J. (1997) Geochemical and paleomagnetic evidence for the occurrence of 'missing' sapropels in Eastern Mediterranean sediments. *Paleoceanography*, **12**, 773–786.
- Van Santvoort P.J.M., De Lange G.J., Thomson J., Colley S., Meysman F.J.R. and Slomp C.P. (2002) Oxidation and origin of organic matter in surficial eastern Mediterranean hemipelagic sediments. *Aquatic Geochem.*, **8**, 153-175.
- Varnavas S.P., Papapioannou J. and Catani J. (1988) A hydrothermal manganese deposit from the Eratosthenes Seamount, Eastern Mediterranean Sea. *Mar. Geol.*, **81**, 205-214.
- Vengosh A., Starinsky A. and Anati D.A. (1994). The origin of Mediterranean interstitial waters - relics of ancient Miocene brines: a re-evaluation. *Earth Planet. Sci. Lett.*, **121**, 613-627.
- Vergnaud Grazzini C., Devaux M. and Znaidi J. (1986) Stable isotope "anomalies" in Mediterranean Pleistocene records. *Mar. Micropal.*, **10**, 35-69.
- Vergnaud-Grazzini C., Ryan W.B.F. and Cita M.B. (1977) Stable isotopic fractionation, climate change and episodic stagnation in the Eastern Mediterranean during the late Quaternary. *Mar. Micropaleontol.*, **2**, 353-370.
- Verosub K.L. and Roberts A.P. (1995) Environmental magnetism: Past, present and future. *J. Geophys. Res.*, **100**, 2175-2192.

Vezzoli L. (1991) Tephra layers in Bannock Basin (eastern Mediterranean). *Mar. Geol.*, **100**, 21-34.

Weaver P.P.E. and Kuijpers A. (1983) Climatic control of turbidite deposition on the Madeira Abyssal Plain. *Nature*, **306**, 360-363.

Wehausen R. and Brumsack H.-J. (1998) The formation of Pliocene Mediterranean sapropels: constraints from high-resolution major and minor element studies. In: *Proc. ODP, Sci. Res.*, **160** (ed. A.H.F. Robertson, K.-C. Emeis and A. Camerlenghi), pp. 207–217.

Westrich J.T. and Berner R.A. (1984) The role of sedimentary organic matter in bacterial sulfate reduction: The *G* model tested. *Limnol. Oceanogr.*, **29**, 236–249.

Wilson T.R.S., Thomson J., Colley S., Hydes D.J., Higgs N.C. and Sørensen J. (1985) Early organic diagenesis: The significance of progressive subsurface oxidation fronts in pelagic sediments. *Geochim. Cosmochim. Acta.*, **49**, 811-822.

Wilson T.R.S., Thomson J., Hydes D.J., Colley S., Culkin F. and Sørensen J. (1986) Oxidation fronts in pelagic sediments: Diagenetic formation of metal-rich layers. *Science*, **232**, 972-975.

Appendix

The samples that were analyzed comprise three fractions: volcanic material, normal oxic or sapropel sediment and pore water. The exact contribution of the different fractions is not known. The following approach is used to calculate the range of concentrations for the composition of each tephra.

A sample consists of two fractions: sediment and tephra. Since the samples are dried, pore water is absent. The pore water concentrations of the various elements are considered to be negligible. The correction will be shown with tephra layer i7 as an example.

1. The element with the lowest concentration in the sample compared to the surrounding sediment is selected. For i7 this is S; the sample contains 73% of the average S found in the surrounding sediment. Assume that the origin of this element in the tephra-containing interval is from the surrounding sediment, in other words the tephra concentration of S is 0. The concentration of S in the sample is 5902 ppm.
2. Determine in the surrounding sediment the ratio between other elements and S. For Al this results in 10.00. The concentrations for surrounding sediment are obtained by determining the average values in two samples immediately above and below the tephra layer (four samples in total).
3. Multiply the value obtained in step 2 by the concentration of that element in the sample and subtract this from the element concentration in the sample. This removes the sediment contribution to the sample. For Al this results in 19125 ppm (original sample concentration is 78145 ppm – (10 · 5902) = 19125).
4. If this results in negative concentrations, then not all S is part of the sediment. Adjust the S concentration in the volcanic fraction until all concentrations show positive amounts.
5. The value obtained in step 3 or 4 is the tephra contribution to the sample. Dividing this value by the total value of that element in the sample gives the percentual contribution to the total composition of the volcanic material. For Al this is 0.25 or 25% (19125 / 78145).
6. The concentration in the sample is the result of the mixing of volcanic material and regular sediment.

$$X \cdot C_{tephra} + (1 - X) \cdot C_{sediment} = C_{sample}$$

C_{sample} and $C_{sediment}$ are analysed. The relative contribution of $X \cdot C_{tephra}$ is obtained in step 5 (F_{tephra}). Therefore, the equation in step 6 evaluates to:

$$(1 - X) \cdot C_{sediment} = (1 - F_{tephra}) \cdot C_{sample}$$

This results in a value for X and subsequent in a value for C_{tephra} . For Al:

$$(1-F_{tephra}) \cdot C_{sample} = (1-0.25) \cdot 78145 = 58998 \text{ ppm.}$$

$$C_{sediment} = 80294 \text{ ppm.}$$

$$X = 0.27.$$

Note that the value for X is one end of a range of possible values for X: if, theoretically, no other sediment is mixed with the volcanic material then X=1. Therefore, the actual X ranges between the value obtained in step 6 and 1. This also means that the elemental concentrations range between the values calculated with the calculated minimum value for X and X=1. In the tables the values for both extremes are listed.

Sulphur is used in this example, other elements are used in other layers. The bold and italic values listed in the tables indicate that this element is used for the correction. Besides the normal values, the Al corrected values are listed. Some elements have not been analyzed for some layers.

Layer	i7		i9		i10		i12	
	Sample	Calc.	Sample	Calc.	Sample	Calc.	Sample	Calc.
X	1	0.27	1	0.78	0.78	0.27	1	0.78
Al (%)	7.8	7.2	9.5	10.0	6.6	7.2	6.5	8.3
Ba (ppm)	288	103	240	245	371	865	354	303
Be (ppm)	2.8	3.1	14	17	-	-	1.9	1.8
Ca (%)	8.6	9.1	2.1	0.5	13.0	12.8	12.7	8.8
Ce (ppm)	79	67	288	341	-	-	61	0
Co (ppm)	30	18	17	12	34	54	23	38
Cr (ppm)	100	122	18	0	70	41	71	58
Cu (ppm)	64	62	19	1	35	41	32	50
Fe (%)	3.8	3.3	2.9	2.7	3.6	4.0	3.7	4.8
K (%)	2.0	2.2	3.1	3.4	1.7	2.1	1.7	1.7
Li (ppm)	56	66	59	59	42	45	43	39
Mg (%)	1.8	1.3	0.8	0.5	1.7	1.7	1.7	1.7
Mn (ppm)	562	540	1300	1516	1044	0	1083	425
Na (%)	1.8	1.0	4.3	5.0	1.7	2.3	1.8	2.8
Ni (ppm)	64	64	21	10	39	21	47	35
P (ppm)	634	92	590	629	850	1304	575	989
S (ppm)	5902	0	1577	1566	-	-	1335	1945
Sc (ppm)	13	14	4	2	10	5	12	16
Sr (ppm)	545	272	191	132	529	498	622	785
Ti (ppm)	4214	3116	3455	3350	3565	3621	4931	9303
V (ppm)	136	137	53	32	102	89	120	194
Y (ppm)	7.8	7.2	57	65	16	8	17	14
Zn (ppm)	288	103	122	128	66	48	97	126
Zr (ppm)	2.8	3.1	525	618	152	285	102	115

Layer X	i14		i17		i20		i25	
	Sample 1	Calc. 0.55	Sample 1	Calc. 0.30	Sample 1	Calc. 0.32	Sample 1	Calc. 0.42
Al (%)	6.9	6.5	5.7	5.7	6.9	9.3	7.0	8.2
Ba (ppm)	312	266	617	323	215	304	328	465
Be (ppm)	3.6	4.4	2.0	2.1	-	-	-	-
Ca (%)	6.7	4.0	14.8	15.8	11.3	0.6	10.9	2.9
Ce (ppm)	187	256	107	114	-	-	-	-
Co (ppm)	42	51	62	110	42	85	28	40
Cr (ppm)	65	27	214	41	105	181	113	155
Cu (ppm)	43	36	152	327	30	43	32	39
Fe (%)	3.4	3.5	3.6	3.4	4.1	5.9	3.6	4.3
K (%)	2.3	2.5	1.4	2.0	1.9	2.6	2.0	2.4
Li (ppm)	30	11	48	41	47	46	47	48
Mg (%)	1.0	0.4	1.4	1.6	1.7	2.3	1.7	2.0
Mn (ppm)	1058	1351	852	0	669	212	622	228
Na (%)	3.9	5.5	1.7	2.4	1.3	1.7	1.2	1.3
Ni (ppm)	40	27	191	180	61	88	50	54
P (ppm)	459	466	675	636	694	1165	631	688
S (ppm)	1937	1241	16631	32898	-	-	-	-
Sc (ppm)	16	20	-	-	13	20	13	16
Sr (ppm)	349	300	630	705	454	0	439	108
Ti (ppm)	3803	4195	2758	2568	3714	4865	3678	4470
V (ppm)	54	0	280	484	116	155	121	148
Y (ppm)	50	71	21	24	18	14	18	12
Zn (ppm)	126	161	107	158	76	75	75	85
Zr (ppm)	679	1085	94	111	60	7	55	0

Layer X	i26		i27		i28		i30	
	Sample 1	Calc. 0.33	Sample 1	Calc. 0.64	Sample 1	Calc. 0.43	Sample 1	Calc. 0.44
Al (%)	7.0	7.9	7.7	9.4	6.9	8.9	8.2	10.9
Ba (ppm)	182	1	194	174	217	295	475	580
Be (ppm)	2.1	2.0	1.3	0.9	2.4	3.0	4.4	5.2
Ca (%)	11.2	11.3	12.5	8.5	10.4	1.3	7.8	0
Ce (ppm)	113	119	58	38	104	71	246	366
Co (ppm)	30	32	13	1	18	10	25	21
Cr (ppm)	84	65	27	0	83	92	54	31
Cu (ppm)	222	613	326	500	58	55	39	44
Fe (%)	3.2	2.9	1.9	1.3	3.4	4.1	2.1	1.4
K (%)	1.9	2.0	2.3	2.9	1.9	2.5	2.3	2.8
Li (ppm)	56	63	40	41	55	71	48	51
Mg (%)	1.7	1.8	0.8	0.5	1.8	2.3	1.1	0.7
Mn (ppm)	630	524	401	91	557	151	493	186
Na (%)	1.3	1.5	3.2	4.4	1.1	1.2	3.3	5.3
Ni (ppm)	73	103	38	26	64	75	50	31
P (ppm)	431	292	522	448	487	432	431	449
S (ppm)	850	1584	1287	1611	625	0	5913	3300
Sc (ppm)	-	-	-	-	-	-	-	-
Sr (ppm)	498	591	670	572	451	97	392	137
Ti (ppm)	3551	4125	4143	5170	3851	5145	2895	3307
V (ppm)	156	247	70	65	109	111	62	40
Y (ppm)	25	35	16	15	23	26	18	19
Zn (ppm)	96	102	71	78	78	96	88	104
Zr (ppm)	100	174	104	102	107	122	346	602

Layer X	i31		i32		i33	
	Sample 1	Calc. 0.85	Sample 1	Calc. 0.33	Sample 1	Calc. 0.57
Al (%)	4.4	4.4	5.1	8.2	5.2	4.5
Ba (ppm)	108	101	148	218	240	267
Be (ppm)	1.9	2.0	-	-	1.7	1.7
Ca (%)	20.5	20.6	20.8	13.1	16.2	17.7
Ce (ppm)	-	-	-	-	57	56
Co (ppm)	39	42	35	68	13	13
Cr (ppm)	61	63	59	93	81	85
Cu (ppm)	214	246	43	77	24	21
Fe (%)	3.4	3.6	2.5	3.6	3.0	2.9
K (%)	1.2	1.2	1.5	2.3	1.6	1.7
Li (ppm)	36	37	46	70	41	36
Mg (%)	1.3	1.3	1.3	1.5	1.6	1.4
Mn (ppm)	757	726	1064	0	953	1107
Na (%)	1.4	1.5	1.4	2.2	1.0	1.0
Ni (ppm)	80	86	47	60	57	61
P (ppm)	571	583	752	1203	855	1039
S (ppm)	914	0	-	-	925	1055
Sc (ppm)	4.3	3.7	9	14	71	85
Sr (ppm)	956	948	1042	887	210	27
Ti (ppm)	2554	2575	2485	3435	1081	0
V (ppm)	103	110	66	92	2310	3142
Y (ppm)	43	47	14	13	81	105
Zn (ppm)	98	107	50	47	31	13
Zr (ppm)	397	451	150	332	87	82

Samenvatting in het Nederlands

Het onderzoeksgebied

De Middellandse Zee is een bijna-gesloten bekken dat wordt omgeven door de Afrikaanse en Euraziatische continenten. De enige verbinding met de oceaan is de smalle en ondiepe Straat van Gibraltar. De drempel in de Straat van Sicilië verdeelt het bekken in een oostelijk en westelijk deel. Het oostelijke bekken is afgebeeld in Figuur 1.1. De verdamping is sterker dan de neerslag en de aanvoer van rivierwater, wat resulteert in zouter oppervlaktewater met een hogere dichtheid. De hoeveelheid water wordt op peil gehouden door het instromen van voedselarm Atlantisch oppervlakte water bij Gibraltar. Tegelijkertijd stroomt er voedselrijk water, afkomstig van groter diepte (Mediterranean Intermediate Water) in de Atlantische Oceaan. Hierdoor treedt er een continue export van nutriënten op en wordt de huidige Middellandse Zee vaak als een voedselwoestijn beschreven. Als gevolg is de aanmaak van organisch materiaal in het oppervlakte water erg laag (bijv. Sarmiento et al., 1988; Béthoux, 1989).

De vorming van diep water vindt plaats in het oostelijke bekken waar het zware, dichte oppervlakte water naar de diepte zakt. Sinds 1987 is dit proces van diep water vorming sterk veranderd. De bron van het diepe water is verplaatst van de Adriatische Zee naar de Aegeïsche Zee. Het huidige diepe water is warmer en zouter dan vroeger, wat tot gevolg heeft dat dezelfde zoutconcentraties nu 500 m minder diep worden aangetroffen (Klein et al., 1999; Lascaratos et al., 1999; Theocharis et al., 2002). Veranderingen zijn ook geconstateerd in de verdeling van voedingsstoffen. Voedselrijk water wordt nu dichter bij de fotische zone (de zone waar het licht nog doordringt in het water) gevonden dan voorheen. Dit kan resulteren in een toename van de biologische activiteit (Klein et al., 1999). Deze omvangrijke wijziging wordt toegeschreven aan belangrijke meteorologische veranderingen in de oostelijke Middellandse Zee en aan veranderingen in de stromingspatronen van het water (Lascaratos et al., 1999). Slechts een lange, droge periode (1988-1993) en een paar bijzonder koude winders (1987, 1992-1993) waren genoeg om dit grootschalige proces van diep water vorming drastisch te veranderen.

Pekelbekkens en moddervulkanen

De geodynamische ontwikkeling van de Middellandse Zee is voor een groot gedeelte bepaald door het samenkomen van Europa en Afrika. Als gevolg van het spreiden van de Atlantische mid-oceanische rug is de Afrikaanse plaat tegen de Euraziatische plaat gestoten en er daarna onder gedoken. Dit proces, dat nog steeds doorgaat, heeft geresulteerd in het ontstaan van vulkanische bogen en andere tectonische fenomenen zoals breuken en scheuren; niet alleen op het land, maar ook onder de zeebodem.

De sedimenten van de Middellandse Zee zijn afgezet bovenop een zeer dikke laag van evaporieten (zout), die gevormd zijn tijdens de zogenaamde “Messiniaanse Zout Crisis”. De meest gangbare verklaring is dat evaporieten zijn afgezet in een diep en opdrogend bekken dat herhaaldelijk afgesloten is geweest van de Atlantische Oceaan. Krijgsman et al. (1999) hebben aangetoond dat het begin van evaporiet vorming, met

astronomische methoden gedateerd op 5,96 miljoen jaar geleden, opvallend genoeg vrijwel in het gehele Middellandse Zee bekken op hetzelfde moment begon. De oorzaak van de “Messiniaanse Zout Crisis” is voornamelijk tectonisch van aard.

Tectonische processen en het feit dat evaporieten een lagere dichtheid hebben dan het sediment, heeft geresulteerd in het de vorming van zoutkoepels die omhoog komen. Het zout wordt snel opgelost als een zoutkoepel de zeebodem bereikt waardoor een diep bekken ontstaat. In de afgelopen jaren zijn een aantal van dit soort bekkens ontdekt: Tyro, Bannock, Atalante, Urania en Discovery Bekken (De Lange and Ten Haven, 1983; Jongma et al., 1983; Scientific staff of Cruise Bannock 1984-2, 1985; MEDRIF Consortium, 1995). De pekels die gevormd zijn tijdens dit oplossingsproces hebben een zeer grote dichtheid en zijn tot tien keer zo zout als zeewater (De Lange et al., 1990b). De overgang van pekkel naar zeewater is zeer scherp: het zoutgehalte verandert van normaal zeewater naar pekkelwaarden binnen tien centimeter. Door het dichtheidsverschil is er geen menging van pekkel met zeewater, wat resulteert in anoxische (zuurstofloze) condities in de pekkel.

Tectonische dislocaties kunnen er voor zorgen dat de druk van het poriewater in niet-doorlatende sedimenten toeneemt (Bray and Karig, 1985), bijvoorbeeld in de Mediterranean Ridge (een onderzees gebergte ten zuiden van Griekenland). Het is vastgesteld dat toenemende druk samen met breuken en plooien het begin kunnen vormen van modder diapieren en vulkanen. Sediment en een vloeibare fase (water en gas) worden uitgestoten tijdens een actieve periode en afgezet op de zeebodem, waardoor de moddervulkaan wordt opgebouwd. Vloeistoffen, die ook tijdens rustige perioden ontsnappen, kunnen op weg naar boven evaporieten oplossen en zijn dan zouter dan het oostelijke Middellandse Zeewater.

Oostelijke Middellandse Zee sedimenten

Sedimenten die hedentendage worden afgezet in hemipelagische gebieden in de oostelijke Middellandse Zee bevatten minder dan een halve gewichtsprocent organisch koolstof (C_{org}). Goed te onderscheiden olijfgroene tot zwarte, organisch rijke lagen (sapropelen) zijn ingebed in deze lichtbruine sedimenten. Kidd et al. (1978) hebben de volgende definitie gegeven: een sapropel is een discrete laag die meer dan 2% organisch koolstof bevat, is afgezet in een open marien milieu en is meer dan 1 cm dik. Sapropelen variëren in dikte van een paar centimeter tot decimeters en kunnen tot 30 gewichtsprocent C_{org} bevatten.

Paleoklimatologische veranderingen in het Middellandse Zee gebied zijn gerelateerd aan het ontstaan van sapropelen. Deze lagen worden gevormd wanneer de instraling van de zon op het noordelijk halfrond maximaal en het klimaat natter was (bijv. Rossignol-Strick et al., 1982; Rossignol-Strick, 1985). Hierdoor vervoeren de rivieren meer water en voedingsstoffen naar de oostelijke Middellandse Zee. De variaties in de instraling worden vooral veroorzaakt door de precessiecyclus van de baan van de aarde, die een periode heeft van ongeveer 23.000 jaar (bijv. Hilgen, 1991; Lourens et al., 1992).

Hoe sapropelen precies ontstaan is nog steeds een punt van discussie. De vele scenario's die zijn voorgesteld kunnen worden onderverdeeld in drie groepen. (1) Als gevolg van een verhoogde nutriënten toevoer, wordt de primaire productie in de fotische zone hoger. Dit zorgt voor een toename van het organisch koolstof gehalte in het sediment. (2) Primaire productie blijft onveranderd tijdens perioden van sapropel vorming, maar het anoxische bodemwater zorgt voor een betere preservatie van het organisch materiaal.

Deze zuurstofloze omstandigheden kunnen worden veroorzaakt door gelaagdheid in de waterkolom waardoor de circulatie van het water (en dus toevoer van zuurstof) stagneert. (3) Een toename in de primaire productie gaat samen met suboxisch tot anoxisch bodemwater.

Diagenese

Vroege diagenetische processen starten onmiddellijk nadat het sediment is afgezet. Het belangrijkste proces is de afbraak van organisch materiaal door bacteriën. De beschikbare oxidanten worden verbruikt in volgorde van afnemende energie productie per mol C_{org} dat wordt geoxideerd, namelijk zuurstof, nitraat, mangaanoxiden, ijzeroxiden en sulfaat (e.g. Froelich et al., 1979). In de meeste organisch rijke sedimenten worden zuurstof en nitraat opgebruikt door bacteriën in de bovenste paar millimeter van het sediment, terwijl zuurstof in organisch arme sedimenten tot op veel grotere diepten wordt aangetroffen. Dieper in het sediment worden andere oxidanten gebruikt voor het afbreken van het organisch materiaal. Het verbruik van de oxidanten heeft tot gevolg dat er verschillende redox zones ontstaan in het sediment. Gewoonlijk wordt het sediment steeds meer gereduceerd met de diepte, waarbij een opeenvolging (van boven naar beneden) wordt gevonden van oxische, suboxische en anoxische sedimenten.

In de suboxische redox zone worden ijzer- en mangaanoxiden in vaste vorm gebruikt voor de oxidatie van C_{org} . Hierdoor komen opgeloste vormen van ijzer en mangaan in het poriewater terecht, evenals sporemetalen die waren geadsorbeerd aan of ingebouwd in de oxiden. Dit opgelost ijzer en mangaan kan diffunderen naar andere plaatsen in het sediment. Als het dichterbij het oppervlak komt, waar weer minimale hoeveelheden zuurstof in het poriewater aanwezig zijn, dan worden deze ionen neergeslagen als oxides.

Wanneer de anoxische omstandigheden blijven bestaan, dan wordt sulfaat gebruikt door bacteriën waardoor er sulfide ontstaat (sulfaatreductie). Sulfide kan met opgelost ijzer het mineraal pyriet vormen. Als gevolg van sulfaatreductie wordt de sulfaat concentratie in het poriewater lager en bariet (bariumsulfaat) kan oplossen. Opgelost barium slaat weer neer op niveaus waar de sulfaat concentratie in het poriewater hoger is.

Dit proefschrift

In dit proefschrift worden diagenetische processen in zowel organisch rijke als organisch arme oostelijke Middellandse Zee sedimenten bestudeerd. Bovendien worden (huidige) fluxen en de variaties van verschillende proxies bediscussieerd. Een proxie is een stof of element waarmee het mogelijk is om het gedrag van een andere stof of element te reconstrueren.

In hoofdstuk 2 wordt gekeken naar de afbraak van C_{org} door zuurstof (aerobe mineralisatie) in de oppervlakte sedimenten van de diepe oostelijke Middellandse Zee. Het modelleerprogramma MEDIA (Modelling Environment for early DIagenetic problems) is gebruikt voor het kwantificeren hiervan. 60-80% van de totale hoeveelheid C_{org} die het sediment bereikt vormt de reactieve fractie. Binnen 10 cm wordt het grootste deel hiervan al weer geoxideerd. Op grotere diepten wordt vooral een niet-reactieve fractie aangetroffen, die 20-40% van de totale flux beslaat. Mineralisatie snelheden in de

oppervlakte sedimenten zijn gelijk aan die in oligotrofe, diepzee milieu's. Naast lage fluxen en snelle remineralisatie van C_{org} is ook de bioturbatie (bepaald met behulp van ^{210}Pb) erg ondiep. Een bioturbatiediepte van slechts 2 cm behoort zelfs tot de ondiepste die zijn gevonden voor oxische mariene sedimenten. De $\delta^{13}C_{org}$ waarden worden minder negatief met toenemende diepte en afnemende C_{org} concentraties. De belangrijkste $\delta^{13}C_{org}$ verandering treedt op in de bovenste 3 tot 4 cm en valt samen met het interval waar de afbraak van organisch materiaal het sterkst is. Schattingen van de paleoproductiviteit, die worden berekend uit de sediment data, wijzen op een lage productiviteit in de oppervlakte wateren.

In hoofdstuk 3 is een semi-kwantitatieve studie gemaakt van sedimentaire zout fluxen naar het diepe water van de oostelijke Middellandse Zee. Verschillende bronnen kunnen worden onderscheiden waarbij modderdiapieren en –vulkanen samen met normale poriewaters de belangrijkste zijn. Deze sediment input is echter relatief klein vergeleken met de verhoging van het zoutgehalte dat door de verdamping wordt veroorzaakt. De invloed op de modellen die gebruikt worden voor de berekening van water- en zoutbudgetten is vrij gering. Het toegevoegde zout uit het sediment is te klein om stagnatie van de waterkolom te initiëren, maar het kan wel een eenmaal gestartte stagnatie versterken.

Diagenetische signalen boven de meest recente sapropel S1 worden bestudeerd in hoofdstuk 4. In het algemeen worden twee Mn-rijke lagen aangetroffen, één direct boven de top van de sapropel, de andere een paar centimeter dicht bij het sediment oppervlak. Poriewater profielen tonen aan dat de onderste piek op dit moment nog groter wordt. Paleoproductiviteitsprofielen, gebaseerd op de relatie tussen barium en organisch koolstof, kunnen worden gebruikt om het oorspronkelijke organisch koolstof profiel van de S1 sapropel te reconstrueren. De profielen die met deze methode worden verkregen, tonen aan dat de oorspronkelijke sapropel dikker was, waarbij de bovenste Mn piek het niveau van de eigenlijke top aangeeft. Dit betekent dus dat het interval tussen de twee Mn pieken, waar nu lage organisch koolstof concentraties worden aangetroffen, oorspronkelijk deel heeft uitgemaakt van de sapropel. De afgezette C_{org} is geoxideerd door een oxidatie front dat steeds dieper is komen te liggen en zich ook nu nog verder naar beneden beweegt. Wanneer de bovenste Mn piek als het einde van de sapropel vorming wordt beschouwd, dan betekent dit dat de vorming van de sapropel recenter is geëindigd koolstofdatering van de zichtbare top van S1 aangeeft.

Het concept van oxidatie van sapropelen wordt verder uitgewerkt in hoofdstuk 5. Het voorkomen van sapropelen hangt samen met maxima in de instraling op het noordelijk halfrond. Niet bij elk maximum wordt echter een sapropel gevonden. Geochemische en magnetische signalen worden gebruikt om volledig geoxideerde ofwel “ontbrekende” sapropelen te identificeren. Een belangrijke parameter hierbij is barium. In zichtbare sapropelen worden altijd verhoogde concentraties Ba aangetroffen en bij gedeeltelijke oxidatie van de sapropel blijft het oorspronkelijke Ba profiel intact. Met behulp hiervan is bij acht van de elf bemonsterde intervallen rond instralingsmaxima een volledig geoxideerde sapropel aangetoond: Ba, de verdeling van spore metalen en magnetische parameters zijn vergelijkbaar met de signalen die gevonden worden bij zichtbare sapropelen.

In hoofdstuk 6 worden de verschillende typen sedimenten besproken die in de oostelijke Middellandse Zee worden aangetroffen. Behalve de normale hemipelagische sedimenten en sapropelen worden ook vulkanische lagen gevonden. Meer dan 5% van het sediment in de bestudeerde lange kern is het gevolg van turbiditische gebeurtenissen. De

samenstelling van deze turbidieten is gelijk aan het sediment wat er boven en onder ligt, wat op een lokaal brongebied wijst. Eén laag wordt aangemerkt als een, waarschijnlijk verplaatste, sapropel met een laag organisch koolstof gehalte. Een vergelijking tussen sapropelen en normaal sediment toont aan dat deze verrassend gelijk zijn. Variaties in het klimaat, de oorzaak voor de vorming van sapropelen, hebben geen significante invloed op de samenstelling van het sediment op deze lokatie. Klimaat gerelateerde cycli zijn dan ook niet gevonden in deze kern.

Dankbetuiging (acknowledgements)

Er zijn veel mensen die me in de afgelopen jaren gesteund en geholpen hebben bij het tot stand komen van dit proefschrift. Een aantal mensen wil ik in het bijzonder danken.

Allereerst ben ik Gert de Lange en Kees van der Weijden dankbaar voor de mogelijkheid om te ontdekken hoe leuk en interessant wetenschap en Mariene Geochemie kan zijn. Zonder hun voortdurende steun en sturing in de afgelopen jaren zou dit proefschrift nooit tot een einde zijn gekomen.

Verder wil ik Gert bedanken voor de mogelijkheden om als niet-wetenschapper toch weer met enige regelmaat op zeegaande reizen mee te kunnen gaan. Het is een mooie mogelijkheid om nog een beetje voeling te houden met het vakgebied en het leven aan boord bevalt elke keer weer prima. Bovendien heeft de deelname aan de Urania 2002 cruise voor een blijvende verandering in mijn leven gezorgd.

Ik dank de co-auteurs voor hun bijdrage en inspanningen. Een speciaal woord van dank aan John Thomson, Caroline Slomp, Luc Lourens, Filip Meysman, Cor Langereis en Mark Dekkers. Hun hulp en de grote hoeveelheid tijd die ze hebben geïnvesteerd waren van grote waarde.

Voor de (technische) ondersteuning op het lab en daarbuiten dank ik Rene Alink, Mark van Alphen, Paul Anten, Hans Bliet, Tilly Bouten, Arnold van Dijk, Chiel Eussen, Tony van de Gon Netscher, Vian Govers, Miranda Klein-Tank, Pieter Kleingeld, Erica Koning Dineke van de Meent, Gijs Nobbe, Guus Peters, Helen de Waard en Theo van Zessen. De koffie bij Helen, Gijs en Mark was (en is nog) altijd een goed begin van de dag!

In alle jaren dat ik, meer of minder frequent, in Utrecht heb rondgelopen hebben de volgende mensen altijd voor een prettig verblijf gezorgd: David Aguilera, Gerard van den Berg, Guiseppe Frapporti, Niels Hartog, Wim Hegeman, Else Henneke, Marcel Hoefs, Andreas Hübner, Ronald Jonckbloedt, Thomas Keijzer, Sieger van der Laan, Peter van der Linde, Dorinda van der Linden, Yvonne van Lith Guus Loch, Jack Middelburg, Pien van Minnen, Gerben Mol, Ivar Nijenhuis, Bertil van Os, Marcel Paalman, Hilde Passier, Peter Pruyssers, Gert-Jan Reichart, Anja Reitz, Arrian Rutten, Dick Schipper, Sjoerd Schenau, Arthur Schmidt, Hendrik-Jan Visser, Simon Vriend, Mariette Wolthers en Berend Wilkens.

Philippe van Cappellen wil ik danken voor de gastvrijheid in het afgelopen jaar en Pien voor het steeds weer regelen van een werkplek.

Mijn ouders en familie dank ik voor de steun die ze altijd hebben gegeven bij de dingen die ik doe. Het geeft een goed gevoel om te weten dat zij er altijd zijn.

Tenslotte wil ik Anke bedanken. Zij is het sprekende voorbeeld dat er aan boord niet alleen ruimte is voor wetenschap. Haar motiverende aanwezigheid heeft er voor gezorgd dat de laatste loodjes een stuk minder zwaar werden.

Curriculum Vitae

Petrus Johannes Maria van Santvoort is op 3 juli 1965 in Rosmalen geboren. In 1977 begon hij zijn middelbare schoolopleiding VWO aan het Jeroen Bosch College te 's-Hertogenbosch. Deze opleiding werd in 1984 afgesloten met het Atheneum B diploma. In datzelfde jaar begon hij met zijn studie aan de Universiteit Utrecht, waar hij in 1986 het propedeutisch examen Geologie behaalde. In augustus 1990 werd door hem het doctoraal examen Geologie behaald. Na een korte periode gewerkt te hebben als Toegevoegd Onderzoeker bij de vakgroep Geochemie te Utrecht, werd hij assistent-in-opleiding bij dezelfde vakgroep. Het in deze hoedanigheid verrichtte onderzoek in de oostelijke Middellandse zee heeft geresulteerd in dit proefschrift. In 1996 is hij begonnen als Software Engineer bij het toenmalige RCC. Naast deze baan heeft hij in 1999 het kort-HBO diploma Bedrijfskundige Informatica en Systeemontwikkeling behaald. Momenteel is hij werkzaam bij PinkRocade Public Sector als ontwikkelaar van internet applicaties.

Other publications

De Lange G.J., Van Os B., Pruyssers P.A., Middelburg J.J., Castradori D., Van Santvoort P., Müller P.J., Eggenkamp H. and Prahl F.G. (1994) Possible early diagenetic alteration of palaeo proxies. *NATO ASI*, **I 17**, 225-258.

De Lange G.J., Van Santvoort P.J.M., Langereis C., Thomson J., Corselli C., Michard A., Rossignol-Strick M., Paterne M. and Anastasakis G. (1999) Palaeo-environmental variations in eastern Mediterranean sediments: a multidisciplinary approach in a prehistoric setting. *Progress in Oceanography*, **44**, 369-386.

Dekkers M.J., Langereis C.G., Vriend S.P., Van Santvoort P.J.M. and De Lange G.J. (1994) Fuzzy *c*-means cluster analysis of early diagenetic effects on natural remanent magnetisation acquisition in a 1.1 Myr piston core from the Central Mediterranean. *Phys. Earth Planet. Int.*, **85**, 155–171.

Langereis C.G., Dekkers M.J., Van Santvoort P.J.M., and De Lange G.J. (1997) Magnetostratigraphy and astronomical calibration of the last 1.1 Myr from a Eastern Mediterranean piston core and dating of short events in the Brunhes. *Geophys. J. Int.*, **129**, 75-94.

Rutten A., De Lange G.J., Ziveri P., Thomson J., Van Santvoort P.J.M., Colley S. and Corselli C. (2000) Recent terrestrial and carbonate fluxes in the pelagic eastern Mediterranean; a comparison between sediment trap and surface sediment. *Palaeogeogr., Palaeoclimatol., Palaeoecol.*, **158**, 197-213.

Thomson J., Higgs N.C., Wilson T.R.S., Croudace I.W., De Lange G.J. and Van Santvoort P.J.M. (1995) Redistribution and geochemical behaviour of redox-sensitive elements around S1, the most recent Eastern Mediterranean sapropel. *Geochim. Cosmochim. Acta*, **59**, 3487–3501.

Thomson J., Mercone D., De Lange G.J. and Van Santvoort P.J.M. (1999) Review of recent advances in the interpretation of Eastern Mediterranean sapropel S1 from geochemical evidence. *Mar. Geol.*, **153**, 77-89.

